Pacific Northwest
NATIONAL LABORATORY

PNNL-30443

Sediment Mineralogy Data Review for the Hanford Central Plateau

September 2020

RJ Serne
Nik Qafoku
JE Szecsody
MJ Truex

U.S. DEPARTMENT OF ENERGY

Prepared for the U.S. Department of Energy
under Contract DE-AC05-76RL01830

DISCLAIMER

PACIFIC NORTHWEST NATIONAL LABORATORY
operated by
BATTELLE
for the
UNITED STATES DEPARTMENT OF ENERGY
under Contract DE-AC05-76RL01830

Printed in the United States of America

Available to DOE and DOE contractors from the
Office of Scientific and Technical Information,
P.O. Box 62, Oak Ridge, TN 37831-0062;
ph: (865) 576-8401
fax: (865) 576-5728
email: reports@adonis.osti.gov

Available to the public from the National Technical Information Service
5301 Shawnee Rd., Alexandria, VA 22312
ph: (800) 553-NTIS (6847)
email: orders@ntis.gov <https://www.ntis.gov/about>
Online ordering: http://www.ntis.gov

PNNL-30443

Sediment Mineralogy Data Review for the Hanford Central Plateau

September 2020

RJ Serne
Nik Qafoku
JE Szecsody
MJ Truex

Prepared for
the U.S. Department of Energy
under Contract DE-AC05-76RL01830

Pacific Northwest National Laboratory
Richland, Washington 99354

Summary

The compendium of Hanford site sediment mineralogy data provided in this report was initiated in 2012 to support flux mitigation technologies and real-time monitoring that could limit contaminant fluxes to the groundwater in the Central Plateau. Recent efforts in advancing spectral induced polarization as a method for monitoring contaminant transformations for active biogeochemical remedies have underscored the need for a published compendium of sediment characterization data. Although the data are primarily focused on the mineralogical composition of Hanford sediments, other soil measurements such as particle size distribution and carbon content are provided. The data have been reproduced from the original reports and are provided here *for information only* (FIO).

In general, the sand and gravel mineralogy of the Hanford formation, Cold Creek unit, and Ringold Formation is similar because of common geologic provenance. Quartz, plagioclase feldspar, and micas (biotite, muscovite, and vermiculitized biotite) have been identified in all size fractions, with illite, smectite, chlorite, and kaolinite as the principal minerals in the clay-size fraction. Detrital and pedogenic calcite are consistently observed in vadose zone sediments, ranging in concentration from ~1% to a maximum of 5%, and averaging 1.79 mass % for the Hanford formation. Pedogenic calcite exists in the form of discrete, but infrequent, caliche layers (~25 cm in thickness) that formed beneath surfaces exposed for extended inter-flood periods during the Pleistocene.

Appendix A contains data on sediment samples obtained from four boreholes in the 200 East Area and two large excavations. Up to 20 samples as a function of depth were characterized in detail so that most of the different lithologies and sediment facies were characterized. Appendix B contains data on sediment samples obtained from five boreholes in the 200 West Area, with up to 20 samples as a function of depth were characterized. Appendix C contains limited characterization data on aquifer sediments from five boreholes.

Acknowledgments

Funding for this work was provided by the U.S. Department of Energy Richland Operations Office under the Deep Vadose Zone – Applied Field Research Initiative. The Pacific Northwest National Laboratory is operated by Battelle Memorial Institute for the Department of Energy under Contract DE-AC05-76RL01830.

Acronyms and Abbreviations

µSXRF	microscanning X-ray fluorescence
µXRD	X-ray microdiffraction
BET	Brunauer–Emmett–Teller
CEC	cation exchange capacity
CERCLA	Comprehensive Environmental Response, Compensation, and Liability Act
DCB	dithionite-citrate-bicarbonate
EDS	energy dispersive spectroscopy
EMP	electron microprobe
EXAFS	extended X-ray absorption fine structure spectroscopy
FIO	for information only
HH	hydroxylamine hydrochloride
ICP	inductively coupled plasma
ICP-MS	inductively coupled plasma mass spectrometry
ICP-OES	inductively coupled plasma optical emission spectrometry
IDF	Integrated Disposal Facility
ILAW	immobilized low-activity waste
K_d	distribution coefficient
NMR-PGSE	nuclear magnetic resonance pulse gradient spin echo technique
RCRA	Resource Conservation and Recovery Act
RI/FS	Remedial Investigation/Feasibility Study
SEM	scanning electron microscopy
SXRF	microscanning X-ray fluorescence
TD	total depth
TEM	transmission electron microscopy
TRLFS	time-resolved spectroscopy laser fluorescence spectroscopy
XAFS	X-ray absorption fine structure spectroscopy
XANES	X-ray adsorption near edge structure spectroscopy
XMP	synchrotron-based X-ray microprobe
XRD	X-ray diffraction
XRF	X-ray fluorescence
WMA	waste management area

Units of Measure

ft bgs	feet below ground surface
g	gram
kg	kilogram
L	liter
µ	micro (prefix, 10^{-6})
M	molar (moles/L)
ppm	parts per million

Contents

Summary ii
Acknowledgments iii
Acronyms and Abbreviations iv
Units of Measure v
Contents vi
1.0 Introduction 1.1
2.0 Analytical Methods 2.1
2.1 Measurement Methods 2.1
2.1.1 X-Ray Diffraction 2.1
2.1.2 Scanning Electron Microscope and Transmission Electron Microscope 2.1
2.2 Total Oxide and Trace Metal Content 2.2
2.2.1 X-ray Fluorescence 2.2
2.2.2 Inductively Coupled Plasma Spectroscopy 2.2
2.3 Hydrous Oxide Content 2.2
2.4 Total Carbon, Inorganic Carbon, and Organic Carbon Content 2.3
2.5 Particle Size Distribution 2.3
2.6 Particle Density 2.3
2.7 Cation Exchange Capacity 2.3
2.8 Specific Surface Area 2.3
3.0 Sediment Characterization 3.1
3.1 Generalized Summary of Hanford Vadose Sediment Mineralogy 3.1
3.2 Mineralogy 3.2
3.2.1 200 West Sediment Analyses 3.2
3.2.2 200 East Sediment Analyses 3.4
3.3 Statistical Mineralogical Analysis of Hanford and Ringold Sediments 3.6
4.0 Summary 4.1
5.0 Quality Assurance 5.2
6.0 References 6.1
Appendix A – Characterization Data for 200 East Area Sediments A.1
Appendix B – Characterization Data for 200 West Area Sediments B.1
Appendix C – Aquifer Sediments C.1

Tables

Table 2.1. Characterization Methods 2.1
Table 3.1. Mineralogical Analyses for 200 West Area Sediments 3.4
Table 3.2. Mineralogical Analyses for 200 East Sediments 3.5

1.0 Introduction

Site characterization plays a critical role in the Comprehensive Environmental Response, Compensation, and Liability Act (CERCLA) Remedial Investigation and Feasibility Study (RI/FS) process in remedy selection and implementation. Exposure assessment, determination of risk-based cleanup levels, and remedial alternative evaluations require knowledge of contaminant transformation and degradation processes that occur in both aqueous and solid phases. Both physical and biogeochemical characterization data are needed for effective decision-making.

As contaminants are transported in the subsurface from the vadose zone to the groundwater, bio-and physiochemical reactions occur between the contaminants and the soil materials. Rates of reactions such as biodegradation, hydrolysis, sorption/desorption, precipitation/dissolution, redox reactions, acid-base reactions, and others are process-limiting characteristics for many remedial alternatives. To effectively identify contaminant transport and transformations, several data types are needed, including soil mineralogy, distribution coefficients, contaminant abiotic/biological degradation rates. The composition of sediment pore fluid and mobility of contaminants in a sediment or soil are limited through adsorption/ desorption and precipitation/dissolution reactions between these minerals and the pore fluid. Therefore, it is important to identify the various minerals and their abundances in sediments used for estimating contaminant-pore water-solid interactions. These data can then be used to determine the nature and extent of contamination, risk analysis, and selection of a remedial alternative.

The objective of this report is to compile available data on the mineralogy of Hanford Site vadose zone sediments, to support flux mitigation technologies and real-time monitoring that could limit contaminant fluxes to the groundwater in the Central Plateau. This report provides a high-level summary of methods used to identify minerals, as well as a general description of mineral composition in the Hanford Central Plateau in Section 2. A literature review of mineralogical analyses is presented as an overview in Section 3, with specific data presented in more detail in Appendix A through Appendix C. In addition to the mineralogy, selected data for other related parameters such as particle size distribution, specific surface area, cation exchange capacity (CEC), total carbon, inorganic carbon, organic carbon, and estimates of hydrous oxide content are also tabulated in appendices. Section 4 provides a brief summary of the content of this report.

Three appendices collate characterization data from different reports. Appendix A contains all the sediment characterization data for vadose zone sediments obtained from the 200 East Area. Appendix B contains all the sediment characterization data for vadose zone sediments obtained from the 200 West Area. Appendix C contains sediment characterization data for aquifer sediments (mostly Ringold Formation sediments). Since the goal of this report is to collate historical characterization data into a single, accessible location, the data *have not* been reviewed for technical accuracy per NQA-1 guidelines. The data have been reproduced from original reports and are provided *for information only* (FIO).

2.0 Analytical Methods

Mineral identification has been carried out on several bulk samples and clay-size fractions of sediments using established techniques such as optical microscopy, X-ray powder diffraction, scanning electron microscopy (SEM), and transmission electron microscopy (TEM). SEM and TEM analyses are often coupled with online instrument capabilities of energy dispersive spectroscopy (EDS), which provide semi-quantitative chemical analyses of the analyzed solids. Depending on the objectives, other instrument techniques may be used to further characterize the composition, morphology, and surfaces of individual minerals in a sediment or rock over a large size range from centimeters to nanometers in scale. For the measurements described in the appendices, Table 2.1 lists the methods used for characterization of Hanford sediments. A compilation of the statistical variability of mineralogy by XRD and SEM in Hanford, Ringold, and Cold Creek formations is found in Xie and others (2003).

Table 2.1. Characterization Methods

Parameter	Method
Mineralogy	XRD and SEM/TEM
Total major constituent oxide and trace metal content	XRF and/or total fusion/digestion
Hydrous oxide content	Chemical extraction
Total and inorganic carbon content	Carbon analyzer
Particle size distribution	Dry sieving and hydrometer
CEC	Various methods
Surface area	BET gas adsorption
Particle density	Pychnometer

BET is Brunauer–Emmett–Teller; XRD is X-ray diffraction; XRF is X-ray fluorescence.

2.1 Measurement Methods

2.1.1 X-Ray Diffraction

Mineralogical studies included X-ray diffraction (XRD) analysis to identify and determine semi-quantitative mineralogical distributions of the minerals present in bulk solid, sand size (<2 mm to 75 μm) and either the silt-clay (<75 μm) or clay-size (<2 μm) fraction of sediment samples. XRD is a laboratory-based technique commonly used for identifying crystalline materials. XRD analysis is based on constructive interference of monochromatic X-rays and a crystalline sample. The X-rays are generated by a cathode ray tube and filtered to produce monochromatic radiation. The characteristic pattern generated in a typical XRD analysis provides a unique “fingerprint” of the crystals present in the sample. When properly interpreted, by comparison with standard reference patterns and measurements, this fingerprint allows for identification of the crystalline form.

2.1.2 Scanning Electron Microscope and Transmission Electron Microscope

There are two common types of electron microscopes: 1) scanning electron microscope and 2) transmission electron microscope. When using an scanning electron microscope, bulk samples are typically prepared by transferring a small aliquot of dilute soil slurry onto a carbon-coated copper support grid to readily reflect electrons. This coating also provides a conducting surface for electrons to avoid

charging of the sample. Samples need to be thin, or they will absorb too much of the electron beam. The incoming electron beam is condensed into a small beam which is scanned over the object. An image is formed by the electrons that bounce off the surface of the specimen and are then collected onto the imaging screen. The observer therefore sees a picture of the surface of the surface of the sample, without any internal information. A transmission electron microscope, on the other hand, produces an image that is a projection of the entire object, including the surface and the internal structures. The incoming electron beam interacts with the sample as it passes through the entire thickness of the sample. Therefore, objects with different internal structures can be differentiated because they give different projections.

2.2 Total Oxide and Trace Metal Content

2.2.1 X-ray Fluorescence

The basis for XRF (X-ray fluorescence) is a non-destructive analytical technique used to determine the elemental composition of materials based on the relationship between an element's mass and frequency. XRF instruments determine the chemistry of a sample by measuring the fluorescent X-ray emitted from a sample when it is excited by an X-ray source. Each of the elements present in a sample produces fluorescent X-rays that serve as a fingerprint unique for that specific element. For the cores described in this report, total oxide and trace metal in the bulk, sand, silt, and clay sized sediment fractions content were determined by using energy and wavelength dispersive XRF.

2.2.2 Inductively Coupled Plasma Spectroscopy

Inductively coupled plasma (ICP) spectrometry is a powerful tool for analyzing trace metals in environmental samples. Inductively coupled plasma optical emission spectrometry (ICP-OES) is mainly used for samples with high total dissolved solids, and is a trace-level, elemental analysis technique. An inductively coupled plasma mass spectrometry (ICP-MS) instrument combines a high-temperature ICP source with a mass spectrometer and is especially useful when lower detection limits are required. ICP-OES is based on the measurement of excited atoms and ions at the wavelength characteristics for the specific elements being measured. ICP-MS, however, measures an atom's mass by mass spectrometry.

The elemental composition of bulk sediment samples for cores in several analyses was determined by a combination of fusion (KOH-KNO_3 treatments) of the sediment with subsequent analysis of the dissolved material by ICP-OES and ICP-MS analyses. Results were compared against known rock and soil standards.

2.3 Hydrous Oxide Content

Chemical extraction methods were used to characterize amorphous and crystalline hydrous-oxide phases in many of the core samples, with an emphasis on determining iron oxide content. The theory behind the extraction methods is that the most mobile metals are removed in the first fraction and continue in order of decreasing mobility. Chemical extraction methods facilitate fractionation. These fractions are often referred to as exchangeable, weakly absorbed, hydrous oxide bound, organic bound, and lattice material components, respectively. To remove the exchangeable fraction, the ionic composition of water is changed, which allows metals sorbed to the exposed surfaces of sediment to be easily removed. An acid solution is used second to remove the carbonate-bound fraction. Metals bound to Fe and Mn oxides are particularly susceptible to anoxic (reducing) conditions, so a solution capable of dissolving insoluble sulfide salts is used third. Organic materials are oxidized to remove metals bound in the organic phase. The residual fraction consists of metals incorporated into the crystal structures of primary and secondary

minerals. This fraction is the hardest to remove and requires the use of strong acids to break down silicate structures.

2.4 Total Carbon, Inorganic Carbon, and Organic Carbon Content

Carbon analyses were carried out using analyzers that measure the CO_2 formed when organic carbon is oxidized and/or when inorganic carbon is acidified. Organic carbon content in cores was estimated by the difference between the inorganic carbon and total carbon concentration. Because the difference between the two values is quite low and often within the analytical error of the two measurements, the organic content of Hanford sediments is often not precisely quantified with this method.

2.5 Particle Size Distribution

Dry sieving and hydrometer methods were used to determine the particle size distribution for selected core samples. Silt/clay, sand, and gravel size fractions were separated by sieving. The silt and clay size fractions were further separated using Stokes' law settling velocities to determine weight percentage of each size-fraction. Each clay fraction and the less than 2 mm (gravel removed) size separate sample were also characterized for mineralogy using XRD. The second particle size measurement technique used the wet sieve/hydrometer method for quantifying the fraction of silt and clay. The silt and clay separates were then used in subsequent mineralogical analyses.

2.6 Particle Density

The particle density of bulk grains was determined using pycnometers, which are suitable for measuring density of coarse-grained soils. A soil particle density analysis involves determining the average density of individual particles that comprise a soil sample based on its mass and volume. Mass of the particle is determined by weighing, using a high-precision analytical balance. The volume of the soil particles is determined using displacement of liquid by the soil particles in a pycnometer (glass flask).

2.7 Cation Exchange Capacity

CEC can be measured replacing cations on the exchange sites with a single cation such as ammonium (NH_4^+), then replacing that exchangeable NH_4^+ with another cation, and then measuring the amount of NH_4^+ exchanged. A similar procedure was used to measure CEC in Hanford sediments that involved fewer extractions to avoid dissolution of calcite. A radiotracer method developed by Routson et al. (1973), which minimizes hydrolysis errors, was also used to identify the CEC of sediments.

The CEC of a soil is a measure of the quantity of negatively charged sites on soil surfaces that can retain positively charged ions (cations) by electrostatic forces. The higher the CEC, the higher the negative charge and the more cations that can be held. At Hanford, vadose zone sediments exhibit a CEC that varies strongly with sediment texture and increases with decreasing particle size (Ward et al. 2006). In general, Hanford sediments are principally calcareous, low-exchange capacity sands and sandy loams with CEC values in the range of 1-5 meq/100 g (Routson et al. 1973).

2.8 Specific Surface Area

Soil-specific surface area was measured using a gas sorption analyzer. The tendency of all solid surfaces to attract surrounding gas molecules gives rise to a process called gas sorption. Before performing a surface area analysis, solid surfaces are freed from contaminants such as water and oils using a degassing technique (e.g., placing a sample of the solid in a glass cell and heating it under a vacuum, or a flow of

dry, inert gas). Once clean, the sample is brought to a constant temperature by means of an external bath using a cryogen such as liquid nitrogen. Then, small amounts of a gas are admitted in steps into the evacuated sample chamber. Gas molecules that stick to the surface in a monolayer are said to be adsorbed. Typically, different gasses used for this technique are nitrogen (N_2) for surface areas above 1 m^2/g and krypton for lower surface areas. The mass of the gas adsorbed to the sediment surface is quantified using an infared detector. The strength with which adsorbed molecules interact with the surface determines if the adsorption process is to be considered physical (weak) or chemical (strong) in nature.

3.0 Sediment Characterization

Minerals are natural inorganic compounds with definite physical, chemical, and crystalline properties. They can be classified into primary (chemically unaltered) or secondary (chemically altered) minerals, silicates and non-silicates, crystalline and noncrystalline minerals. Major soil mineral groups include silicates, carbonates, sulfides, oxides and hydroxides, halides, sulfates, carbonates and phosphates.

This section provides an overview of the mineralogical analyses that have been performed in the Hanford Central Plateau, and include sediments associated with Waste Management Areas (WMAs) S-SX, T, A-AX, and B-BX-BY, the Integrated Disposal Facility, and boreholes within the B Complex. Sediment core samples from WMAs U (Brown et al. 2007, TX-TY (Serne et al. 2004a,b), and C (Brown et al. 2006, 2007 are available but have not been characterized in any detail, although some total carbon, inorganic carbon, and particle size distribution data have been collected and reported in the cited borehole reports. No mineralogic characterization has been performed to date on the cores from WMAs U, TX-TY, and C.

3.1 Generalized Summary of Hanford Vadose Sediment Mineralogy

In general, the sand and gravel mineralogy of the Hanford formation, Cold Creek unit, and Ringold Formation is similar because of common geologic provenance. Gravel-sized clasts generally consist of >50% subangular to subrounded basalt rock fragments (DOE/RL 2002). Sand facies generally contain 50% basaltic lithic fragments and 50% granitic fragments, whereas silt is typically dominated by quartz, various feldspars, and micas (biotite and muscovite) (Ginder-Vogel et al. 2005; Tallman et al. 1979; Zachara et al. 2002). The clay fraction of Hanford Site vadose zone sediments is remarkably consistent between different vadose zone samples (Knepp 2002, Zachara et al. 2002) and is dominated by expansible phyllosilicates (smectite), ferroan chlorite (clinochlore), and mica (both biotite and muscovite). Serpentine-group minerals (antigorite and lizardite) have also been reported (Ginder-Vogel et al. 2005).

Although the relative abundances of individual minerals vary widely, the bulk samples (<2-mm size fraction) of these sediments are largely dominated by quartz (SiO_2), plagioclase feldspar [general formula $(Na,Ca)Al(Al,Si)Si_2O_8$], and alkali (potassium) feldspar ($KAlSi_3O_8$) with quartz usually the dominating, and plagioclase more abundant than alkali feldspar. The bulk sediment samples also generally contain minor amounts of mica, chlorite, amphibole, smectite, and/or detrital calcite ($CaCO_3$, calcium carbonate).[1]

Detrital and pedogenic calcite are consistently observed throughout the Hanford formation vadose zone sediments, ranging in concentrations from ~1% to a maximum of 5% and averaging 1.79 mass% (Serne et al., 2004a). Pedogenic calcite exists in the form of discrete, but infrequent, caliche layers (~25 cm in thickness) that formed beneath surfaces that were exposed for extended inter-flood periods during the Pleistocene. Other names used to describe these facies have included “caliche” and “calcrete” (Reidel and Chamness 2007). A calcite-indurated paleosol (calcrete) with 35% to 45% calcite frequently occurs in the lower Cold Creek unit (CCU_c). The concentration of calcium carbonate within the CCU_c varies over a wide range and can be as large as 70 wt%. In sediments at the Hanford Site, the CCU_c is known to react strongly with uranium, binding it and retarding its migration deeper into the subsurface. The Cold Creek unit is immediately below the contact with the Hanford formation (Fig. 3; Serne et al., 2004a).

[1] Mica, chlorite, amphibole, smectite, and apatite are mineral groups that are each characterized by specific structural features and some general ranges in composition. Each group consists of numerous minerals that have these same structural features and specific compositions within the compositional range for that mineral group. Unless the name of a specific mineral within such a mineral group is given, it’s generally not possible to list a specific composition when reporting the presence of a mineral group such as “mica.”

The zeolite laumontite ($CaAl_2Si_4O_{12}$•$4H_2O$) was identified as a minor constituent phase in some of the XRD analyses reported in Lindenmeier et al. (2003) and Serne et al. (2008a, b). Laumontite is known to be naturally present in uncontaminated Hanford formation sediments and therefore is not considered always to be a unique alteration product resulting from reactions where leaked tank wastes are present (Serne et al. 2008a). Although more laumontite may be present where tank liquors have altered the sediments.

Zachara et al. (2007) noted that the vadose zone sediments at the Hanford Site invariably contain a magnetic, iron-rich mineral fraction (probably less than 2 mass%) that contains magnetite ($Fe^{II}Fe_2^{III}O_4$), ilmenite ($FeTiO_3$), Fe(II)/Fe(III) phyllosilicates, and Fe(III) oxides (ferrihydrite [nominally $5Fe_2O_3$•$9H_2O$]); and goethite [α-FeO(OH)]), based on XRD and transmission Mössbauer spectroscopy (e.g., Ginder-Vogel et al. 2005). Zachara et al. (2007) indicated that this potentially reactive iron-bearing mineral fraction has not been well-studied and is expected to show considerable variation both between and within stratigraphic units.

Hanford formation sediments are only modestly weathered because of its youthful age, whereas the Ringold Formation sediments can be significantly weathered and show more hydrous oxide coatings of iron, manganese, and aluminum compared to the young Hanford formation sediments. The Cold Creek unit is expected to show intermediate amounts of weathering based on its age and often shows signs of soil pedogenesis. All Hanford sediments not impacted by Hanford wastes exhibit a soil water pH near neutrality because of high concentrations of dissolved bicarbonate in pore water and the frequent presence of calcite.

3.2 Mineralogy

Although this section is primarily focused on minerals present in the clay-size fractions (<2 μm) of sediments, analyses of larger sized fractions are also presented. References for all analyses are provided in Table 3.1 and Table 3.2 for 200 West and 200 East sediments, respectively. In general, clay-sized sediments are dominated by four primary minerals: illite {general formula $(K,H_3O)(Al,Mg,Fe)_2(Si,Al)_4O_{10}[(OH)_2,H_2O]$}, smectite, chlorite, and kaolinite [$Al_2Si_2O_5(OH)_4$] Quartz, plagioclase feldspar, and micas (biotite, muscovite, and vermiculitized biotite) were identified in all size fractions. Illite has also been identified in clays in lesser amounts, which is particularly noteworthy because it can irreversibly adsorb cesium within the interlayer sites of its crystal structure.

Specific mineralogy for sediments at discrete locations (e.g., boreholes, excavations, and outcrops) is provided in Appendix A through Appendix C.

3.2.1 200 West Sediment Analyses

The TEM/EDS analyses of the clay fractions of sediment samples from the WMA S-SX reported in Serne et al. (2002, 2008d, 2008f) indicate that the compositions of chlorites typically ranged from that of magnesium-rich chamosite [general formula $(FeII,Mg,FeIII)_5Al(Si_3,Al)O_{10}(OH,O)_8$] to iron-rich clinochlore [general formula $(Mg,FeII)_5Al(Si_3,Al)O_{10}(OH,O)_8$]. The TEM/EDS analyses also identified the presence of iron oxide(s), anatase (TiO_2), apatite, and sepiolite [$Mg_4Si_6O_{15}(OH)_2$•$6H_2O$] (Serne et al. 2008d,e,f,b). Some of the samples analyzed by TEM/EDS in Serne et al. (2008f) contained platy particles of weathered muscovite [$KAl_2(Si_3Al)O_{10}(OH)_2$] and, in lesser amounts, weathered biotite [$K(Mg,FeII)_3(Al,FeIII)Si_3O_{10}(OH,F)_2$].

Detailed mineralogical characterization analyses in support of research studies of contaminant reactions with Hanford sediments have also been completed. McKinley et al. (2001a,b, 2004), Zachara et al. (2002), and Liu et al. (2003) investigated cesium adsorption-desorption reactions, and Zachara et al.

(2004) studied chromium speciation and mobility. The S-SX analyses are summarized in Table 3.2. An extensive part of the mineralogical characterization studies described in Table 3.2 is summarized in McKinley et al. (2001b). Key results from the mineralogical studies by McKinley et al. (2001b) and Zachara et al. (2002, 2004) are briefly summarized below. Similar mineralogical information is given in Liu et al. (2003) and McKinley et al. (2004).

Characterization of the sediment samples studied by Zachara et al. (2002, p 193) shows that the mineralogy of the size fractions greater than 2 μm was dominated by quartz with lesser amounts of plagioclase and potassium feldspars, micas, chlorite, vermiculite [$(Mg,Fe^{II},Al)_3(Al,Si)_4O_{10}(OH)_2 \bullet 4H_2O$], and smectite. Anorthite ($CaAl_2Si_2O_8$) was the dominant feldspar mineral. The clay-size fraction (<2 μm) contained smectite, chlorite (clinochlore), and mica. Based on XRD of a mica concentrate hand-picked from the sand fraction (0.5–2.0 mm), Zachara et al. (2002) identified the micas muscovite, biotite, and vermiculitized biotite. Zachara et al. (2002) also observed a cream-colored encrustation on the basal surfaces of biotite and vermiculitized biotite, which they identified as feldspar using XRD. These analyses showed the basal surfaces of some of the biotite to be highly weathered to vermiculite, whereas the internal surfaces of the biotite were unaltered (Zachara et al. 2002). Bright red and dark brown colors of the vermiculite and biotite grains, respectively, determined by optical microscopy were consistent with oxidation of octahedrally-coordinated iron during weathering (Zachara et al. 2002).

The mineralogy determined by McKinley et al. (2001b) on S-SX sediment samples was essentially identical to that described in Zachara et al. (2002). Quartz, plagioclase feldspar, and micas (biotite, muscovite, and vermiculitized biotite) were identified in all size fractions, with kaolinite, quartz, plagioclase, smectite, and micas being the principal minerals in the clay-size fraction (McKinley et al. 2001b). McKinley et al. (2001b, p. 3433) used digital phosphor-plate images to identify the mineral particles in their sediment samples responsible for sorbing ^{137}Cs. Their autoradiograph analyses indicated that the cesium-bearing particles were individual grains of mica or agglomerates of smectite, mica, quartz, and plagioclase.

Table 3.1. Mineralogical Analyses for 200 West Area Sediments

Waste Management Area	Reference	Borehole/Well	Stratigraphic Unit	Method
S-SX	McKinley et al. (2001b)	Borehole 41-09-39		Autoradiography, optical microscopy, XRD
S-SX	Zachara et al. (2002)	SX-108 slant borehole and Borehole 41-09-39		Optical microscopy, XRD
S-SX	Serne et al. (2008d)	299-W22-48 299-W22-50 Four composite samples	Hanford Ringold Cold Creek	XRD, TEM, and EDS
S-SX (near SX-115)	Serne et al. (2002)	Well 299-W23-19	Hanford Cold Creek	XRD, TEM and EDS
S-SX (near SX-109)	Serne et al. (2008f)	Borehole 41-09-39	Hanford	XRD, TEM, and EDS
S-SX (below SX-108)	Serne et al. (2008b)	SX-108 slant borehole	Hanford Cold Creek	XRD, TEM, and EDS
S-SX	Liu et al. (2003)	SX-108 slant borehole and Borehole 41-09-39		SEM, XMP
S-SX	McKinley et al. (2004)	Borehole not specified		EMP, SEM/EDS, TEM, XMP
S-SX	Zachara et al. (2004)	SX-108 slant borehole and Borehole 41-09-39		SEM/EDS, XANES, XRD, SXRF
T (southwest of Tank T-106)	Serne et al. (2004a,b)	Borehole C4105	Hanford Cold Creek Ringold	XRD

EMP is electron microprobe; XANES is X ray adsorption near edge structure spectroscopy; XMP is synchrotron-based X-ray microprobe; SXRF is microscanning X-rayfluorescence.

Mineralogical characterization by Zachara et al. (2004) shows evidence that dissolution and precipitation reactions have occurred in sediment samples from the SX-108 slant borehole as a result of contact with tank liquid wastes. Although the surfaces of mica grains in uncontaminated Hanford sediments show no alteration, the SEM analyses of muscovite and biotite grains in sediment samples from SX-108 slant borehole (samples 3A and 7A) found that they were highly coated with poorly crystalline sodium aluminosilicates. Zachara et al. (2004) noted that, based on the SEM analyses, the degree of alteration of the sediments decreased with depth and distance from the tank.

XANES analyses of chromium-rich sediment samples from the SX-108 slant borehole indicated the presence of both Cr(VI) and Cr(III). Zachara et al. (2004) found that the largest Cr(III) concentration [smallest Cr(VI)] was observed in sample 7A, which had the largest extent of mineral alteration of the samples analyzed by XANES, whereas the highest Cr(VI) concentrations were in the samples deeper in the core, where mineral alteration was minimal. Zachara et al. (2004) also speculated that the most altered sediment samples—3A and 7A—should also contain secondary zeolites that formed from reaction with the liquid tank wastes. Zachara et al. (2004) identified grains of quartz that had sodium aluminosilicate precipitates on their surfaces. Because these surface coatings did not exist on uncontaminated sediments, Zachara et al. (2004) assumed these surface precipitates were zeolites that formed from reaction with the waste liquids.

3.2.2 200 East Sediment Analyses

Specialized mineralogical analyses to determine the geochemical reactions controlling the sorption and speciation of ^{90}Sr was studied in McKinley et al. (2007) in contaminated sediments from borehole 299-E33-46, located near tank B-110. Uranium in contaminated sediment samples from BX 102 borehole 299-

E33-45 have also been analyzed (Catalano et al. 2004; Liu et al. 2004; Wang et al. 2005; Liu et al. 2006; McKinley et al. 2006, Freedman et al. 2002). These analyses are summarized in Table 3.2. These studies focused on establishing the reaction mechanisms controlling the geochemical behavior of specific contaminants in these sediments. In general, the same types and relative amounts of minerals as discussed above for vadose sediments from the SX Tank Farm are present in the vadose zone sediments from the B and BX Tank Farms.

Similar minerals and mineral volumes were identified in S-SX and B-BX vadose sediments. For the contaminated sediments directly below the tanks, the B and BX Tank Farm sediments had less alkaline attack that resulted in predominantly zeolite formation. This may be attributed to two factors: 1) the tank fluids are not as caustic and are less concentrated; and 2) the boreholes are more distant from the tanks themselves than for the studies at the SX Tank Farm.

Table 3.2. Mineralogical Analyses for 200 East Sediments

Waste Management Area	Reference	Borehole/Well	Stratigraphic Units	Method
A-AX (southwest/south of A-AX)	Brown et al. (2005)	299-E25-46 299-E24-19	Hanford formation	XRD, TEM, and EDS
B-BX-BY (BX-102)	Serne et al. (2008c)	Well 299-E33-45	Hanford formation Cold Creek unit	XRD, TEM, and EDS
B-BX-BY (B-110)	Serne et al. (2008a)	Well 299-E33-46	Hanford formation Cold Creek unit	XRD, TEM, and EDS
B-BX-BY (southeast of B Tank Farm)	Lindenmeier et al. (2003)	299-E33-338	Hanford formation Cold Creek unit	XRD, TEM, and EDS
T (southwest of Tank T-106)	Serne et al. (2004a,b)	Borehole C4105	Hanford formation Cold Creek Ringold	XRD
B-BX-BY (BX-102)	Catalano et al. (2004)	Borehole 299-E33-45	EXAFS, µXRD, µSXRF, XAFS, XANES	XRD
B-BX-BY (BX-102)	Liu et al. (2004)	Borehole 299-E33-45	EMP, SEM, XMP	XRD, TEM, and EDS
B-BX-BY (BX-102)	Wang et al. (2005)	Borehole 299-E33-45	TRLFS, XRD	XRD
B-BX-BY (BX-102)	Liu et al. (2006)	Borehole 299-E33-45	NMR-PGSE, SEM, XRD	XRD
B-BX-BY (BX-102)	McKinley et al. (2006)	Borehole 299-E33-45	EMP, SEM/EDS, TEM, XRM	
B-BX-BY (B-110)	McKinley et al. (2007)	Borehole 299-E33-46	SEM/EDS, digital micro-autoradiography	

µSXRF is microscanning X-ray fluorescence; µXRD is X-ray microdiffraction; EXAFS is extended X-ray absorption fine structure spectroscopy; NMR PGSE is nuclear magnetic resonance pulsed field-gradient spin echo; TRLFS is time-resolved spectroscopy laser fluorescence spectroscopy; XAFS is X-ray absorption fine structure spectroscopy.

3.3 Statistical Mineralogical Analysis of Hanford and Ringold Sediments

Xie et al. (2003) used statistical methods (such as principal component analysis, discriminant function analysis, and machine learning methods) to try to classify sediments from the Hanford formation and Ringold Formation using mineralogical and geochemical data. Although the Hanford and Ringold formations comprise the majority of the vadose zone sediments at the Hanford Site, quantitative methods do not exist, and visual examinations are not always conclusive for distinguishing between samples from these formations. The statistical analyses by Xie et al. (2003) were based on analyses of mineralogy and composition by electron microprobe (EMP), optical petrographic polarizing microscopy, and XRF of sediment samples from the 200 West and 200 East Areas of the Hanford Site.

Xie et al. (2003) relied on the stratigraphic unit designations in the source documents used in their analysis, which may not correspond to current nomenclature. Acronyms were used to refer to the three types of data used in their report: EM (electron microscopy), Petro, and XRF, respectively. The EMP analysis data used by Xie et al. (2003) were from Tallman et al. (1979), and the petrographic data were from Bjornstad (1990). The XRF analyses data used by Xie et al. (2003) were from Serne et al. (2002) and unpublished data from B. N. Bjornstad (PNNL). Xie et al. (2003) also noted they did not use mineralogical data determined by XRD (e.g., Serne et al. 2008d,e), because they considered mineral abundances determined by XRD to be semiquantitative, which would make direct comparison of petrographic and XRD data difficult.

Results of the statistical analyses by Xie et al. (2003) show significant differences in the EM, Petro, and XRF variables between the Hanford and Ringold formations. They found that Hanford formation samples contained higher percentages of plagioclase, pyroxenes, sphene ($CaTiSiO_5$), and mica, and lower percentages of calcite and ilmenite ($FeTiO_3$) than sediments designated as Ringold Formation. The reader is referred to Xie et al. (2003) for a detailed presentation of their datasets, statistical methods, and results. Their results also indicated that XRF data and trace element data could be useful in developing classification algorithms to differentiate Hanford formation and Ringold Formation samples over wider geographic areas.

4.0 Summary

Data that provide the technical basis for the distribution of minerals in the Central Plateau region (vadose zone and groundwater) at Hanford have been summarized in this report. In addition to the mineralogy of the Hanford, Cold Creek, and Ringold formations, the data for other related parameters such as particle size distribution, specific surface area, CEC, total carbon, inorganic carbon, organic carbon, and estimates of hydrous oxide content have been provided. These physical and geochemical data can be used as inputs for contaminant transport models to estimate hydraulic conductivity or contaminant sorption used to evaluate risk and identify remedial alternatives. In addition, these data support electrical methods that monitor biogeochemical transformations that may occur for in situ remedy approaches. Knowledge of contaminant sources, contaminant chemistry, and soil interactions are pertinent to determining the nature and extent of contamination, risk assessment, and selection of remedial techniques. These are critical data needed to understand contaminant mobility, bioavailability, and selection of appropriate remedial options. For example, the fate and transport of contaminants in soil depends significantly on the chemical form and speciation. Once in the soil, contaminants can be adsorbed by initial fast reactions (minutes, hours), followed by slow adsorption reactions (days, years) and are, therefore, redistributed into different chemical forms with varying bioavailability, mobility, and toxicity. This distribution is controlled by soil reactions, such as (i) mineral precipitation and dissolution; (ii) ion exchange, adsorption, and desorption; (iii) aqueous complexation; and (iv) biological immobilization.

5.0 Quality Assurance

This work was performed in accordance with the Pacific Northwest National Laboratory (PNNL) Nuclear Quality Assurance Program (NQAP). The NQAP complies with the United States Department of Energy Order 414.1D, Quality Assurance. The NQAP uses NQA-1-2012, Quality Assurance Requirements for Nuclear Facility Application as its consensus standard and NQA-1-2012 Subpart 4.2.1 as the basis for its graded approach to quality.

This report is intended to inform investigators of the existing data available for RI/FS tasks and provide a centralized location for the data needed to support site evaluations. The data have not been reviewed for technical accuracy per NQA-1 guidelines but have been reproduced from the original reports and are provided here for information only (FIO).

6.0 References

Bjornstad, B. 1990. Geohydrology of the 218-W-5 burial ground, 200-West area, Hanford site. PNL-7336. Pacific Northwest National Laboratory. Richland, WA.

Brown CF, RJ Serne, HT Schaef, BA Williams, MM Valenta, VL LeGore, MJ Lindberg, KN Geiszler, SR Baum, IV Kutnyakov, TS Vickerman, and RE Clayton. 2005. *Investigation of Accelerated Casing Corrosion in Two Wells at Waste Management Area A-AX*. PNNL-15141, Pacific Northwest National Laboratory, Richland, Washington.

Brown, C., R. Serne, B. Bjornstad, D. Horton, D. Lanigan, R. Clayton, M. Valenta, T. Vickerman, I. Kutnyakov, K. Gieszler, S. Baum, K. Parker, M. Lindberg. 2006. Characterization of vadose zone sediments below the C tank farm borehole C4297 and RCRA borehole 299-E27-22. PNNL-15503, Pacific Northwest National Laboratory, Richland, WA.

Brown, C., M. Valenta, R. Serne, B. Bjornstad, D. Lanigan, C. Iovin, R. Clayton, K. Geiszler, E. Clayton, I. Kutnyakov, S. Baum, M. Lindberg, R. Orr. 2007. Characterization of direct push vadose zone sediments from the 241-U single-shell tank farm. PNNL-17163. Pacific Northwest National Laboratory, Richland, WA.

Catalano JG, SM Heald, JM Zachara, and GE Brown Jr. 2004. "Spectroscopic and Diffraction Study of Uranium Speciation in Contaminated Vadose Zone Sediments from the Hanford Site, Washington State." *Environmental Science & Technology* 38(10):2822−2828.

Freedman V, M Williams, C Cole, M White, and M Bergeron. 2002. *Field Investigation Report for Waste Management Area B-BX-BY*. RPP-10098, prepared for the U.S. Department of Energy, Office of River Protection, Pacific Northwest National Laboratory, PNNL-13949, Richland, Washington.

DOE/RL (U.S. Department of Energy Richland Operations Office). 2002. *Standardized Stratigraphic Nomenclature for Post-Ringold Formation Sediments within the Central Pasco Basin*. DOE/RL-2002-39, Rev. 0, Richland, Washington.

Ginder-Vogel M, T Borch, MA Mayes, PM Jardine, and S Fendorf. 2005. "Chromate Reduction and Retention Processes within Arid Subsurface Environments." *Environmental Science & Technology* 39(20):7833−7839.

Knepp, A. 2002. Field investigation report for waste management area S-SX Volume 1 and 2, CH2M Hill Hanford Group, Richland WA, 1256p.

Lindenmeier CW, RJ Serne, BN Bjornstad, GW Gee, HT Schaef, DC Lanigan, MJ Lindberg, RE Clayton, VL LeGore, IV Kutnyakov, SR Baum, KN Geiszler, CF Brown, MM Valenta, TS Vickerman, and LJ Royack. 2003. *Characterization of Vadose Zone Sediment: RCRA Borehole 299-E33-338 Located Near the B-BX-BY Waste Management Area*. PNNL-14121, Pacific Northwest National Laboratory, Richland, Washington.

Liu CX, JM Zachara, SC Smith, JP McKinley, and CC Ainsworth. 2003. "Desorption Kinetics of Radiocesium from Subsurface Sediments at Hanford Site, USA." *Geochimica et Cosmochimica Acta* 67(16):2893−2912.

Liu CX, JM Zachara, and SC Smith. 2004. “A Cation Exchange Model to Describe Cs+ Sorption at High Ionic Strength in Subsurface Sediments at Hanford Site, USA.” *Journal of Contamination Hydrology* 68(3-4):217−238.

Liu CX, JM Zachara, W Yantasee, PD Majors, and JP McKinley. 2006. “Microscopic Reactive Diffusion of Uranium in the Contaminated Sediments at Hanford, United States.” *Water Resources Research* 42(12): Art. No. W12420.

McKinley JP, CJ Zeissler, JM Zachara, RJ Serne, RM Lindstrom, HT Schaef, and RD Orr. 2001a. “Distribution and Retention of Cs-137 in Sediments at the Hanford Site, Washington.” *Environmental Science & Technology* 35(17):3433-3441.

McKinley JP, JM Zachara PL Gassman, CC Ainsworth, B Arey, S McKinley, HT Schaef, SC Smith, J Kimberling, DL Bish, SJ Chipera, and P Snow. 2001b. “S-SX Site Mineralogy.” In *Appendix D: Digest of S&T Program Evaluations*, RPP-7884, Rev. 0, AJ Knepp (ed.), pp. D10-D35. CH2M Hill Hanford Group Inc., Richland, Washington.

McKinley JP, JM Zachara, SM Heald, A Dohnalkova, MG Newville, and SR Sutton. 2004. “Microscale Distribution of Cesium Sorbed to Biotite and Muscovite.” *Environmental Science & Technology* 38(4):1017−1023.

McKinley JP, JM Zachara, CX Liu, SC Heald, BI Prenitzer, and BW Kempshall. 2006. “Microscale Controls on the Fate of Contaminant Uranium in the Vadose Zone, Hanford Site, Washington.” *Geochimica et Cosmochimica Acta* 70(8):1873−1887.

McKinley JP, JM Zachara, SC Smith, and C Liu. 2007. “Cation Exchange Reactions Controlling Desorption of 90Sr2+ from Coarse-Grained Contaminated Sediments from the Hanford Formation, Washington.” *Geochimica et Cosmochimica Acta* 71(2):305−325.

Reidel SP and MA Chamness. 2007. *Geology Data Package for the Single-Shell Tank Waste Management Areas at the Hanford Site*. PNNL-15955, Pacific Northwest National Laboratory, Richland, Washington.

Routson, R. 1973. A review of studies of soil-waste relationships on the Hanford reservation from 1944 to 1967, BNWL-1464, Battelle Pacific Northwest Laboratories, Richland, WA

Serne RJ, BN Bjornstad, GW Gee, HT Schaef, DC Lanigan, RG McCain, CW Lindenmeier, RD Orr, VL LeGore, RE Clayton, JW Lindberg, IV Kutnyakov, SR Baum, KN Geiszler, MM Valenta, TS Vickerman, and LJ Royack. 2008a. *Characterization of Vadose Zone Sediment: Borehole 299-E33-46 Near B-110 in the B-BX-BY Waste Management Area*. PNNL-14119, Rev. 1, Pacific Northwest National Laboratory, Richland, Washington.

Serne RJ, GV Last, HT Schaef, DC Lanigan, CW Lindenmeier, CC Ainsworth, RE Clayton, VL LeGore, MJ O’Hara, CF Brown, RD Orr, IV Kutnyakov, TC Wilson, KB Wagnon, BA Williams, and DB Burke. 2008b. *Characterization of Vadose Zone Sediment: Slant Borehole SX-108 in the S-SX Waste Management Area*. PNNL-13757-4, Rev.1, Pacific Northwest National Laboratory, Richland, Washington.

Serne RJ, GV Last, GW Gee, HT Schaef, DC Lanigan, CW Lindenmeier, MJ Lindberg, RE Clayton, VL LeGore, RD Orr, IV Kutnyakov, SR Baum, KN Geiszler, CF Brown, MM Valenta, and TS Vickerman. 2008c. *Characterization of Vadose Zone Sediment: Borehole 299-E33-45 Near BX-102 in the B-BX-BY*

Waste Management Area. PNNL-14083, Rev. 1, Pacific Northwest National Laboratory, Richland, Washington.

Serne RJ, BN Bjornstad, HT Schaef, BA Williams, DC Lanigan, DG Horton, RE Clayton, AV Mitroshkov, VL LeGore, MJ O'Hara, CF Brown, KE Parker, IV Kutnyakov, JN Serne, GV Last, SC Smith, CW Lindenmeier, JM Zachara, and DS Burke. 2008d. *Characterization of Vadose Zone Sediment: Uncontaminated RCRA Borehole Core Samples and Composite Samples*. PNNL-13757-1, Rev. 1, Pacific Northwest National Laboratory, Richland, Washington.

Serne RJ, HT Schaef, BN Bjornstad, DC Lanigan, GW Gee, CW Lindenmeier, RE Clayton, VL LeGore, RD Orr, MJ O'Hara, CF Brown, GV Last, IV Kutnyakov, DS Burke, TC Wilson, and BA Williams. 2008e. *Characterization of Vadose Zone Sediment: Borehole 299-W23-19 [SX-115] in the S-SX Waste Management Area*. PNNL-13757-2, Rev. 1, Pacific Northwest National Laboratory Richland, Washington.

Serne RJ, GV Last, GW Gee, HT Schaef, DC Lanigan, CW Lindenmeier, RE Clayton, VL LeGore, RD Orr, MJ O'Hara, CF Brown, DS Burke, AT Owen, IV Kutnyakov, TC Wilson, KB Wagnon, BA Williams, and DS Burke. 2008f. *Characterization of Vadose Zone Sediment: Borehole 41-09-39 in the S-SX Waste Management Area*. PNNL-13757-3, Rev. 1, Pacific Northwest National Laboratory, Richland, Washington.

Serne RJ, BN Bjornstad, DG Horton, DC Lanigan, CW Lindenmeier, MJ Lindberg, RE Clayton, VL LeGore, RD Orr, IV Kutnyakov, SR Baum, KN Geiszler, MM Valenta, and TS Vickerman. 2004a. *Characterization of Vadose Zone Sediments Below the TX Tank Farm: Probe Holes C3830, C3831, C3832 and 299-W10-27*. PNNL-14594, Rev. 1, Pacific Northwest National Laboratory, Richland, Washington.

Serne RJ, BN Bjornstad, DG Horton, DC Lanigan, CW Lindenmeier, MJ Lindberg, RE Clayton, VL LeGore, KN Geiszler, SR Baum, MM Valenta, IV Kutnyakov, TS Vickerman, RD Orr, and CF Brown. 2004b. *Characterization of Vadose Zone Sediments Below the T Tank Farm: Boreholes C4104, C4105, 299-W10-196 and RCRA Borehole 299-W11-39*. PNNL-14849, Rev. 1, Pacific Northwest National Laboratory, Richland, Washington.

Tallman, A M, Fecht, K R, Marratt, M C, and Last, G V. 1979. *Geology of the Separation Areas, Hanford site, South-Central Washington*. United States, Rockwell International Corp. RHO-ST-23. Richland, WA.

Wang ZM, JM Zachara, PL Gassman, CX Liu, O Qafoku, W Yantasee, and JG Catalan. 2005. "Fluorescence Spectroscopy of U(VI)-Silicates and U(VI)-Contaminated Hanford Sediment." *Geochimica et Cosmochimica Acta* 69(6):1391−1403.

Ward, A. 2006. Vadose zone transport field study summary report, Pacific Northwest National Laboratory, PNNL-15443, Richland WA

Xie, Y., CJ Murray, GR Last, and R. Mackley. 2003. Mineralogical and bulk-rock geochemical signatures of Ringold and Hanford formation sediments, Pacific Northwest National Laboraties, PNNL-14202.

Zachara JM, SC Smith, CX Liu, JP McKinley, RJ Serne, and PL Gassman. 2002. "Sorption of Cs+ to Micaceous Subsurface Sediments from the Hanford Site, USA." *Geochimica et Cosmochimica Acta* 66(2):193−211.

Zachara JM, CC Ainsworth, GE Brown Jr., JG Catalano, JP McKinley, O Qafoku, SC Smith, JE Szecsody, SJ Traina, and JA Warner. 2004. “Chromium Speciation and Mobility in a High Level Nuclear Waste Vadose Zone Plume.” G*eochimica et Cosmochimica Acta* 68(1):13−30.

Zachara JM, RJ Serne, MD Freshley, FM Mann, FJ Anderson, MI Wood, TE Jones, and DA Myers. 2007. “Geochemical Processes Controlling Migration of High Level Wastes in Hanford's Vadose Zone.” *Vadose Zone Journal* 6(4):985−1003.

Appendix A – Characterization Data for 200 East Area Sediments

This appendix contains detailed characterization data on vadose zone sediments from four boreholes drilled in the 200 East Area and two near surface excavation sites. Full details are found in the technical reports cited in the text. Since the goal of this report is intended to inform investigators of the existing data available for RI/FS tasks and provide a centralized location to support site evaluations, the data *have not* been reviewed for technical accuracy per NQA-1 guidelines, but reproduced from original reports and provided *for information only* (FIO).

A.1 Borehole 299-E1-21

Borehole 299-E17-21 is located in the southwest corner of the proposed Integrated Disposal Facility (IDF) site in the 200 East Area. Reidel and Reynolds (1998) and Reidel and Horton (1999) contain analyses of the geological data; Meyer and Serne (1999) report on the physical and chemical properties of the sediment samples from borehole 299-E17-2.1 The pH, cation exchange capacity (CEC), and distribution coefficients for selected radionuclides were determined by Kaplan et al. (1998).

The 299-E17-21 borehole was drilled in the spring of 1998 (Reidel and Reynolds, 1998). A total of 45 cores were collected in liners. Thirty of the 45 liners had an 8.26-cm (3.25-in.) internal diameter and came from depths between 45 and 175 ft. The remaining fifteen liners had a 9.53-cm (3.75-in.) internal diameter and came from depths between 175 and 242 ft. All the sediment from the depth interval from 0 to 45 ft went to the tracer task for Cl-36 tracer-specific analyses to determine long-term recharge. Undisturbed cores from this interval were not necessary for hydraulic property measurements because these sediments will not exist in an undisturbed state once the disposal facility is built. No vadose zone cores were collected below 242 ft because this zone was open framework gravel (i.e., gravel that supports itself with little to no finer grained material) and could not be sampled with the method used.

A.1.1 Particle Size Characterization

Twenty 299-E17-21 borehole cores were analyzed for hydraulic and physical properties and selected on the basis of providing somewhat evenly spaced coverage of the sampled vadose zone. Table A.1 lists the sample numbers, depths, and diameters.

Table A.1. Borehole 299-E17-21 Liner Samples Analyzed for Hydrologic Properties. Data are FIO. (Kaplan et al. 1998)

Sample ID	Total Depth Interval (ft)	Internal Diameter (in.)	Depth Interval of Intact Core (ft)
B8500-07A	45.9 to 47.9	3.25	46.3 to 46.8
B8500-10A	57.8 to 59.8	3.25	58.0 to 58.5
B8500-12A	69.4 to 70.95	3.25	69.8 to 70.3
B8500-14A	80.3 to 82.8	3.25	80.8 to 81.3
B8500-15A	90.5 to 93.0	3.25	90.8 to 91.3
B8500-16A	100.5 to 103.0	3.25	102.0 to 102.5
B8500-17A	109.8 to 112.2	3.25	111.3 to 111.8
B8500-19A	121.0 to 123.5	3.25	122.6 to 123.1
B8500-20A	129.7 to 132.0	3.25	131.1 to 131.6
B8500-21A	141.5 to 144.0	3.25	141.8 to 142.3
B8500-22A	151.9 to 154.4	3.25	153.7 to 154.2
B8500-23A	160.4 to 162.9	3.25	162.1 to 162.6
B8500-24A	180.7 to 182.7	3.75	181.9 to 182.4
B8500-25A	189.7 to 191.7	3.75	190.9 to 191.4
B8500-27A	199.3 to 201.3	3.75	200.5 to 200.9
B8500-29A	209.4 to 211.4	3.75	210.6 to 211.1
B8500-31A	219.6 to 221.6	3.75	220.9 to 221.3
B8500-32A	226.1 to 228.1	3.75	227.4 to 227.9
B8500-34A	236.1 to 238.1	3.75	237.2 to 237.7
B8500-35A	239.5 to 241.5	3.75	240.7 to 241.2

Two types of subsamples were removed from each liner. One subsample was an intact portion of the liner that retained its undisturbed nature. This intact core was used to determine unsaturated conductivity, bulk density, and porosity. The depth intervals of these intact cores are listed in Table A.1. A second subsample was taken from a 4-to-5-in. portion of the liner next to the intact core. This loose material was used to determine particle size distribution, particle density, initial water content, and water retention using pressure plates and vapor adsorption. These samples were also used to determine distribution coefficients.

Table A.2 shows the results for the particle distribution measurements. In all but two samples, the gravel content was less than 2%. In contrast, samples 34A and 35A had 13% and 25% gravel, respectively. These were the deepest samples that were analyzed (between 236 and 242 ft). This depth range corresponds to the lower gravel sequence of the Hanford formation.

Table A.2. Particle Size Distribution of Material Adjacent to the 299-E17-21 Cores. Data are FIO. (Kaplan et al. 1998)

Sample 7A		Sample 10A		Sample 12A		Sample 14A	
Particle Diameter (µm)	% Less Than Diameter	Particle Diameter (µm)	% Less Than Diameter	Particle Diameter (µm)	% Less Than Diameter	Particle Diameter (µm)	% Less Than Diameter
2000	99.8	2000	100.0	2000	99.3	2000	99.8
1000	99.3	1000	95.6	1000	93.9	1000	96.5
500	94.7	500	52.3	500	68.6	500	76.5
250	74.2	250	33.8	250	36.1	250	34.1
106	41.5	106	24.1	106	17.3	106	15.2
75	30.7	75	19.8	75	13.8	75	12.2
53	24.3	53	14.4	53	11.5	53	10.4
52.0	23.4	53.4	13.7	53.2	11.4	53.7	11.1
30.4	18.0	31.1	10.0	30.9	9.3	31.1	9.1
16.9	12.7	17.1	7.2	17.0	8.1	17.1	6.6
9.8	12.1	9.9	6.5	9.8	8.1	9.9	6.3
6.9	9.8	7.0	5.5	6.9	7.0	7.0	6.3
5.7	8.9	5.7	5.2	5.7	5.8	5.7	5.2
4.9	6.8	5.0	5.0	4.9	5.1	5.0	5.0
1.4	5.2	1.4	2.7	1.4	4.4	1.4	4.5
Sample 15A		Sample 16A		Sample 17A		Sample 19A	
Particle Diameter (µm)	% Less Than Diameter	Particle Diameter (µm)	% Less Than Diameter	Particle Diameter (µm)	% Less Than Diameter	Particle Diameter (µm)	% Less Than Diameter
2000	99.5	2000	98.5	2000	99.7	2000	100.0
1000	90.7	1000	87.5	1000	97.3	1000	99.1
500	58.6	500	56.7	500	87.9	500	95.8
250	29.7	250	29.3	250	60.8	250	73.6
106	17.9	106	18.0	106	33.5	106	33.1
75	14.9	75	15.4	75	27.0	75	21.4
53	13.0	53	13.3	53	22.0	53	15.4
53.4	12.4	53.4	15.9	52.4	19.1	52.6	15.1
31.0	10.0	31.1	12.3	30.7	13.8	30.8	10.2
17.1	7.2	17.2	9.6	16.9	11.3	16.9	8.3
9.9	6.0	10.0	7.2	9.8	8.8	9.8	6.2
7.0	4.8	7.1	6.2	7.0	7.4	7.0	4.9
5.7	4.8	5.8	6.5	5.7	6.4	5.7	4.5
5.0	4.5	5.0	5.3	5.0	5.5	4.9	4.5
1.4	4.8	1.4	2.9	1.4	5.1	1.4	3.2

Table A.2 (cont.)

Sample 20A		Sample 21A		Sample 22A		Sample 23A	
Particle Diameter (µm)	% Less Than Diameter	Particle Diameter (µm)	% Less Than Diameter	Particle Diameter (µm)	% Less Than Diameter	Particle Diameter (µm)	% Less Than Diameter
2000	99.8	2000	99.6	2000	98.4	2000	100.0
1000	98.3	1000	96.6	1000	88.2	1000	99.9
500	87.1	500	80.7	500	46.5	500	98.2
250	54.2	250	44.5	250	19.3	250	75.5
106	25.3	106	19.5	106	10.6	106	35.6
75	19.0	75	14.7	75	8.7	75	28.1
53	14.8	53	11.6	53	7.3	53	23.5
53.1	14.0	53.4	11.2	54.2	10.5	53.0	23.2
31.0	10.2	30.9	10.8	31.3	9.2	31.0	18.2
17.1	7.6	17.1	7.1	17.3	5.9	17.1	13.4
9.9	6.4	9.9	6.0	10.0	3.6	9.9	11.5
7.0	4.7	7.0	4.3	7.1	3.3	7.1	8.9
5.7	4.0	5.7	3.0	5.8	3.6	5.8	8.4
5.0	4.5	5.0	3.2	5.0	3.3	5.0	8.4
1.4	4.3	1.4	4.1	1.4	1.6	1.4	3.6
Sample 24A		Sample 25A		Sample 27A		Sample 29A	
Particle Diameter (µm)	% Less Than Diameter	Particle Diameter (µm)	% Less Than Diameter	Particle Diameter (µm)	% Less Than Diameter	Particle Diameter (µm)	% Less Than Diameter
2000	99.8	2000	99.7	2000	98.3	2000	98.7
1000	95.8	1000	96.5	1000	89.3	1000	91.5
500	75.0	500	79.5	500	58.9	500	62.2
250	37.3	250	28.6	250	18.9	250	14.6
106	17.0	106	10.1	106	8.3	106	-1.8
75	13.4	75	7.5	75	6.6	75	-4.3
53	11.0	53	5.9	53	5.5	53	-5.9
54.2	13.2	54.2	7.8	54.1	8.4	54.1	9.9
31.5	9.7	31.4	6.4	31.4	6.4	31.4	8.1
17.3	8.5	17.2	5.4	17.2	5.7	17.3	4.9
10.0	7.9	10.0	4.2	10.0	4.4	10.0	4.2
7.1	8.2	7.1	4.7	7.1	4.7	7.1	4.2
5.8	7.3	5.8	4.7	5.8	4.9	5.8	4.4
5.0	7.3	5.0	4.0	5.0	4.9	5.0	3.5
1.4	2.9	1.4	2.6	1.4	3.7	1.4	2.7

Table A.2 (cont.)

Sample 31A		Sample 32A		Sample 34A		Sample 35A	
Particle Diameter (μm)	% Less Than Diameter	Particle Diameter (μm)	% Less Than Diameter	Particle Diameter (μm)	% Less Than Diameter	Particle Diameter (μm)	% Less Than Diameter
2000	99.8	2000	98.2	2000	87.0	2000	75.7
1000	99.4	1000	86.3	1000	54.4	1000	42.8
500	98.4	500	45.4	500	23.1	500	18.8
250	96.4	250	13.7	250	10.1	250	9.8
106	72.9	106	5.5	106	4.6	106	5.5
75	46.9	75	4.1	75	3.5	75	4.5
53	28.2	53	3.2	53	2.9	53	3.8
51.7	29.2	54.3	7.6	53.6	5.9	53.2	8.5
30.8	15.8	31.5	5.9	31.1	4.5	30.8	6.7
17.0	10.8	17.3	4.8	17.0	4.5	16.9	5.7
9.9	8.3	10.0	3.8	9.8	4.1	9.8	5.0
7.0	7.2	7.1	3.8	7.0	2.7	6.9	4.5
5.7	7.0	5.8	3.8	5.7	2.3	5.7	4.7
5.0	6.2	5.0	3.3	4.9	2.5	4.9	4.5
1.4	5.2	1.4	2.5	1.4	1.8	1.4	2.0

A.1.2 Mineralogy

A total of eight representative core samples from the Hanford formation were selected for mineralogical analysis (see Table A.3). These were three samples from Layer 1 (24A, 31A, and 35A), three samples from Layer 2 (12A, 14A, and 16A), and two samples (7A and 10A) from Layer 3. The particle size descriptions of these core samples, as provided by Reidel and Horton (1999), are listed in Table A.2. The data show that these samples consisted mainly of sand-size material derived from roughly equal proportions of basaltic and felsic parent materials. Many of the samples contained calcium carbonate as coatings, discrete particles, and cementitious material.

Table A.3. Description of Select Core Sample from Borehole 299-E17-2. Data are FIO. (Horton et al., 2003)

Core Number	Core Interval (ft)	Description
7A	45.9 – 47.9	Medium to fine-grained sand with minor silts; sparse pebbles up to 1 inch; 50% basalt, 50% felsic. 45.9 $CaCO_3$ cementing sand into poorly consolidated nodules.
10A	57.8 – 59.8	57.8 – 58.1 Medium- to coarse-grained sand with some $CaCO_3$ 58.1 – 58.5 Cemented soil zone; fine- to medium-grained sand 58.5 – 59.8 Medium-grained sand
14A	80.3 – 82.8	Compacted medium- to fine-grained sand; some silt; 50% basalt, 50% felsic; minor $CaCO_3$ probably as grain coatings.
16A	100.5 – 103.0	Medium-grained sand; some $CaCO_3$ coating grains.
20A	129.7 – 132.2	Fine- to medium-grained sand, some silt; less than 50% basalt; some $CaCO_3$ as discrete particles and grain coatings.
24A	180.7 – 182.7	Fine- to medium-grained sand; uniform grain size; 50% basalt, 50% felsic; no bedding; well compacted, minor $CaCO_3$ cement.
31A	219.6 – 221.6	Fine-grained sand compacted by not cemented; faint bedding. 219.0 Pebbles of basalt and andesite; rounded.
35A	239.5 – 241.5	239.5 – 240.0 Granular to pebbly gravel (1/8 inch), mainly basalt; no sand matrix, open framework. 240.0 – 240.4 Grading into coarser gravel (1/4 to 1/2 inch); no sand matrix, open framework.

	240.4 – 240.9 Coarse gravel with sand matrix; gravel up to 1 inch in diameter; coarse-grained sand; 50% basalt, 50% felsic.

The particle size analysis of the eight cores used for mineralogy measurements indicated that the sand content of these soils ranged from about 78% to 98%, the silt content varied from about 1% to 10%, and the clay fraction constituted about 0.6% to 7% (Table A.4). All the sediment samples were classified as sand, except for 10A and 14A, which were classified as sandy loam.

Table A.4. Particle Size Distribution for Select Sediment Borehole 299-E17-21 Samples. Data are FIO. (Horton et al., 2003)

Sample #	Sand > 75 μm	Silt 75 – 2 μm	Clay < 2 μm
7A	92.1	5.5	2.4
10A	82.1	14.6	3.3
14A	79.4	13.6	7.0
16A	94.7	3.8	1.4
20A	90.0	8.8	1.2
24A	91.3	6.1	2.6
31A	88.4	10.0	1.5
35A	98.3	1.1	0.6

The mineralogical compositions of the sand, silt, and clay fractions of the sediments are tabulated (Table A.5 through Table A.9). About 5% wt% of corundum was detected in all sand samples, which was contamination resulting from grinding the soil in a corundum containing mortar and pestle. The semi-quantitative mineral contents of sand fractions, therefore, were normalized to eliminate the corundum content.

The dominant minerals in the sand fractions of all samples were quartz (~66% to 82% by mass) and feldspars (~15% to 31%) (Table A.5). These minerals (quartz, and anorthite and orthoclase, both feldspars) constituted approximately 92% to 99% of the total mass of the sediment samples. Trace quantities of muscovite mica, chamosite (a type of chlorite), and ferrotschermakite (an amphibole mineral) were also detected in the sand fractions.

The silt fractions of these samples were also dominated by quartz (~61% to 76%) and feldspars (~19% to 44%) (Table A.6). Relative to the sand fractions, the silt fractions contained higher amounts of muscovite and chamosite (~1% to 5%), and ferrotschermakite (1% to 10%). Illitic mica was the dominant mineral (~42% to 60% by mass) in the clay fractions of all the sediment samples (Table A.7). About 14% to 17% chlorite and about 21% to 28% kaolinite were also found in clay fractions. Minor amounts (3% to 12%) of smectite (a high-surface, high-CEC mineral) were also detected in the clay fractions of all samples.

Overall, quartz and feldspars dominated the sand fractions, whereas the clay fractions were dominated by illitic mica and chlorite. These size-dependent mineral distributions are typical of primary (quartz and feldspars) and secondary (illite, chlorite, kaolinite, and smectite) mineral occurrence in soils undergoing chemical weathering. The mineralogy of these sediments was typical of published mineralogy of other Hanford formation sediments (Xie et al., 2003). Based on the mineralogy data (Table A.5 through Table A.7) and the mass distribution of particles in each size fraction (Table A.4), the mineral distribution on the bulk soil basis were computed (Table A.8 and Table A.9). As expected, in all samples (predominantly sandy in texture), the quartz and feldspars that dominate in the sand and silt also dominate the mineralogy of bulk soils (~91% to 95%). All other minerals occur in minor to trace concentrations in these soils.

Although the mineralogy of these soils is dominated by quartz and feldspar minerals, other minerals such as illite, chlorite, smectite, and kaolinite that have characteristics such as high surface areas, ionizable exchange sites, and specific adsorption interlayer sites significantly influence bulk soil chemical properties such as CEC. Therefore, calculations were performed to assess the contribution of each mineral to the overall CEC of whole soil. The results (Table A.10) show that although the minerals mica, chlorite, smectite, and kaolinite together constitute only about 5% to 9% of the total soil mass, they account for about 40% to 60% of the total exchange capacity of the whole soils. Only trace amounts (<0.6%) of smectite were detected in these soils; however, because this mineral has a very high surface area, it accounts for about 4% to 17% of the CEC of the whole soils. Also, it is well-established that minerals such as illitic mica in Hanford sediments specifically adsorb radionuclides such as ^{137}Cs (Kaplan et al. 1998). Therefore, although mica constitutes only 3% to 5% of the soil mass, it could significantly affect the specific adsorption of alkali cations such as Cs and K.

Also, the calculated CEC of the soils agreed reasonably well with the measured CEC values except in the case of samples 24A, 31A, and 35A. The measured CEC values for these samples were about twice as high as the calculated values. Because the mineralogy of these sample was not significantly different from the other core samples, the anomalously high measured CEC values were attributed to the presence of trace amounts of carbonates in these sediments.

Table A.5. Semi-quantitative Estimates (wt%) of Minerals Identified in Sand Fractions of Select Sediment Samples from Borehole 299-E17-21. Data are FIO. (Horton et al., 2003)

Mineral Group	Mineral Species	Typical Chemical Composition	Sample #							
			7A	10A	14A	16A	20A	24A	31A	35A
Quartz	Quartz	SiO_2	82	74	66	76	76	66	74	71
Feldspar	Anorthite	$(Ca, Na)(Al,Si)_2Si_2O_8$	10	20	30	20	20	31	21	25
Feldspar	Orthoclase	$KalSi_3O_8$	5	5	1	1	1	1	1	1
Mica	Muscovite	$(K, Na)(Al, Mg, Fe)_2(Si_3Al_{0.9}O_{10}(OH)_2$	1	1	1	1	1	1	1	1
Chlorite		$(Fe, Al, Mg, Mn)_6(Si, Al)_4O_{10}(OH)_8$	1	1	1	1	1	1	1	1
Amphibole		$Ca_2Fe_3Al_2(Si_6Al_2)O_{22})OH)_2$	--	--	1	1	1	--	1	1

Table A.6. Semi-quantitative Estimates (wt%) of Minerals Identified in Silt Fractions of Select Sediment Samples from Borehole 299-E17-21. Data are FIO. (Horton et al., 2003)

Mineral Group	Mineral Species	Typical Chemical Composition	Sample #							
			7A	10A	14A	16A	20A	24A	31A	35A
Quartz	Quartz	SiO_2	65	71	49	61	64	62	73	76
Feldspar	Anorthite	$(Ca, Na)(Al,Si)_2Si_2O_8$	20	14	39	31	20	19	19	20
Feldspar	Orthoclase	$KalSi_3O_8$	5	5	5	1	1	5	5	1
Mica	Muscovite	$(K, Na)(Al, Mg, Fe)_2(Si_3Al_{0.9}O_{10}(OH)_2$	5	5	5	5	1	5	1	1
Chlorite		$(Fe, Al, Mg, Mn)_6(Si, Al)_4O_{10}(OH)_8$	5	5	1	1	5	5	1	1
Amphibole		$Ca_2Fe_3Al_2(Si_6Al_2)O_{22})(OH)_2$	--	--	1	1	10	5	1	1

Table A.7. Semi-quantitative Estimates (wt%) of Minerals Identified in Clay Fractions of Select Sediment Samples from Borehole 299-E17-21. Data are FIO. (Horton et al., 2003)

Mineral Group	Mineral Species	Typical Chemical Composition	Sample #							
			7A	10A	14A	16A	20A	24A	31A	35A
Smectite	--	$(Ca, Mg, Na, K)_{0.66}(Si, Al)_8(Al, Fe, Mg)_4O_{22}(OH)_4$	8	5	4	3	8	8	12	8
Mica	Illite	$K_2(Al, Si, Mg, Fe)_8Al_4O_{20}(OH)_4$	56	60	60	59	55	51	44	42
Kaolinite	Kaolinite	$Al_4Si_4O_{10}(OH)_8$	22	21	22	21	22	26	28	25
Chlorite	--	$(Al, Mg, Fe, Ni, Mn)_{12}(Si_6Al_2)O_{20}(OH)_{16}$	14	14	14	17	15	15	15	25

Table A.8. Calculated Mineral Distribution in Each Fraction (on Whole Soil Basis (wt%)) in Select Sediment Samples from Borehole 299-E17-21. Data are FIO. (Horton et al., 2003)

Mineral Group	7A			10A			14A			16A			20A			24A			31A			35A		
	Sand	Silt	Clay	Sand	Silt	Clay	Sand	Silt	Clay	Sand	Silt	Clay	Sand	Silt	Clay	Sand	Silt	Clay	Sand	Silt	Clay	Sand	Silt	Clay
Quartz	62	12	--	63	8	--	59	3	--	66	6	--	65	6	--	59	5	--	53	17	--	68	1	--
Feldspar	12	5	--	21	3	--	28	2	--	19	3	--	18	2	--	28	5	--	16	5	--	25	--	--
Mica	1	1	3	1	Tr	2	1	Tr	3	1	Tr	2	1	Tr	2	1	Tr	2	1	Tr	2	1	--	1
Chlorite	1	1	1	1	1	Tr	1	Tr	1	1	Tr	Tr	1	1	1	1	Tr	1	1	Tr	1	1	--	1
Amphibole	--	--	--	--	--	--	1	Tr	--	1	Tr	--	1	1	--	--	Tr	--	1	Tr	--	1	--	--
Smectite	--	--	Tr	--	--	Tr	--	--	Tr	--	--	Tr	--	--	Tr	--	--	Tr	--	--	Tr	--	--	Tr
Kaolinite	--	--	1	--	--	1	--	--	1	--	--	1	--	--	1	--	--	1	--	--	2	--	--	1

Table A.9. Calculated Mineral Distribution (wt%) in Bulk (<2 mm) Sediment Samples from Borehole 299-E17-21. Data are FIO. (Horton et al., 2003)

Mineral Group	7A	10A	14A	16A	20A	24A	31A	35A
	wt%							
Quartz	74	71	62	72	71	64	70	69
Feldspars	17	23	30	22	20	30	22	25
Mica	4	3	4	3	3	2	3	2
Chlorite	3	2	2	1	3	2	2	1
Amphibole	--	--	1	1	2	Tr	1	1
Smectite	Tr	Tr	Tr	Tr	Tr	Tr	Tr	Tr
Kaolinite	1	1	1	1	1	1	2	1

Table A.10. Comparison of Calculated and Measured CEC Based on Mineralogy of Select Sediment Samples from Borehole 299-E17-21. Data are FIO. (Horton et al., 2003)

	7A			10A			14A			16A		
Mineral Group	Wt%	Calc CEC (meq)	% Total CEC	Wt%	Calc CEC (meq)	% Total CEC	Wt%	Calc CEC (meq)	% Total CEC	Wt%	Calc CEC (meq)	% Total CEC
Quartz, Feldspar, Amphibole	91	1.82	40.9	94	1.88	53.4	93	1.86	49.6	95	1.90	59.9
Mica, Chlorite	8	2.00	44.9	5	1.25	35.5	6	1.5	40.0	4	1.00	31.5
Smectite	0.4	0.48	10.8	0.2	0.24	6.8	0.2	0.24	6.4	0.1	0.12	3.8
Kaolinite	1	0.15	3.4	1	0.15	4.3	1	0.15	4.0	1	0.15	4.7
Calc. Total CEC (meq/100g)		4.55			4.27			4.65			3.77	
Meas. CEC (meq/100g)		**5.07**			**4.73**			**4.62**			**2.32**	
	20A			24A			31A			35A		
Mineral Group	Wt%	Calc CEC (meq)	% Total CEC	Wt%	Calc CEC (meq)		Wt%	Calc CEC (meq)	% Total CEC	Wt%	Calc CEC (meq)	% Total CEC
Quartz, Feldspar, Amphibole	93	1.86	48.1	94	1.89	55.6	93	1.86	45.0	95	1.90	62.5
Mica, Chlorite	6	1.50	38.8	4	1.00	29.4	5	1.25	30.3	3	0.75	24.7
Smectite	0.3	0.36	9.3	0.3	0.36	10.6	0.6	0.72	17.4	0.2	0.24	7.9
Kaolinite	1	0.15	3.9	1	0.15	4.4	2	0.30	7.3	1	0.15	4.9
Calc. Total CEC (meq/100g)		4.77			4.00			4.88			3.49	
Meas. CEC (meq/100g)		**4.67**			**9.03**			**10.98**			**6.65**	

Kaplan et al. 1998 [PNNL-11966] also measured CEC for 12A, 15A, 17A, 19A, 21A, 22A, 23A,25A,27A,29A,32A, and 34A; see Table A.1, column 2, for depths.
CEC values (meq/100 g) are: 12A = 4.6, 15A = 4.11, 17A = 4.98, 19A = 4.72, 21A = 4.56, 22A = 7.33, 23A = 8.41, 25A = 6.63, 27A = 8.36, 29A = 7.77, 32A = 8.39, and 34A = 6.21

A.2 Geochemistry of Borehole 299-E24-21 (C3177)

Borehole 299-E24-21 was drilled at the northeast corner of the IDF disposal site in 2001. The borehole was drilled with a Becker hammer and a near-continuous core was collected from 45 ft below ground surface (bgs) to total depth at 335 ft bgs (see Figure A.1 for lithology). The drill core was retrieved in 2-ft-long plastic liners that were capped as soon as possible after being removed from the split-tube sampler. Details of the drilling activities and the geologist's log are given in Reidel et al. (2001).

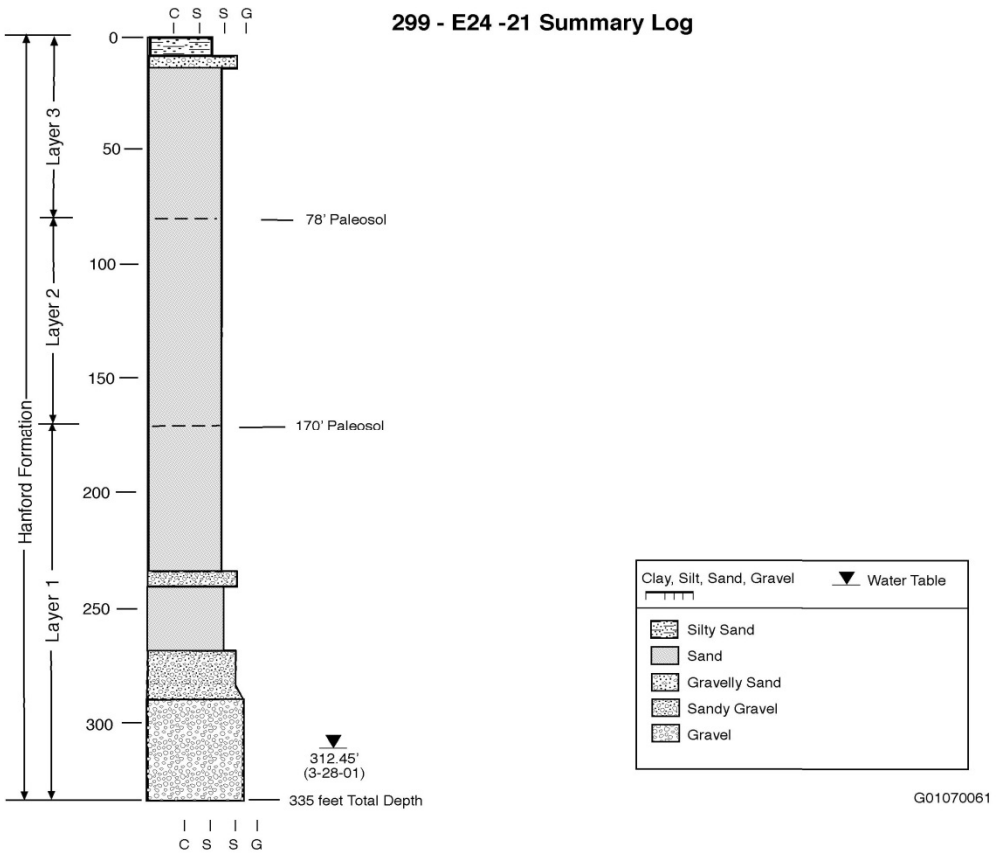

Figure A.1. Lithology of Sediments in IDF Borehole 299-E24-21 (Reidel et al. 2001).

Twelve samples were selected from the core for detailed analyses. Table A.11 lists the samples and gives a short description of each. Samples are identified by the borehole number with a depth (in feet bgs) suffix. Two types of samples were collected: composite samples and discrete depth samples. Composite samples were made by combining several 2-ft sections of core. Each composite was homogenized in 5-gallon buckets before subsampling for analyses. Composite samples are identified in Table A.11.

Depth discrete samples were collected to characterize specific features. The sample at 80.3 ft depth was collected to characterize a paleosol identified by the geologist during description of the core. The paleosol was identified at 78 ft bgs whereas the sample collected for this effort was taken at 80.3 ft bgs. Thus, the sample used for this study probably represents the sediment immediately below the paleosol and not the paleosol itself. The sample collected at 113.3 ft bgs represents a discrete, thin (~1/2-in.-thick) silt lens typical of silt lenses found in the Hanford formation sand-dominated sequence. The sample from 168.5 ft bgs is from the bottom of the R2 paleomagnetic layer and represents a discrete sample of the Hanford formation sand-dominated, Layer 2. The sample from 170.4 ft bgs is the paleosol identified at that depth by Reidel et al. (2001) during core logging. The two samples from 223.5 and 242.0 ft bgs are from above and below the N1/R1 paleomagnetic boundary and were collected to characterize any differences above and below that contact.

Table A.11. Samples Collected from Borehole 299-E24-21. Data are FIO. (Horton et al., 2003)

#	Sample ID	Description
1	C3177-45	Composite sample; Hanford formation Layer 3
2	C317	Sediment associated with paleosol at the Hanford formation Layer 3/Layer 2 boundary; bedded, medium-grained sand; beds are distinguished by color and hardness
3	C3177-110	Composite sample; Hanford formation Layer 2
4	C3177-113.3	Silt lens in the Hanford formation Layer 2
5	C3177-150	Composite sample; Hanford formation Layer 2
6	C3177-168.5	Hanford formation Layer 2; bedded, medium-grained sand with a trace of silt; sample is from the base of the R2 (paleomagnetic) layer
7	C3177-170.4	Paleosol at the Hanford formation Layer 2/Layer 1 boundary; fine-grained sand to silt; bioturbated and bleached with calcite cement
8	C3177-200	Composite sample; Hanford formation Layer 1
9	C3177-215	Composite sample; Hanford formation Layer 1
10	C3177-223.5	Hanford formation Layer 1; coarse-grained sand; slight reaction to HCl; bottom of the N1 (paleomagnetic) layer
11	C3177-242.0	Hanford formation Layer 1; sandy gravel; near the top of the R1 (paleomagnetic) layer
12	C3177-251	Composite sample; Hanford formation Layer 1

Characterization data generated for the sediments from 299-E24-21 included particle size, total oxide content via X-ray fluorescence (XRF) after the sediment was fused using dilithium tetraborate ($Li_2B_4O_7$), total and inorganic carbon analysis, semi-quantitative mineralogy of various particle size fractions by X-ray diffraction (XRD), surface area by multipoint Brunauer–Emmett–Teller (BET), hydrous oxide content, and CEC.

A.2.1 Particle Size for Borehole 299-E24-21 Sediments

Table A.12 contains the particle size distributions as determined by wet sieve and hydrometer methods normalized to 100% for the composite samples from borehole 299-E24-21.

Table A.12. Particle Size Distributions for 299-E24-21 Sediments. Data are FIO. (Horton et al., 2003)

Sample Number	% Gravel	% Sand	% Silt	%Clay	Classification
C3177-45	1.05	92.16	5.41	1.38	Sand
C3177-110	3.85	88.60	6.19	1.36	Sand
C3177-150	1.27	91.60	6.12	0.99	Sand
C43177-200	5.25	89.36	4.44	0.94	Slightly gravelly sand
C3177-215	22.94	73.12	3.20	0.74	Gravelly sand
C3177-251	0.60	93.31	5.28	0.80	Sand

A.2.2 Chemical Composition of 299-E24-21 Sediments

The bulk compositions of each of the 12 samples as weight percent oxides are shown in Table A.13. All iron in the samples is assumed to be ferrous iron. Weight percent FeO can be converted to weight percent Fe_2O_3 by multiplying the wt% of FeO by 0.44887.

With the exception of the deepest sample from 251 ft bgs, the samples from the Hanford formation Layer 1 appear to have lower SiO_2 and bound water content (from LOI) and greater FeO, CaO, and MgO than do samples from the Hanford formation Layer 2 and Layer 3. However, the number of samples is small and the number of variables is large, so that no general trends can be assumed without a larger database of analyses. In general, the bulk composition of sediments from borehole 299-E24-21 appears to be typical of the Hanford formation sand-dominated sequence.

A.2.3 Carbon Content in 299-E24-21 Sediments

The total carbon, inorganic carbon, and organic carbon (by difference) concentrations are shown in Table A.14. Also shown on the table are the equivalent weight percents calcium carbonate calculated from the inorganic carbon concentrations. Almost all carbon in the Hanford formation is present as calcium carbonate (calcite). As expected, the coarser grained sediments, with significant gravel components, contain less weight percent calcium carbonate than finer grained sediments (with the exception of the sample from 251 ft depth). Somewhat surprising, however, is the relatively low calcium carbonate content of the paleosols. The paleosols present in borehole 299-E24-21 did not develop over the extensive lengths of time available for development of other, more developed, paleosols such as those found as part of the Plio-Pleistocene unit that commonly contains up to 4.5 to 5 wt% carbon (or about 38 wt% calcium carbonate). Instead, the paleosols in the Hanford formation at borehole 299-E24-21 probably developed in only a few thousand years between flood deposits. The paleosols at C3177 were recognized by their mud content, bioturbated, and bleached nature (Reidel et al. 2001) and not as a well-developed caliche.

Table A.13. Bulk Sediment Composition of Twelve Samples from Borehole 299-E24-21. Data are FIO. (Horton et al., 2003)

Oxide	C3177-45 % wt.	C3177-80.3 % wt.	C3177-110 % wt.	C3177-113.3 % wt.	C3177-150 % wt.	C3177-168.5 % wt.	C3177-170.4 % wt.	C3177-200 % wt.	C3177-215 % wt.	C3177-223.5 % wt.	C3177-242.0 % wt.	C3177-251 % wt.
LOI	2.52	2.81	2.32	2.68	2.15	2.07	2.01	2.07	1.76	2.11	1.79	1.95
Major Element Oxides												
SiO_2	71.82	72.19	70.44	72.21	71.45	71.41	72.23	68.43	64.92	67.06	68.44	70.61
Al_2O_3	13.06	13.03	13.24	12.86	13.29	13.23	13.19	13.36	13.65	13.54	13.49	13.53
TiO_2	0.571	0.572	0.672	0.64	0.568	0.545	0.486	0.831	1.118	0.94	0.82	0.603
FeO*	3.97	3.82	4.42	3.85	3.91	3.95	3.45	5.51	6.91	6	5.27	4.19
MnO	0.066	0.069	0.077	0.07	0.072	0.072	0.064	0.098	0.114	0.1	0.091	0.076
CaO	3.31	3.19	3.72	3.44	3.35	3.42	3.22	4.16	5.15	4.52	4.18	3.61
MgO	1.73	1.67	1.87	1.7	1.72	1.71	1.6	2.04	2.62	2.24	2.07	1.72
K_2O	2.63	2.74	2.54	2.36	2.47	2.4	2.44	2.25	2	2.16	2.13	2.25
Na_2O	2.73	2.61	2.87	2.71	3.05	3.13	3.2	3.16	3.31	3.25	3.33	3.28
P_2O_5	0.126	0.123	0.153	0.155	0.131	0.128	0.121	0.169	0.219	0.194	0.174	0.138
BaO	0.088	0.088	0.090	0.079	0.095	0.097	0.100	0.089	0.086	0.092	0.090	0.094
SrO	0.043	0.043	0.044	0.044	0.048	0.050	0.049	0.048	0.047	0.048	0.049	0.051
ZrO_2	0.020	0.023	0.020	0.036	0.019	0.020	0.016	0.018	0.019	0.018	0.018	0.017
Trace Elements (μg/g)												
Ni	20	19	20	23	22	26	28	20	19	20	22	24
Cr	39	43	51	55	53	68	61	55	43	41	47	50
Sc	14	7	11	13	13	15	13	18	27	21	14	17
V	81	62	99	76	81	80	66	120	174	132	131	90
Ba	792	786	810	712	847	865	899	793	767	821	806	842
Rb	87	92	80	77	75	73	72	69	56	66	62	69
Sr	364	362	376	373	404	423	418	404	401	403	414	433
Zr	145	170	145	270	141	145	117	136	140	134	132	123
Y	22	24	22	26	18	19	17	22	28	22	20	18

Trace Elements (μg/g)												
Nb	10.6	11.7	11.5	13.2	10.5	11.2	9.8	11	11.2	10.8	10.1	9.4
Ga	16	15	16	11	17	16	14	16	19	17	13	18
Cu	20	23	22	21	23	23	22	19	27	28	21	18
Zn	49	52	55	53	47	49	49	62	78	67	65	49
Pb	13	13	10	13	9	11	10	8	9	10	12	8
La	29	26	19	29	23	15	23	32	19	36	13	20
Ce	46	51	50	56	49	46	35	46	37	38	40	36
Th	7	5	7	10	6	5	6	6	6	2	3	9
Total (% wt.) Majors	102.68	102.98	102.48	102.84	102.32	102.23	102.18	102.23	101.92	102.27	101.94	102.12

Table A.14. Total Carbon, Inorganic Carbon, Equivalent Calcium Carbonate, and Organic Carbon Concentrations in Borehole Samples from 299-E24-21. Data are FIO. (Horton et al., 2003)

Sample Number	Description	Total Carbon (wt%)	Mean Total Carbon (wt%)	Inorganic Carbon (wt%)	Mean Inorganic Carbon (wt%)	Equivalent Calcium Carbonate (wt%)	Organic Carbon[(a)] (wt%)
C3177-45	Composite, Layer 3 Sand	0.26 0.25	0.25	0.24 0.24 0.24	0.24	1.99	0.01
C3177-80.3	Paleosol	0.22		0.22		1.83	0.00
C3177-110	Composite, Layer 2 Sand	0.20		0.19		1.58	0.01
C3177-113.3	Silt lens	0.23		0.21		1.75	0.02
C3177-150	Composite, Layer 2 Sand	0.20		0.17		1.42	0.03
C3177-168.5	Sand, R2	0.21		0.15		1.25	0.06
C3177-170.4	Paleosol	0.20		0.17		1.42	0.03
C3177-200	Composite, Layer 1 slightly gravelly sand	0.18		0.14 0.15	0.14	1.16 1.25	0.04
C3177-215	Composite, Layer 1 gravelly sand	0.11		0.7		0.58	0.04
C3177-223.5	Sand, N1	0.14		0.10		0.83	0.04
C3177-242.0	Sand, R1	0.19 0.22	0.21	0.16		1.33	0.05
C3177-251	Composite, Layer 1 sand	0.17		0.13		1.08	0.04

(a) Organic carbon calculated by difference.

A.2.4 Mineralogy of 299-E24-21 Sediments

XRD analysis of 299-E24-21 sediments shows that all the sediments are mineralogically similar. The sediments are dominated by quartz and feldspar (both plagioclase and alkali-feldspar), with lesser amounts of mica, chlorite, and an amphibole. Figure A.2 is an example XRD pattern of the sediment from 80.3 ft depth. The main reflection for quartz is at 26.63° 2θ, followed by less intense reflections at 20.86, 36.53, 39.46, 42.43, 50.12, and 59.92° 2θ. The main reflections associated with feldspar minerals are between 27.34° 2θ and 27.92° 2θ, with the higher 2θ values belonging to the plagioclase series. Chlorite and mica minerals were identified on the X-ray tracings by the reflections at 6.3° 2θ and 8.8° 2θ, respectively. The presence of an amphibole was established by the characteristic 100% reflection at 10.5° 2θ. Additionally, trace amounts of the zeolite, laumontite, were identified in most of the samples by a diffraction peak positioned at 9.36° 2θ.

Analysis results are provided in Table A.15. Quartz concentrations range from 26 to 46 wt%, with an average quartz concentration of 38 ± 6 wt%. Plagioclase feldspar is present at concentrations between 15 to 40 wt% and potassium feldspar concentrations are between 16 to 31 wt%. Plagioclase feldspar was more abundant than potassium feldspar in all samples except C3177-45, C3177-80.3, C3177-113.3, and C3177-170.4. Overall the feldspar content (both plagioclase and alkali feldspars) averaged about 47 ± 5 wt%. The amphibole phase comprised <4 wt% at most, with the majority of samples having concentrations in the 2 to 4 wt% range. Samples from Layer 1 have higher plagioclase and lower quartz

concentrations than do samples from Layer 2 or Layer 3. Also, the paleosols and the silt lens have greater potassium feldspar concentrations than do the other samples.

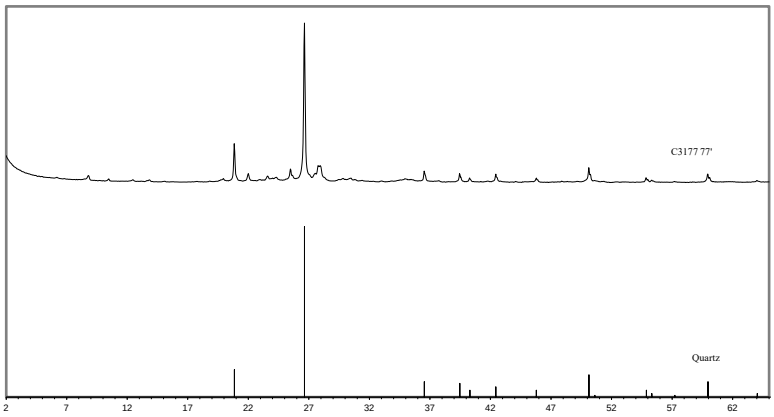

Figure A.2. XRD Tracing of Sample C3177-80.3 along with a Standard Reference Pattern for Quartz. Data are FIO. Reidel et al., 2001)

Table A.15. Semi-quantitative XRD Results of Bulk Samples from ILAW Borehole 299-E24-21. Data are FIO. (Horton et al., 2003)

	Mineral Phase (wt%)						
Sample ID	Quartz	Amphibole	Plagioclase	K-Spar	Mica	Chlorite	Goodness of Fit[(a)]
C3177-45	43	2	20	20	11	3	0.87
C3177-80.3	41	2	15	28	16	2	0.94
C3177-110	46	1	25	19	9	2	0.70
C3177-113.3	40	4	15	31	8	2	1.22
C3177-150	42	3	25	18	3	8	0.81
C3177-168.5	40	4	23	22	10	2	1.00
C3177-170.4	43	3	21	23	8	2	1.04
C3177-200	37	4	31	16	10	3	0.77
C3177-215	26	3	40	18	11	3	0.73
C3177-223.5	33	4	34	18	8	3	0.56
C3177-242.0	32	2	31	18	14	3	0.95
C3177-251	32	4	35	18	9	3	0.67

(a) Values closest to 1.0 represent an ideal refinement.

Clay minerals identified in the whole rock sediment include mica and chlorite. Mica concentrations range from a low of 3 wt% to a high of 16 wt% (the paleosol at 80.3 ft bgs, with an average concentration of 10 ± 3 wt%. Chlorite concentrations were <3 wt% in all sediments analyzed with the exception of sample C3177-150, which had 8 wt% chlorite. Smectite and kaolinite minerals were not identified in the whole rock samples due in part to the sample preparation technique and to their low overall concentrations.

The results of XRD analysis of the <2 micron fraction of each sample are shown in Table A.16. The clay fraction is dominated by four clay minerals: smectite, chlorite, illite, and kaolinite with minor amounts of quartz and feldspar. Figure A.3 provides an example XRD pattern of a typical clay assemblage (sample C3177.80.3) following four different treatments. Smectite is the fraction of the Mg-saturated sub-sample

that gives a basal reflection at 5.85° 2θ and expands to 5.28° 2θ after solvation with ethylene glycol. Saturation with K^+ causes the reflection to shift to 7.3° 2θ and heating the sample at 575° 2θ for 1 hour causes the smectite reflection to irreversibly collapse to 8.88° 2θ. Illite is the easiest of the four clay minerals to identify in the immobilized low-activity waste (ILAW) samples. The basal reflections for illite are at 8.88, 17.8, and 26.7° 2θ. The various treatments including cation saturation, solvation with ethylene glycol, and heating do not affect the position of these reflections. An increase in intensity of the 8.88° 2θ reflection between the heated and the unheated K-saturated specimens in the example patterns in Figure A.3 is due to the collapse of the smectite reflection to 8.88° 2θ, where it is superimposed on the illite reflection.

Table A.16. Semi-quantitative XRD Results of Clay Minerals Separated from the Sediment Collected from ILAW Borehole C3177 Samples. Data are FIO. (Horton et al., 2003)

Sample ID	Mineral Phase (wt%)				Normalization Factor
	Smectite	Illite	Chlorite	Kaolinite	
C3177-45	24	54	14	8	0.67
C3177-80.3	34	44	14	9	0.78
C3177-110	26	51	16	7	0.89
C3177-113.3	39	43	12	6	0.9
C3177-150	25	50	18	7	0.77
C3177-168.5	27	47	19	6	0.9
C3177-170.4	18	50	24	9	1.4
C3177-200	27	50	16	8	1.36
C3177-215	30	46	20	4	1.5
C3177-223.5	NA	NA	NA	NA	NA
C3177-242.0	27	44	18	10	1.16
C3177-251	NA	NA	NA	NA	NA

NA = not analyzed

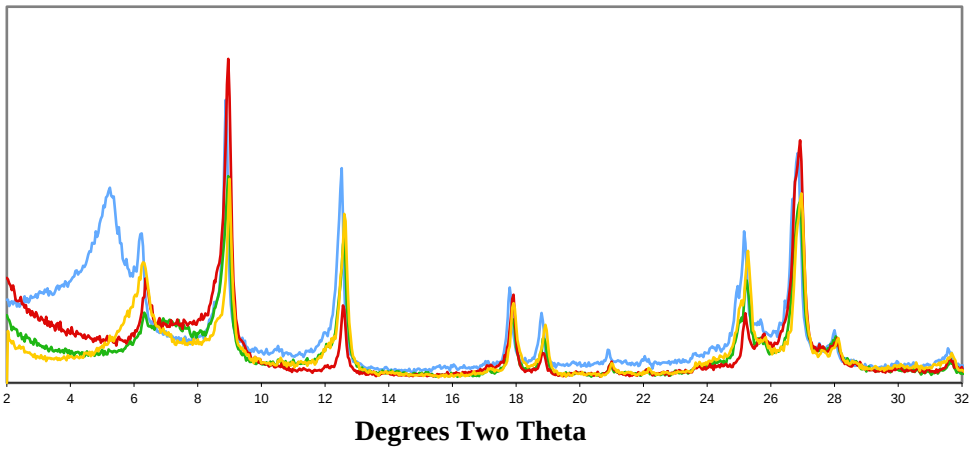

Figure A.3. XRD Tracings of Preferentially Oriented < 1.4 μm Specimen from Sample C3177-80.3 The yellow line represents the Mg-saturated fraction and the blue line represents the same fraction solvated with ethylene glycol. The green line indicates the K+ saturation and the red line is the K+-saturated sample heated to 575°C for 1 hour. Data are FIO. (Horton et al., 2003)

Chlorite is identified by a basal series of diffraction peaks at 6.24, 12.5, 18.8, and 25.2° 2θ, which are unaffected by cation saturation or ethylene glycol solvation. Heating to 575°C shifts the first order reflection to 6.37° 2θ and tends to diminish or eliminate the intensity of the higher order reflections (12.5, 18.8, and 25.2° 2θ). Kaolinite is difficult to identify in the presence of chlorite. Basal reflections characteristic of kaolinite are at 12.5 and 24.9° 2θ and are superimposed on the even-ordered chlorite reflections. Kaolinite reflections are unaffected by cation saturation and ethylene glycol solvation. After heating, the kaolinite structure becomes amorphous and the reflections are eliminated. Positive identification of kaolinite in the presence of chlorite can be determined by differentiating kaolinite basal reflection at 24.9° 2θ from the chlorite reflection at 25.2° 2θ. Published reports characterizing clay fractions of Hanford formation sand-dominated sediment from other studies identify kaolinite by electron microscopy (Xie et al., 2003).

Trace amounts of quartz in the < 2 μm fractions are evident by the diffraction peak located at 20.85° 2θ. The 100% reflection for quartz (26.6° 2θ) is hidden by the third-order basal reflection of illite located at 26.6° 2θ. Plagioclase feldspar is also identified in the clay fractions by the minor diffraction peak at 27.8° 2θ.

Examination of samples C3177-80.3 and C3177-251 by transmission electron microscopy (TEM) allowed detailed characterization of the various clay minerals identified by XRD. Overall, illite and chlorite particles dominated the coarser component of the clay fractions, with individual grain sizes commonly measuring 1 to 4 μm in length. Figure A.4 is an example of a representative illite particle measuring about 4 μm in length. The particle exhibits a thin platy habit, making it easily distinguishable from other clay minerals. Using data from TEM analysis and assuming all iron as Fe^{3+}, the following structural formula was calculated:

$$\left[K^{+}_{0.63}Ca^{2+}_{0.01}\right]^{+0.65}\left[(Al^{3+}_{1.58}Mg^{2+}_{0.30}Fe^{3+}_{0.21}Ti^{4+}_{0.02})^{+0.05}(Si^{4+}_{3.29}Al^{3+}_{0.71})^{-0.71}\right]^{-0.64}O_{10}(OH)_2.$$

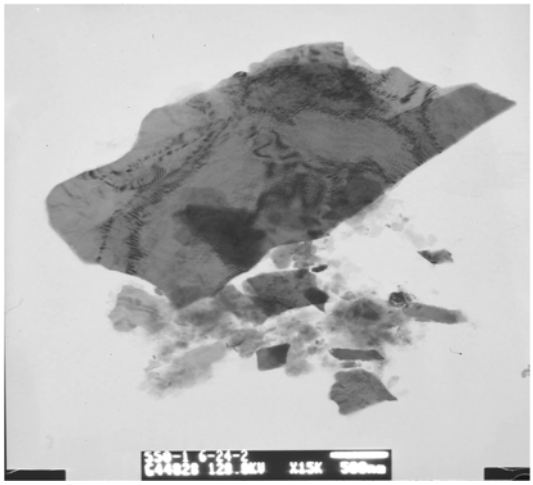

Figure A.4. Large Illite Particle from Sample C3177-80.3. The particle is about 4 mm long. (Horton et al., 2003)

As in muscovite, the layer charge for the illite originates in the tetrahedral sheet (-0.71), with a slight positive contribution from the octahedral sheet (+0.05), resulting in a 2:1 layer charge of –0.64. The interlayer charge of +0.65 balances the charge on the 2:1 silicate structure. Iron content of eight illite particles examined by TEM ranged between 0.08 and 0.54 atoms per $O_{10}(OH)_2$ and octahedral Al^{3+} ranged between 1.07 and 1.70 atoms per $O_{10}(OH)_2$. Traces of Ti^{+4} were detected in most of the illites.

Chlorite particles displayed platy habits and often appeared similar in shape and texture to illite. Figure A.5 is an example of a typical chlorite particle about 1 μm in size found in the clay fraction of sample C3177-251. Chlorite particles were found to be generally smaller than illite particles, with sizes ranging between 1 to 2 μm. Developing a structural formula for this particular particle from by TEM data results in the following:

$$\left[K^{+}_{0.01}\right]^{+0.01}\left[(Al^{3+}_{1.45}Mg^{2+}_{2.90}Fe^{2+}_{1.44})^{+1.03}(Si^{4+}_{2.92}Al^{3+}_{1.08})^{-1.08}\right]^{-0.05}O_{10}(OH)_8.$$

The structural formula shows that the negative charge in the tetrahedral sheet, originating from the substitution of Al^{3+} for Si^{4+}, is balanced by the inclusion of the trivalent cation, Al^{3+}, and divalent cations, Mg^{2+} and Fe^{2+}, into the octahedral sheets. The total number of cations occupying octahedral sites is 5.79 per $O_{10}(OH)_8$. TEM analysis of four individual chlorite grains showed Fe^{2+} concentrations ranging from 0.96 to 1.44 atoms per $O_{10}(OH)_8$ and Mg^{2+} ranging from 2.90 to 3.26 atoms per $O_{10}(OH)_8$. Small amounts of K^{+} were included in the structural formula, but are most likely from very small illite grains that could not be separated from the chlorite grains during the analysis.

Smectite dominates the finer particles of the clay fractions. Smectite is typically found as fine-grained flakes in the <0.5 μm range and occasionally as aggregates up to 1 to 2 μm in size. Figure A.6 is an example of several dense smectite aggregates measuring less than 2 μm. The aggregates consist of a dense center from which delicate thin films of individual smectite flakes extend outward. These individual films can be seen curling up around the edge of the aggregate. Although individual smectite flakes or aggregates were never sufficiently isolated during the TEM analysis to obtain data for developing a structural formula, using data collected from the EDS during TEM analysis showed smectite aggregates to be rich in iron, with minor amounts of magnesium and aluminum. The iron concentrations were consistent from particle to particle but the magnesium and aluminum concentrations varied.

Figure A.5. Chlorite Aggregate from C3177-251. The aggregate is a little over 1 micron in size. (Horton et al., 2003)

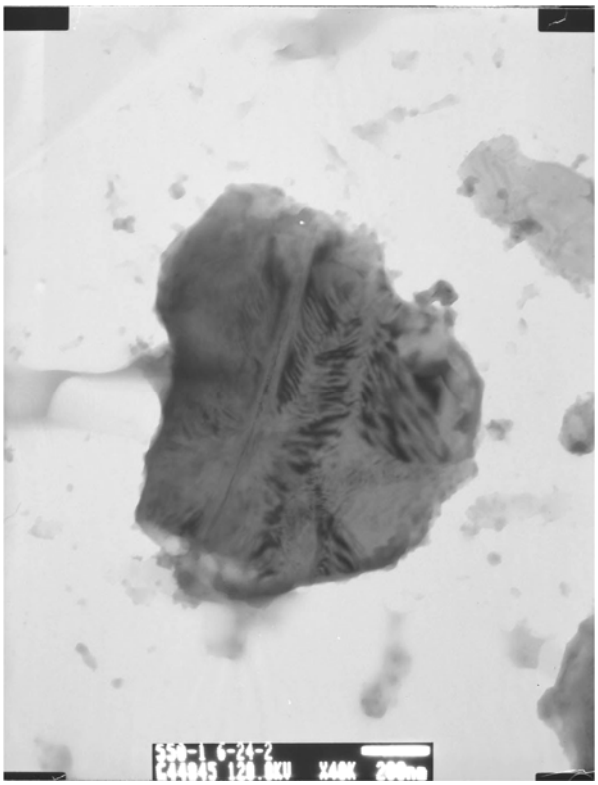

Figure A.6. TEM Photomicrograph of the Clay Fraction of Sample C3177-80.3 Showing the Morphology of Individual Smectite Aggregates (Horton et al., 2003)

Crystalline phases not detected in the XRD analysis, but observed by TEM, included various oxides of iron, manganese, chromium, and titanium. These oxides were associated with the finest grain size fractions and are generally < 0.1 μm in size. Additionally, individual rhomboid shaped grains of apatite (calcium-phosphate) were found throughout the sample.

Results of the clay minerals in the < 2 μm fractions are presented in Table A.16. Total recoveries were normalized to 100% and the normalization factor used for each sample is provided in the last column. Smectite concentrations range from 18 to 39 wt%. Illite concentration varies from 43 to 54 wt% with an average concentration of 48 wt%. Chlorite and kaolinite are the least abundant of the clay minerals identified in the samples, with concentrations equal to or less than 24 wt% and 9 wt%, respectively. Quartz and feldspar minerals were present as trace amounts in the clay fraction and therefore were not included in totals presented in Table A.17.

No general trends are noted in the data in Table A.16 from the 12 samples. The silt lens sample (C3177-113.3) has the highest smectite concentration and the lower paleosol sample (C3177-170.4) has the highest chlorite concentration. Overall, the mineralogy of the clay fractions from borehole C3177 are similar to clay fractions analyzed from clean boreholes and other composite samples of the Hanford formation sand-dominated sequence characterized by Serne et al. (2004a).

Total clay recoveries are within ±15% of the "ideal" 100% for samples C3177-110, C3177-113.3, C3177-168.5, and C3177-242.0. Most other samples have recoveries within 30% of the "ideal" 100%. Factors affecting the semi-quantitative procedure (preparation and condition of the clay filter cake) were generally controlled and not considered to be significant, based on an error margin of ± 20% for minerals whose concentrations are less than 20 wt% (Moore and Reynolds 1989).

The most common plagioclase feldspar in Columbia River basalts is labradorite (An_{45} – An_{65}). Visual inspection of most Hanford formation sediment samples shows that both biotite and muscovite micas are also present. These are difficult to distinguish by XRD in multi-mineral samples such as the Hanford formation sand-dominated sequence without detailed work in the laboratory.

A.2.5 Surface Area of 299-E24-21 Sediments

The surface areas of the bulk sediment (with particles > 7 mm excluded) and the clay-size fraction (<2 μm) were measured for each of the composite samples. Several other sediment sample clay-size fractions were also measured and the data are given in Table A.17. The data represent the external surface area per gram of sample that is available to react with non-polar molecules. (Note: In this case, N_2 was used for the measurement. N_2 does not readily penetrate the interlayers of the clay minerals so that only the external surfaces contribute to the measurement.)

Generally, the surface area of the bulk sediments from the ILAW borehole are low. The composite sample from 215 ft bgs, however, contains a high percentage of both coarse pebbles and fine sand/silt that yielded higher surfaces areas than the other bulk sediments in the borehole (15.58, 7.51, and 7.92 m^2/g, for the three aliquots used in this analysis). As shown in Table A.15, this sample appears to contain less quartz and more plagioclase than the other composite samples. The surface areas are consistent with published clay fractions in Grim (1968) for mono-mineralic samples, who reports surface areas for smectite at 30 to 82 m^2/g, illite at 56 to 113 m^2/g, and kaolinite at 16 to 22 m^2/g.

Table A.17. Surface Areas of 12 Bulk Sediments and Clay-Size Fractions from Borehole 299-E24-21. Data are FIO. (Horton et al., 2003)

Sample ID	Bulk Sediment (m^2/g)	Clay Fraction (m^2/g)
C3177-45	3.94	51.1
C3177-80.3	NA	53
C3177-110	5.11	41.8
C3177-113.3	NA	21.1
C3177 150	3.52	38.4
C3177-168.5	NA	28.3
C3177-170.4	NA	35.1
C3177-170.4 re-run	NA	35
C3177-200	5.30	52.5
C3177-215	7.15	52.2
C3177-215 (re-run)	10.3 ± 4.5[(a)]	
C3177-223.5	NA	58.5
C3177-242.0	NA	36.9
C3177-251	4.43	46.8

(a) Sample has high % of pebbles that can't fit in analyzer AND high % of fine sand/silt. Three aliquots (pebbles excluded) were run.

(b) Not analyzed

A.2.6 Hydrous Oxide Content of 299-E24-21 Sediments

Results from the iron extraction experiments are presented in Figure A.7. As expected, the solutions containing sodium dithionite containing removed more iron from the composite soil samples than the less aggressive extraction solutions. Overall, the total percentages of iron extracted from the various samples are lower than those reported from similar tests performed on an exposed Hanford soil collected in the vicinity of the 300 Area (Serne et al., 2004a). The relatively low extractable iron concentrations in the 299-E24-21 samples may be attributed to short times that these Hanford formation sediments were exposed to the weathering environment. The samples are sands that were rapidly deposited from glacial floods and probably were not exposed to the weathering environment for any appreciable time before being buried by overlying sediment. This is further supported by the extraction data, which indicate that iron oxide precipitates and coatings constitute less than 0.3 total weight percent in all of the composite samples. These data suggest that iron oxide measurements taken from exposed faces and outcroppings can potentially overestimate the percentages available in buried Hanford formation flood deposits, excepting known paleosols. It is difficult to discern from the data the overall effectiveness of the respective solutions to target discrete iron phases (i.e., amorphous versus crystalline); spectroscopic techniques (scanning electron microscopy and XRD) would need to be used to further evaluate whether the classical extraction techniques can differentiate amorphous from crystalline ferric oxides in Hanford formation sands, which are relatively young and unweathered.

A.2.7 Cation Exchange Capacity of 299-E24-21 Sediments

Figure A.8 shows the CEC of three composite samples from 299-E24-21 using three separate radio-tracer techniques. For comparison, some of the samples were pretreated with a slightly acidic sodium acetate solution to remove discrete carbonate solids and carbonate coatings from the soil. In general, agreement between the three techniques is quite good (average relative standard deviation of 11%), with the largest portion of error attributed to the ^{22}Na replicate analysis for sample C3177-45. Slightly better agreement was achieved using the Cs and Sr tracers; therefore, future analyses will utilize the ^{85}Sr radio-tracer method. An interesting result to note is that the relative standard deviation is actually lower (less than 11%) when the calculation is performed using both the sodium acetate treated and non-treated results. Furthermore, a t-test calculation performed on the respective data shows no significant difference among the three radio-tracer methods or between the sodium acetate treated and untreated samples. These data imply that the presence of small concentrations of carbonate minerals and coatings does not bias the CEC values measured by releasing calcium to compete with the tracers or by coating grain surfaces and reducing the number of available exchange sites.

Figure A.9 shows the total CEC of samples from 299-E24-21 as a function of depth using the ^{85}Sr radio-tracer technique. In general, there is sufficient overlap of error bars such that there is no measurable difference in CEC for the borehole samples as a function of depth. This result is not surprising given the results of the particle size analysis (Table A.12) and bulk sediment composition (Table A.13), which indicate that the borehole samples are primarily composed of sand and have very similar elemental and mineralogical compositions. The average CEC of all samples and replicates tested was 3.87 meq/100g with a relative percent standard deviation of 15.7%. Overall, this indicates good agreement given the relatively small sample size (approximately 2 grams) and the inherent heterogeneity of soil samples. Furthermore, the calculated CECs in Figure A.8 are consistent with the typical range (2-5 meq/100g) for Hanford soils (Serne et. al 2004a).

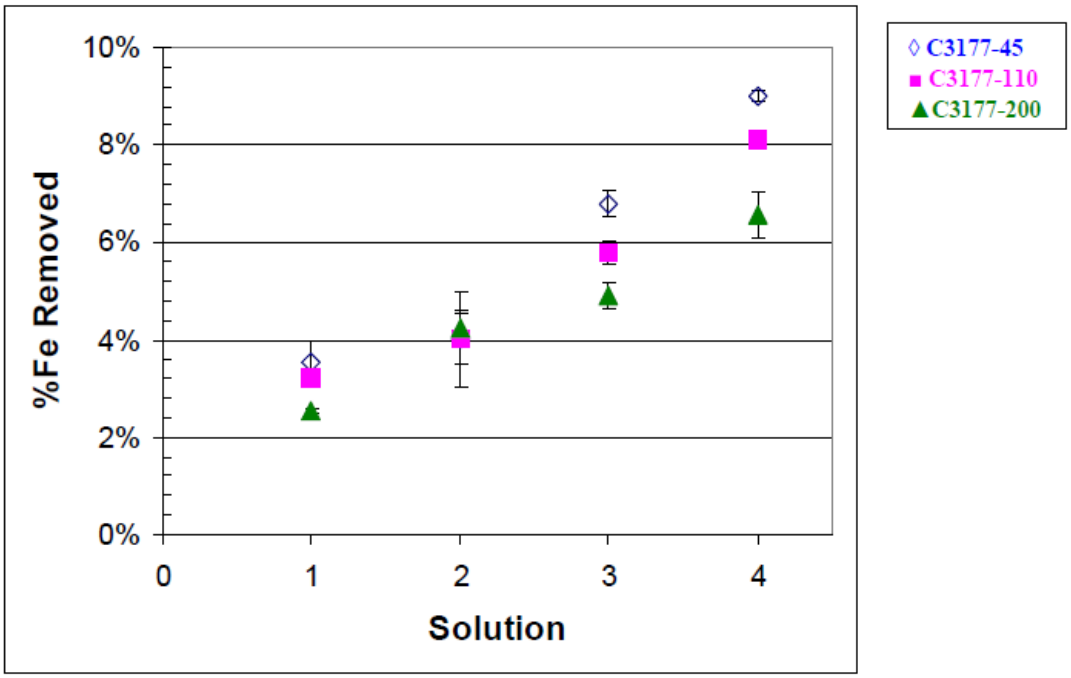

Figure A.7. Percentage of Iron Extracted from ILAW C3177 Borehole Composite Samples (plotted as percentage of total iron). The solution numbers on the y-axis correspond to the following solutions: 1–hydroxylamine hydrochloride/acetic acid, 2–ammonium oxalate/oxalic acid, 3–sodium dithionite/sodium citrate/sodium bicarbonate, and 4–sodium dithionite/sodium citrate/citric acid. Data are FIO. (Horton et al., 2003)

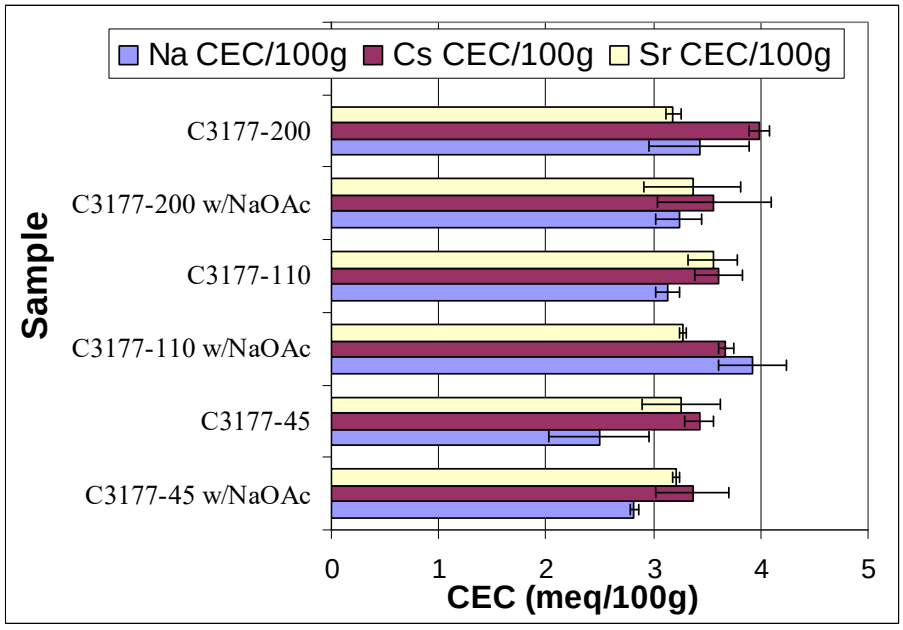

Figure A.8. Calculated Cation Exchange Capacities of Composite Samples from 299-E24-21. Samples identified by "...w/NaOAc" were pretreated with acidic sodium acetate solution to remove discrete carbonate solids and carbonate coatings from the soil. Data are FIO. (Horton et al., 2003)

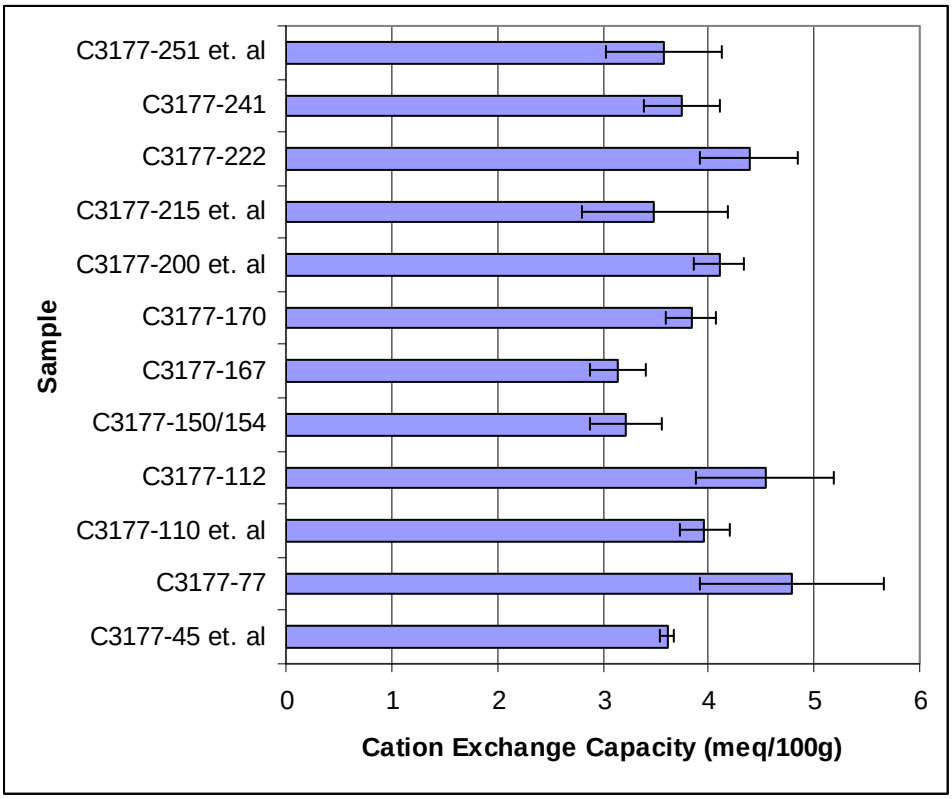

Figure A.9. Cation Exchange Capacities of 299-E24-21 Samples. Data are FIO. (Horton et al., 2003)

A.3 Borehole 299-E33-46

Borehole 299-E33-46 was drilled close to tank B-110 in the B Tank Farm to investigate a vadose zone plume known to contain elevated ^{90}Sr concentrations. Borehole 299-E33-46 was drilled using the cable-tool technique and is located approximately 15 ft (5 m) from the northeast edge of single-shell tank 241-B-110 (Figure A.10). Total depth of the borehole was 264.4 ft bgs; the groundwater table was encountered at 255.8 ft bgs. The surveyed well elevation is 657.3 ft above mean sea level; geographic coordinates are N13728.365 and E573792.553.

Thirty-three split spoon core samples were collected between 10 and 254 ft bgs—an average of every 7.5 ft. Grab samples were collected between these core sample intervals to yield near continuous samples to a depth of 78.3 m (257 ft). The split spoon samples were taken ahead of the casing by driving a split spoon sampler into the undisturbed formations below the casing. Four 0.5-ft-long stainless-steel core liners were used in each 2-ft split spoon. Core extraction was performed later in a radiologically controlled laboratory. Geologic logging occurred after each core segment was emptied into an open plastic container, followed by photographing and sub-sampling for physical and chemical characterization. The plastic containers were sealed shut and placed into cold storage. The complete list of split spoon cores collected, depth interval, and sediment description is listed in Table A.18. Core recovery was excellent (95% to 100%) in the finer grained sediments, decreasing significantly in the coarser materials.

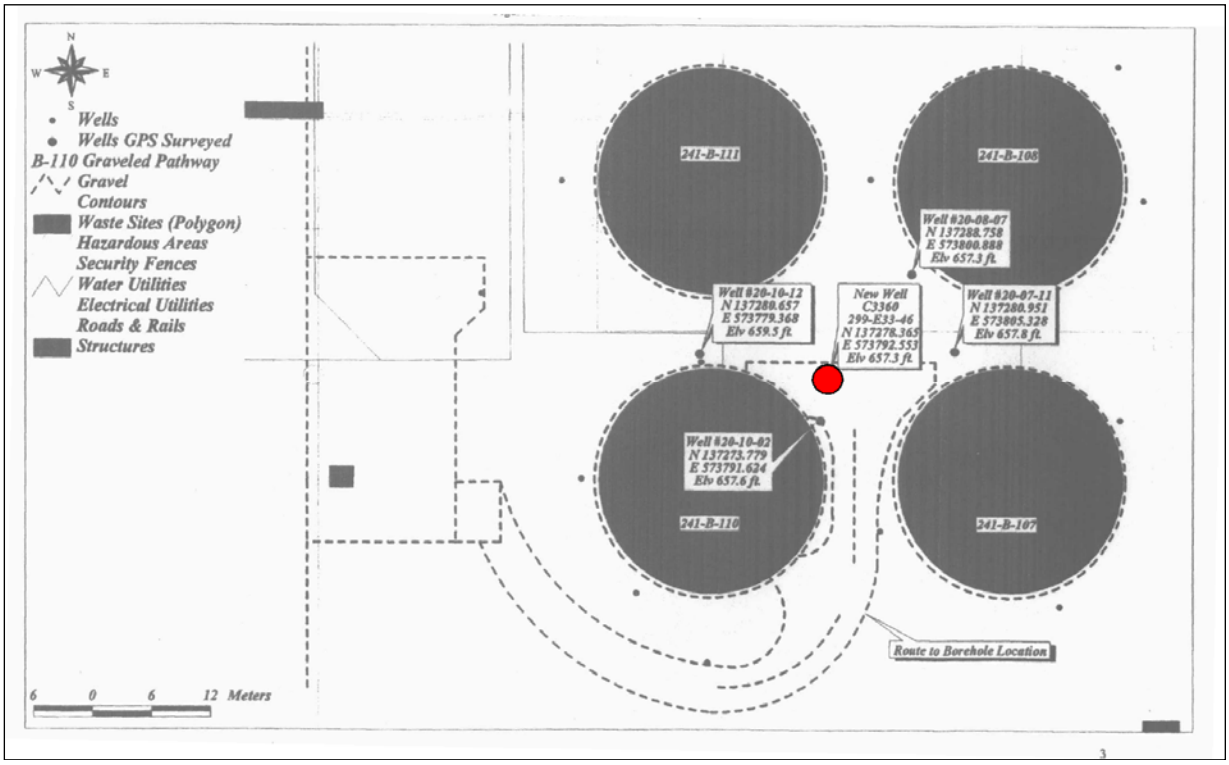

Figure A.10. Location of Borehole 299-E33-46 with B Tank Farm. (Horton et al., 2003)

Table A.18. Composite Grab and Split Spoon Shoe Samples from 299-E33-46. Data are FIO. (Horton et al., 2003)

Sample No.	Top Depth (ft)	Bottom Depth (ft)	Sampled Interval Thickness (ft)	Sample Type	Sample Description	Stratigraphic Unit
S01052-03	11.80	14.07	2.27	Composite Grab	*	*
S01052-04	14.07	15.90	1.83	Composite Grab	*	*
S01052-05	15.90	18.00	2.10	Composite Grab	*	*
S01052-06	21.37	21.60	0.23	Split spoon Shoe	*	*
S01052-07	21.60	24.10	2.50	Composite Grab	*	*
S01052-08	24.10	26.00	1.90	Composite Grab	*	*
S01052-09	26.00	27.70	1.70	Composite Grab	*	*
S01052-10	29.67	30.00	0.33	Split spoon Shoe	*	*
S01052-11	30.00	31.70	1.70	Composite Grab	*	*
S01052-12	31.70	33.30	1.60	Composite Grab	*	*
S01052-13	33.30	35.40	2.10	Composite Grab	*	*
S01052-14	35.40	37.80	2.40	Composite Grab	*	*
S01052-15	37.80	40.00	2.20	Composite Grab	*	*
S01052-16	41.97	42.30	0.33	Split spoon Shoe	*	*
S01052-17	44.27	44.60	0.33	Split spoon Shoe	*	*
S01052-18	46.67	47.00	0.33	Split spoon Shoe	*	*
S01052-19	47.00	48.90	1.90	Composite Grab	*	*
S01052-20	50.87	51.20	0.33	Split spoon Shoe	*	*
S01052-21	53.27	53.60	0.33	Split spoon Shoe	*	*
S01052-22	53.60	55.60	2.00	Composite Grab	*	*

Sample No.	Top Depth (ft)	Bottom Depth (ft)	Sampled Interval Thickness (ft)	Sample Type	Sample Description	Stratigraphic Unit
S01052-23	53.60	55.60	2.00	Composite Grab	*	*
S01052-24	55.60	57.80	2.20	Composite Grab	*	*
S01052-25	57.80	59.00	1.20	Composite Grab	*	*
S01052-26	60.97	61.30	0.33	Split spoon Shoe	*	*
S01052-27	61.30	62.90	1.60	Composite Grab	*	*
S01052-28	62.90	64.90	2.00	Composite Grab	*	*
S01052-29	64.90	67.20	2.30	Composite Grab	*	*
S01052-30	67.20	68.70	1.50	Composite Grab	*	*
S01052-31	70.70	71.00	0.30	Split spoon Shoe	*	*
S01052-32	71.00	72.70	1.70	Composite Grab	*	*
S01052-33	72.70	74.30	1.60	Composite Grab	*	*
S01052-34	74.30	76.50	2.20	Composite Grab	Medium sand	H2
S01052-35	76.50	78.20	1.70	Composite Grab	*	*
S01052-36	80.50	80.50	0.00	Split spoon Shoe	*	*
S01052-37	80.50	81.30	0.80	Composite Grab	*	*
S01052-38	83.30	83.60	0.30	Split spoon Shoe	Medium sand	H2
S01052-39	83.60	85.50	1.90	Composite Grab	Medium sand	H2
S01052-40	85.50	87.10	1.60	Composite Grab	*	*
S01052-41	87.10	88.60	1.50	Composite Grab	*	*
S01052-42	90.87	90.90	0.03	Split spoon Shoe	*	*
S01052-43	90.90	92.00	1.10	Composite Grab	Slightly pebbly coarse sand	H2
S01052-44	92.00	94.30	2.30	Composite Grab	Medium sand	H2
S01052-45	94.30	96.00	1.70	Composite Grab	Medium sand	H2
S01052-46	96.00	97.90	1.90	Composite Grab	*	*
S01052-47	99.87	100.20	0.33	Split spoon Shoe	Medium to coarse sand	H2
S01052-48	100.20	102.90	2.70	Composite Grab	Coarse sand	H2
S01052-49	102.90	104.80	1.90	Composite Grab	Medium to coarse sand	H2
S01052-50	104.80	106.60	1.80	Composite Grab	Medium to coarse sand	H2
S01052-51	106.60	108.30	1.70	Composite Grab	Medium to coarse sand	H2
S01052-52	108.30	109.70	1.40	Composite Grab	*	*
S01052-53	111.67	112.00	0.33	Split spoon Shoe	*	*
S01052-54	112.00	114.00	2.00	Composite Grab	Coarse sand	H2
S01052-55	114.00	115.80	1.80	Composite Grab	Medium to coarse sand	H2
S01052-56	115.80	118.20	2.40	Composite Grab	Medium to coarse sand	H2
S01052-58	120.70	122.30	1.60	Composite Grab	Medium to coarse sand	H2
S01052-59	122.70	124.30	1.60	Composite Grab	Medium sand	H2
S01052-60	122.70	124.30	1.60	Composite Grab	Medium sand	H2
S01052-61	124.30	125.80	1.50	Composite Grab	Medium to coarse sand	H2
S01052-62	125.80	127.70	1.90	Composite Grab	Medium to coarse sand	H2
S01052-63	127.70	130.10	2.40	Composite Grab	Medium to coarse sand with silt lens	H2
S01052-64	132.10	132.40	0.30	Split spoon Shoe	*	*
S01052-65	132.40	133.30	0.90	Composite Grab	Coarse sand	H2
S01052-66	133.30	135.10	1.80	Composite Grab	Coarse sand	H2
S01052-67	135.10	136.90	1.80	Composite Grab	Medium to coarse sand	H2
S01052-68	136.90	138.30	1.40	Composite Grab	Coarse sand	H2
S01052-69	140.30	140.60	0.30	Split spoon Shoe		
S01052-70	140.60	142.20	1.60	Composite Grab	Medium to coarse sand	H2
S01052-71	142.20	144.50	2.30	Composite Grab	Medium to coarse sand	H2
S01052-72	144.50	146.50	2.00	Composite Grab	Medium to coarse sand	H2
S01052-73	146.50	148.40	1.90	Composite Grab	Medium to coarse sand	H2
S01052-74	150.40	150.70	0.30	Split spoon Shoe	*	*

Sample No.	Top Depth (ft)	Bottom Depth (ft)	Sampled Interval Thickness (ft)	Sample Type	Sample Description	Stratigraphic Unit
S01052-75	150.70	152.20	1.50	Composite Grab	Medium to coarse sand	H2
S01052-76	152.20	154.40	2.20	Composite Grab	Medium to coarse sand	H2
S01052-77	154.40	156.60	2.20	Composite Grab	Medium to coarse sand	H2
S01052-78	156.60	158.60	2.00	Composite Grab	Medium to coarse sand	H2
S01052-79	160.40	160.70	0.30	Composite Grab	Medium to coarse sand	H2
S01052-80	160.70	162.80	2.10	Composite Grab	Medium sand	H2
S01052-81	160.70	162.80	2.10	Composite Grab	Medium sand	H2
S01052-82	164.80	165.10	0.30	Composite Grab	Medium to coarse sand	H2
S01052-83	167.10	167.40	0.30	Composite Grab	Medium to coarse sand	H2
S01052-84	167.50	169.40	1.90	Composite Grab	*	*
S01052-85	168.10	168.40	0.30	Composite Grab	Fine sandy silt	H2
S01052-86	171.40	171.70	0.30	Composite Grab	Coarse sand	H2
S01052-87	171.70	174.10	2.40	Composite Grab	Medium to coarse sand	H2
S01052-88	174.10	176.10	2.00	Composite Grab	Medium to coarse sand	H2
S01052-89	176.10	178.10	2.00	Composite Grab	Pebbly sand	H3
S01052-90	180.10	180.40	0.30	Composite Grab	Pebbly sand	H3
S01052-91	180.40	183.10	2.70	Composite Grab	Fine to medium sand with silty fine sand lens	H3
S01052-92	183.10	184.30	1.20	Composite Grab	Pebbly sand	H3
S01052-93	184.30	185.90	1.60	Composite Grab	Pebbly sand	H3
S01052-94	185.90	187.80	1.90	Composite Grab	Medium sand	H3
S01052-95	187.80	189.10	1.30	Composite Grab	Medium sand	H3
S01052-97	191.40	193.50	2.10	Composite Grab	*	*
S01052-98	193.50	195.10	1.60	Composite Grab	*	*
S01052-99	195.10	197.50	2.40	Composite Grab	*	*
S01052-100	197.50	199.20	1.70	Composite Grab	*	*
S01052-102	201.50	203.30	1.80	Composite Grab	*	*
S01052-103	203.30	205.80	2.50	Composite Grab	*	*
S01052-104	201.50	203.30	1.80	Composite Grab	*	*
S01052-105	210.20	210.70	0.50	Composite Grab	*	*
S01052-106	210.70	213.70	3.00	Composite Grab	*	*
S01052-107	213.70	215.70	2.00	Composite Grab	*	*
S01052-108	215.70	217.70	2.00	Composite Grab	Fine sand	CCUz
S01052-109	219.90	220.00	0.10	Composite Grab	Fine sand over silt	CCUz
S01052-110	222.40	222.70	0.30	Composite Grab	Fine sandy silt	CCUz
S01052-111	222.70	224.30	1.60	Composite Grab	Silty fine sand	CCUz
S01052-112	222.70	224.30	1.60	Composite Grab	Silty fine sand	CCUz
S01052-113	224.30	227.50	3.20	Composite Grab	*	*
S01052-114	227.70	229.20	1.50	Composite Grab	Sandy gravel	CCUg
S01052-116	231.70	233.70	2.00	Composite Grab	*	*
S01052-117	233.70	235.70	2.00	Composite Grab	*	*
S01052-118	235.70	238.00	2.30	Composite Grab	*	*
S01052-119	238.00	239.40	1.40	Composite Grab	*	*
S01052-121	241.70	243.80	2.10	Composite Grab	*	*
S01052-122	243.80	245.20	1.40	Composite Grab	*	*
S01052-124	246.00	247.50	1.50	Composite Grab	*	*
S01052-125	247.50	249.50	2.00	Composite Grab	*	*
S01052-126	249.50	252.40	2.90	Composite Grab	*	*
S01052-128	254.70	255.10	0.40	Composite Grab	*	*
S01052-129	254.70	255.10	0.40	Composite Grab	*	*

* Not examined

A.3.1 Particle Size Data for Sediments from Borehole 299-E33-46

The hydrometer method was used to determine the particle size distributions of several samples from 299-E33-46 as shown in Table A.19. No wet sieving was done to separate the gravel and sand fractions from each other so the particle size data shows only combined gravel + sand, silt, and clay fractions. The thin fine-grained lenses and CCU_z silts are highlighted in yellow shading in the table. One sample at the very top of the CCU_z (sample 109A) does not contain very much silt and clay even though it is assigned to the silt layer. The same situation was found at borehole 299-E33-45 (near tank BX-102) such that we conclude that the uppermost portion of the CCU_z unit near these two tank farms in the 200 East Area is in fact coarser grained than the middle and deepest portions.

Table A.19. Particle Size Distribution (percent by weight) in 299-E33-46 Sediments. Data are FIO. (Serne et al., 2008a)

ID	Depth (ft bgs)	% Gravel plus % Sand	%Silt	%Clay
Backfill				
No sample analyzed				
Hanford H2 Sand (upper sequence) Unit				
16A	41.72	95.90	2.60	1.50
26A	60.72	96.16	1.92	1.92
31B	69.95	96.10	2.96	0.94
Thin Fine Grained Lens				
No sample analyzed				
Hanford H2 Sand (middle sequence) Unit				
42A	90.62	91.31	2.79	5.91
74A	150.15	91.43	5.83	2.74
Hanford H2 Fine Grained Lens				
84	168.45	68.06	28.85	3.08
Hanford H3 Sand Unit				
96A	190.8	96.54	2.21	1.25
CCU Mud Unit---CCU_z				
109A	219.45	89.48	8.97	1.55
110A	222.05	7.00	85.73	7.27
113	225.9	53.74	39.82	6.44
CCU Gravel Unit---CCU_g				
120B	240.95	87.44	9.81	2.76

Fine grained samples are highlighted in yellow.

A.3.2 Particle Density for Sediments from Borehole 299-E33-46

The particle density for each of the 299-E33-46 borehole samples that were used in the hydrometer procedure is shown in Table A.20. The values are similar to those for uncontaminated sediment from the same lithologic facies found in the 200 West Area, and in general, about 0.05 to 0.10 g/cm^3 higher than values measured for the uncontaminated sediments from borehole 299-E33-338 located east of the B Tank Farm. The differences in particle density between the sediment samples from this contaminated borehole and the samples from the uncontaminated borehole are likely caused by analyst artifacts. Differences on the order of 0.1 g/cm^3 have been found on identical samples that were analyzed by three different lab staff during the characterization of the SX Tank Farm vadose zone sediments. There do not appear to be any statistically significant differences in the particle densities for the 299-E33-46 or for that

matter 299-E33-338 clean or background sediments versus lithologic unit. The average value for all the Hanford formation sediments for boreholes 299-E33-46 and 299-E33-338 is 2.76 ± 0.14 g/cm^3, similar to the value 2.78 g/cm^3 often used for Hanford formation sediments. The average particle density for the Cold Creek unit sediments from the two boreholes is 2.78 ±0.07 g/cm^3.

Table A.20. Particle Density of Bulk Sediment from 299-E33-46. Data are FIO. (Serne et al., 2008a)

ID	Depth[(a)] (ft bgs)	Ave. Particle Density (g/cm^3)	σ (g/cm^3)
Backfill			
No sample analyzed			
Hanford H2 Sand (upper sequence) Unit			
16A	41.72	2.81	0.097
26A	60.72	2.65	0.028
31B	69.95	2.90	0.238
Thin Fine-Grained Lens			
No sample analyzed			
Hanford H2 Sand (middle sequence) Unit			
42A	90.62	2.89	0.017
74A	150.15	2.91	0.047
Fine Grained Lens			
84	168.45	2.79	0.019
Hanford H3 Sand Unit			
96A	190.8	2.91	0.018
Plio-pleistocene Mud Unit			
109A	219.45	2.91	0.020
110A	222.05	2.82	0.024
113	225.9	2.71	0.061
Plio-pleistocene Gravel Unit			
120B	240.95	2.78	0.024

A.3.3 Oxide Composition of Sediments from Borehole 299-E33-46

Eleven samples of the bulk vadose zone sediment from the 299-E33-46 borehole were crushed and analyzed with XRF to obtain the complete composition of the sediment. The total oxide composition of the bulk sediments was used to aid in the quantification of mineralogy that will be discussed later.

The total elemental oxide composition for the bulk sediment is shown in Table A.21. Two types of XRF instruments were used. Assuming that the beryllium, boron, fluorine, and lithium contents of the sediment were small; the oxide mass of the sediment was calculated. All iron was also assumed to be Fe_2O_3. The mass balances for the bulk sediment vary from 90.3 to 99.3 wt%. The low mass balances for samples in the CCU_z unit appear to be caused by low silica and alumina values. Calcium, carbonate, iron, magnesium, potassium, sodium, and titanium comprise most of the oxides. The total concentration of many trace metals in the 299-E33-46 sediments are shown in Table A.22.

Table A.21. Total Composition of the Vadose Zone Sediment from 299-E33-46 Percent Weight as Oxides. Data are FIO. (Serne et al., 2008a)

ID	16A	26A	31B	42A	74A	84	96A	109A	110A	113	120B
Depth (ft)[a]	41.72	60.72	69.95	90.62	150.15	168.45	190.8	219.45	222.05	225.9	240.95
Unit	H2 upper	H2 upper	H2 upper	H2 middle	H2 middle	Thin silt	H3	CCU_z	CCU_z	CCU_z	CCUg
CO_2	0.66	0.29	0.55	0.51	0.48	0.48	0.40	0.46	0.99	0.81	0.29
Na_2O	2.23	2.37	1.98	2.53	2.65	2.73	2.52	2.15	1.06	1.67	2.20
MgO	1.00	1.15	1.16	1.25	1.43	1.27	1.05	1.72	1.32	1.96	1.19
Al_2O_3	11.80	12.28	11.76	12.00	12.61	12.98	11.67	12.79	13.91	12.06	10.94
SiO_2	69.96	70.38	65.68	68.67	71.03	70.38	66.96	66.32	60.54	60.97	64.61
P_2O_5	<0.275	<0.275	<0.275	<0.275	<0.275	<0.275	<0.298	<0.298	<0.275	<0.451	<0.298
SO_3	<0.062	<0.070	<0.080	<0.085	<0.085	<0.080	<0.085	<0.087	<0.080	<0.082	<0.090
Cl	<0.012	<0.013	<0.013	<0.012	<0.013	<0.012	<0.012	<0.013	<0.013	<0.012	<0.013
K_2O	2.25	2.36	2.42	2.19	2.25	2.17	1.92	2.09	2.28	1.86	1.61
CaO	3.68	3.53	3.12	3.54	3.51	3.50	3.96	3.47	2.88	3.97	4.11
TiO_2	0.70	0.66	0.60	0.69	0.63	0.64	0.80	0.63	0.87	0.80	0.98
V_2O_5	0.011	0.006	0.006	<0.006	<0.006	0.006	0.012	0.009	0.011	0.011	0.018
Cr_2O_3	0.004	0.005	0.006	0.006	0.008	0.009	0.006	0.010	0.010	0.008	0.006
MnO	0.063	0.058	0.058	0.069	0.072	0.067	0.073	0.067	0.070	0.099	0.095
Fe_2O_3	4.09	3.92	3.39	4.39	4.12	4.03	4.89	3.85	5.89	5.35	6.21
CoO	<0.006	0.009	<0.005	<0.006	0.006	<0.006	0.009	0.006	<0.006	<0.006	0.010
NiO	0.001	0.002	0.003	0.003	0.003	0.003	0.003	0.004	0.005	0.004	0.002
CuO	0.002	0.002	0.002	0.002	0.002	0.002	0.002	0.002	0.004	0.003	0.002
ZnO	0.007	0.006	0.005	0.006	0.006	0.006	0.006	0.006	0.011	0.008	0.008
Rb_2O	0.009	0.009	0.009	0.008	0.007	0.008	0.007	0.007	0.011	0.007	0.005
SrO	0.049	0.042	0.047	0.049	0.053	0.054	0.055	0.057	0.037	0.049	0.045
YO_2	0.003	0.002	0.002	0.002	0.002	0.003	0.002	0.002	0.004	0.003	0.003
ZrO_2	0.019	0.015	0.014	0.015	0.011	0.015	0.012	0.014	0.029	0.022	0.015
BaO	0.093	0.086	0.090	0.094	0.088	0.088	0.096	0.087	0.084	0.090	0.080
ThO_2	<0.001	<0.001	<0.001	0.001	0.001	0.001	0.001	<0.001	0.001	0.001	0.001
UO_3	0.004	0.002	0.002	0.002	0.001	0.001	0.001	<0.001	0.003	<0.001	<0.001
Total	96.99	97.54	91.28	96.41	99.34	98.82	94.85	94.14	90.40	90.31	92.83

Table A.22. Total Trace Constituents in Vadose Zone Sediment from 299-E33-46 in ug/g (ppm). Data are FIO. (Serne et al., 2008a)

ID	16A	26A	31B	42A	74A	84	96A	109A	110A	113	120B
Depth (ft)[a]	41.72	60.72	69.95	90.62	150.15	168.45	190.8	219.45	222.05	225.9	240.95
Unit	H2 upper	H2 upper	H2 upper	H2 middle	H2 middle	thin silt	H3	CCU_z	CCU_z	CCU_z	CCU_g
Ga	14.5	15.2	12.9	15.9	13	15.1	13.2	16	19	16.5	14.7
As	5.4	5.1	4.6	<2.5	4.8	5.8	<2.3	4.6	9.6	7.4	3.8
Se	1.7	<1.6	<1.6	<1.6	1.7	<1.7	<1.6	<1.6	<1.7	<1.7	<1.7
Br	<1.3	<1.3	<1.2	<1.3	<1.3	<1.3	<1.1	<1.1	<1.3	<1.3	<1.3
Nb	7.3	6.9	6.3	7.5	6.6	6.3	5.8	6.8	14.4	12.03	6.08
Mo	<1.9	<1.5	<1.5	1.7	1.5	1.7	1.5	<1.4	2.34	<1.8	<1.4
Ru	14	<9.9	<10	10	9.1	12	10	<8.4	<9.7	<11	<7.9
Rh	<14	<11	<11	11	10	13	11	<8.6	<10	<12	<8.1
Pd	<15	<11	<12	12	11	13	11	<9.9	<11	<12	<8.9
Ag	17	<13	<13	13	12	15	12	<10	<12	<13	<10
Cd	<19	<14	<15	14	13	17	14	<11	<14	<15	<11
In	<21	<16	<16	17	14	19	16	<13	<16	<17	<13
Sn	<23	<18	<18	18	16	21	17	<15	<17	<18	<14
Sb	<25	<19	<19	20	19	23	20	<17	<19	<20	<16
Te	<30	<22	<23	21	19	26	20	<17	<23	<22	<16
I	<37	<24	<27	29	23	33	27	<20	<27	<30	<20
Cs	<42	<35	<34	36	33	42	35	<28	35	<37	<27
La	<51	<38	<38	38	37	46	40	<33	<39	<39	<33
Ce	<67	<57	<60	62	60	75	57	<48	81	<66	<47
Hg	<3.7	<3.6	<3.5	<3.7	<3.8	4.9	<3.8	<3.6	<3.7	<3.8	<3.9
Pb	8.9	9.7	14.7	12.5	9.5	7.9	13.7	9	22.1	11.4	12.2

A.3.4 Carbon Content of Sediments from Borehole 299-E33-46

Table A.23 shows the total carbon, inorganic carbon, and organic carbon contents of the 299-E33-46 vadose zone sediment at selected depths along with average values for uncontaminated sediments. The inorganic carbon was also converted to the equivalent calcium carbonate content. The sediments in the backfill, upper sand sequence, and middle sand sequence of the H2 unit are relatively low in carbonate and organic carbon, with the calcium carbonate equivalent content ranging from 1.14% to 1.33% by weight. The two thin lenses in the Hanford H2 unit have slightly higher calcium carbonate contents (1.5 to 2.1 wt%). The Hanford H3 unit has only 1.1 wt% calcium carbonate equivalent content. The fine-grained CCU_z shows slightly higher calcium carbonate, averaging 1.7 wt%.

Table A.23. Carbon Content in Vadose Sediment from 299-E33-46. Data are FIO. (Serne et al., 2008a)

ID	Depth[a]	Total Carbon (wt%)	Inorganic Carbon (wt%)	Organic Carbon (wt%)	IC as $CaCO_3$ (wt%)
			Backfill		
02A	13.7	0.22	0.17	0.05	1.42
06A	21.12	0.18	0.13	0.05	1.08
10A	29.42	0.18	0.11	0.07	0.92
			Hanford H2 Sand (upper sequence) Unit		
16A	41.72	0.25	0.18	0.06	1.50
17A	44.02	0.29	0.24	0.05	2.00
18A	46.42	0.3	0.23	0.07	1.92
20A	50.62	0.28	0.22	0.06	1.83
21A	53.02	0.236	0.184	0.050	1.53
22	54.6	0.08	0.07	0.01	0.58
24	56.7	0.02	0.16	0.04	1.33
25	58.4	0.19	0.14	0.05	1.17
26C	59.72	0.18	0.13	0.05	1.08
26-A	60.72	0.17	0.08	0.09	0.67
27	62.1	0.17	0.13	0.04	1.08
29	66.05	0.14	0.09	0.05	0.75
31B	69.95	0.19	0.15	0.04	1.25
31A	70.45	0.23	0.19	0.05	1.58
33	73.5	0.23	0.17	0.06	1.42
35	77.35	0.2	0.2	0	1.67
36A	79.95	0.18	0.14	0.04	1.17
38A	83.05	0.21	0.17	0.04	1.42
Background Upper H2 Sand					**1.23±0.23**
			Thin Fine Grained Lens		
39	84.55	0.25	0.18	0.07	1.50
			Hanford H2 Sand (middle sequence) Unit		
41	87.85	0.16	0.1	0.06	0.83
42A	90.62	0.19	0.14	0.04	1.17
46	96.8	0.19	0.15	0.04	1.25
47A	98.62	0.15	0.12	0.03	1.00
53A	111.42	0.22	0.18	0.04	1.50
57A	119.92	0.18	0.14	0.04	1.17
64A	131.85	0.14	0.1	0.04	0.83
69A	140.05	0.38	0.31	0.07	2.58
74A	150.15	0.165	0.13	0.035	1.08

ID	Depth[a]	Total Carbon (wt%)	Inorganic Carbon (wt%)	Organic Carbon (wt%)	IC as $CaCO_3$ (wt%)
79A	160.15	0.14	0.09	0.05	0.75
82A	164.55	0.18	0.12	0.06	1.00
83A	166.85	0.18	0.14	0.04	1.17
Background Middle H2 Sand					**1.23±0.23**
			Fine Grained Lens		
84	168.45	0.19	0.13	0.06	1.08
Background Fine Grained Lens					**NA**
			Hanford H2 Sand Unit		
86A	171.15	0.33	0.25	0.08	2.08
			Hanford H3 Sand Unit		
90A	179.85	0.19	0.16	0.03	1.33
96A	190.8	0.13	0.11	0.02	0.92
101A	200.95	0.19	0.15	0.04	1.25
105A	209.95	0.14	0.1	0.04	0.83
Background H3 Sand					**0.67±0.01**
			CCU_z Mud Unit		
109A	219.45	0.175	0.125	0.05	1.04
110A	222.05	0.34	0.27	0.09	2.25
113	225.9	0.22	0.22	0.00	1.83
Background CCU_z					**1.69±0.28**
			CCU_g Gravel Unit		
115A	230.75	0.13	0.09	0.04	0.75
120B	240.95	0.09	0.08	0.01	0.67
120A	241.45	0.1	0.06	0.04	0.50
123A	245.75	0.03	0	0.03	0.00
127A	253.15	0.08	0.02	0.06	0.17
Background CCU_g					**0.72**

A.3.5 Mineralogy of Sediments from Borehole 299-E33-46

XRD analysis of the 11-bulk sediment samples shows the samples collected from the Hanford formation (16A, 26A, 31B, 42A, 74A, and 84A) to be mineralogically similar. The sediments are mostly quartz and feldspar (both plagioclase and alkali-feldspar), with trace amounts of mica, chlorite, and an amphibole. Samples examined from the lower Hanford unit [H3] along with samples from the Cold Creek Mud unit [CCU_z] and Cold Creek Gravel unit [CCU_g] contain quartz and feldspars, along with significant amounts of clay material, predominantly mica and chlorite.

The XRD tracing of a typical sediment sample (110A) from the CCU_z is provided in Figure A.11, along with a quartz reference pattern. The main reflection for quartz is 26.63° 2θ, followed by less intense reflections at 20.86, 36.53, 39.46, 42.43, 50.12, 59.92° 2θ. The main reflections associated with feldspar minerals are found between 27.34° 2θ and 27.92° 2θ, with the higher 2θ values belonging to the plagioclase series. Chlorite and mica minerals were identified on the X-ray tracings by the reflections at 6.3° 2θ and 8.8° 2θ, respectively. The presence of an amphibole was established by the characteristic 100% reflection at 10.5° 2θ. Additionally, trace amounts of the zeolite, laumontite, were identified in most of the samples by a diffraction peak positioned at 9.36° 2θ.

The XRD tracings from samples 96A and 109A indicate an unusually high concentration of the amphibole mineral (hornblende) compared to all the other samples. Hornblende is typically found in most Hanford sediments, but only in trace amounts.

Mineral analysis results are provided in Table A.24. Quartz concentrations ranged from 22.4 wt% (96A) to 43.5 wt% (31B), with an average concentration of 33±6 wt%. The borehole sediment contained plagioclase feldspar concentrations from 10 to 34 wt% and potassium feldspar content measured between 8 to 37 wt%. Plagioclase feldspar was more abundant than potassium feldspar in all but three samples (16A, 26A, and 84A). Overall, the feldspar content (both plagioclase and alkali feldspars) averaged about 43±6 wt%. The amphibole phase comprised <9 wt% at most, with the majority of samples having concentrations in the 2 to 4 wt% range.

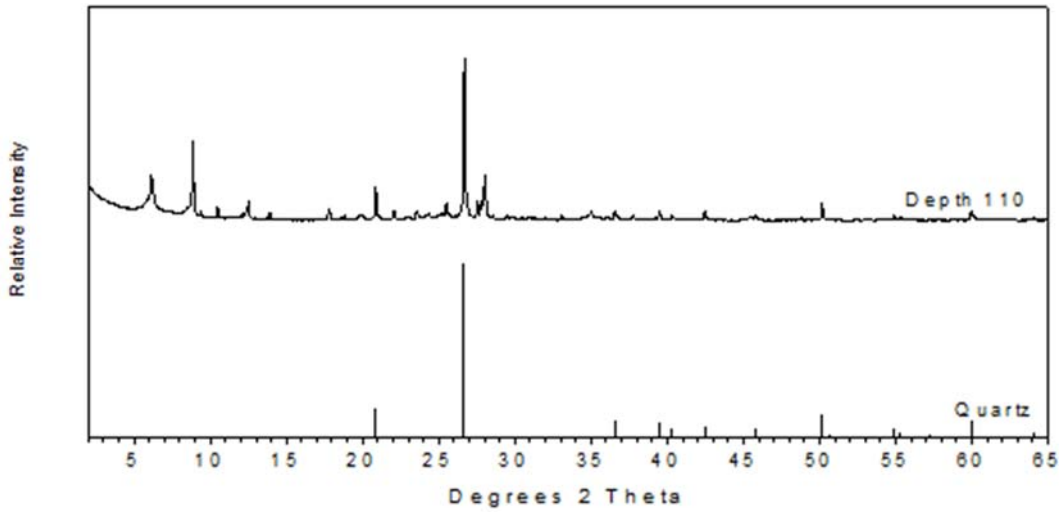

Figure A.11. XRD Tracing of Sample 110A along with the Standard Reference Pattern for Quartz. Data are FIO. (Serne et al., 2008a)

Table A.24. Semi-quantitative XRD Results of Minerals from the S01052 Borehole. Data are FIO. (Serne et al., 2008a)

	Mineral Phase (wt%)						Goodness of fit[(a)]
Sample ID	Quartz	Amphibole	Plagioclase	K-Spar	Mica	Chlorite	
Hanford H2 Sand (upper sequence) Unit							
16A	34.8	1.0	12.7	36.6	10.4	4.5	0.57
26A	33.3	0.5	9.6	37.2	14.2	5.2	0.78
31B	43.5	2.8	27.4	13.2	9.1	4.0	0.46
Hanford H2 Sand (middle sequence) Unit							
42A	38.5	3.1	28.5	16.5	9.4	4.0	0.41
74A	39.6	2.0	23.0	20.2	11.8	3.5	0.71
H2 Fine Grained Lens							
84A	34.5	2.9	19.5	29.1	8.5	5.6	0.81
Hanford H3 Sand Unit							
96A	22.4	4.0	29.1	12.3	27.0	5.2	0.22
CCU_z Mud Unit							
109A	31.1	7.6	27.9	14.3	7.5	11.7	0.22
110A	26.5	4.7	14.1	18.8	14.6	21.2	0.30
113A	25.3	3.5	24.8	7.8	31.7	6.9	0.17
CCU_g Gravel Unit							
120B	32.6	8.7	34.1	13.4	6.5	4.6	0.20

(a) 1.0 represents ideal goodness of fit.

Clay minerals identified in the whole rock sediment included mica and chlorite. Mica concentrations ranged from a low of 6.5 wt% (120B) to a high of 32 wt% (113A), with most of the intervals having concentrations between 7 and 15 wt%. Chlorite concentrations were <7 wt% in all sediments analyzed with the exception of two samples in the CCU_z. Samples 109A and 110A contained 11.7 and 21.2 wt% chlorite, respectively. Smectite and kaolinite minerals were not identified in the whole rock sediment samples due in part to the sample preparation technique and the low overall concentration.

XRD analysis was performed on the <2 micron fraction of each sample, and the results are presented below. The clay fraction is dominated by four clay minerals: smectite, chlorite, illite, and kaolinite with minor amounts of quartz and feldspar. Figure A.12 provides XRD-tracings of a typical clay fraction (from sample 110A) following four different treatments. Smectites are considered the fraction of the Mg-saturated sub-sample that gives a basal reflection at 5.85° 2θ and expands to 5.28° 2θ upon solvation with ethylene glycol (Amonette 1991). Saturation with a K^+ cation shifts the reflection down to 7.3° 2θ followed by the irreversible collapse to 8.88° 2θ after heating for 1 hour at 575°C.

Illite is the simplest of the four clay mineral phases to identify in this sediment. The basal reflections are located at 8.88, 17.8, and 26.7° 2θ. The various treatments including cation saturation, solvation with ethylene glycol, and heating do not affect the structure of the illite. This is shown in Figure A.12 by examination of the illite basal reflection at 8.88° 2θ. The increase in intensity of the 8.88° 2θ reflection between the heated and the unheated K-saturated sample is due to the incorporation of the smectite reflection resulting from the smectite structure collapsing.

Chlorites are identified by their basal series of diffraction peaks at 6.24, 12.5, 18.8, and 25.2° 2θ, which are unaffected by cation saturation or ethylene glycol solvation. Heating to 575°C shifts the first order reflection to 6.37° 2θ and also tends to diminish or eliminate the higher order reflections (12.5, 18.8, and 25.2° 2θ) as shown in Figure A.12. Kaolinite is difficult to identify in the presence of a chlorite mineral. Basal reflections characteristic to kaolinite are positioned at 12.5 and 24.9° 2θ, which are superimposed on the even-order chlorite peaks. These kaolinite reflections are unaffected by cation saturation and ethylene glycol solvation. When heated, the kaolinite structure becomes amorphous and the reflections are eliminated. Positive identification of kaolinite in the presence of chlorite can be determined by examination of the 24.9 to 25.2° 2θ region of the XRD tracing. The kaolinite basal reflection at 24.9° 2θ can be distinguished from the chlorite 25.2° 2θ reflection (Figure A.12).

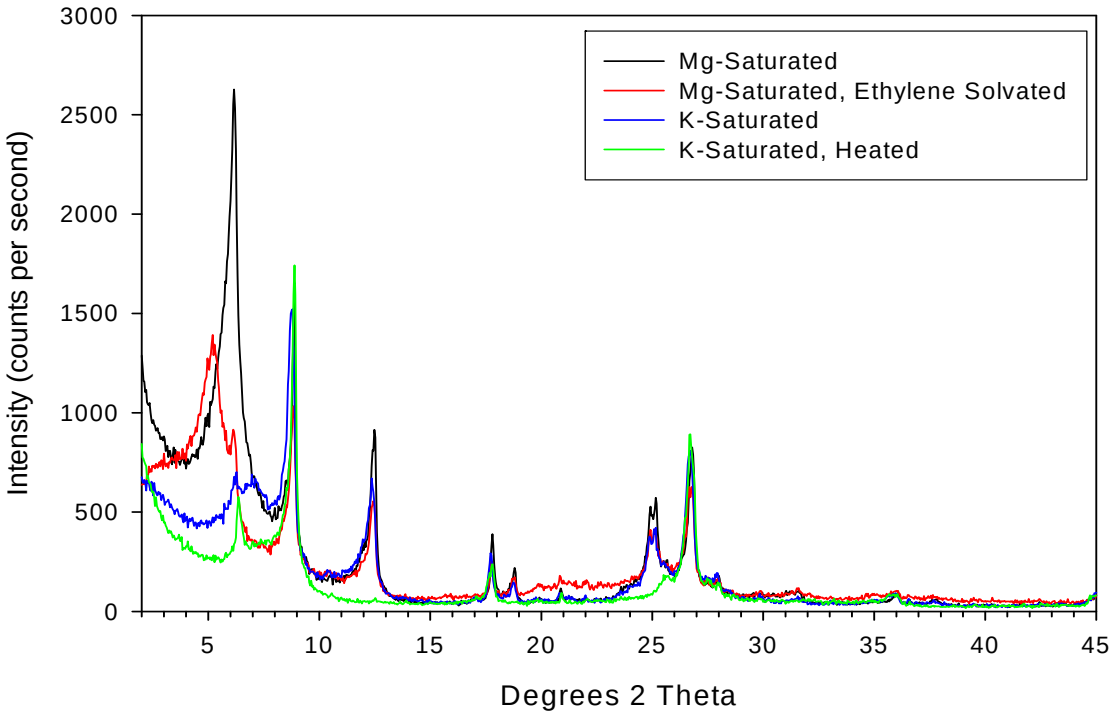

Figure A.12. XRD Tracings of Preferentially Oriented Clay Slides Taken from Borehole 299-E33-46 Sample 110A. The scans were collected from 2 to 45° 2θ with a 0.04° step and 2-second dwell time. The black line represents the Mg-saturated fraction and the red line represents the same fraction solvated with ethylene glycol. The blue line indicates the saturation with K+ cation and the green line is the K+-saturated sample heated to 575°C for 1 hour. Data are FIO. (Serne et al., 2008a)

Trace amounts of quartz are evident by the diffraction peak located at 20.85° 2θ. The 100% reflection for quartz (26.6° 2θ) is hidden by the third basal reflection of illite located at 26.6° 2θ.
Plagioclase feldspar is also identified in the clay fraction by the minor diffraction peak at 27.8° 2θ.

Results of the clay minerals in the < 2 micron fraction are presented in Table A.25. Total recoveries were normalized to 100%, and the normalization factor used for each sample is provided in the last column. Smectites ranged in concentrations from a low of 22 wt% (74A) to a high of 50 wt% (110A). Illite amounts varied from 30 to 56 wt% with the majority of samples having concentrations in the 40 to 50 wt% range. Chlorite and kaolinite were the least abundant of the clay minerals identified in the samples with concentrations equal to or less than 20 wt% and 9 wt%, respectively. Quartz and feldspar minerals were present as trace amounts in the clay fraction and therefore were not included in totals presented in Table A.25.

Total clay recoveries were within ±25% of the ideal target for 8 of the 11 samples analyzed. Factors affecting the semi-quantification procedure (preparation and condition of the clay filter cake) were generally controlled and not thought to be a significant factor. Quantitative analysis is considered reasonable if errors amount to ±10% of the amounts present for major constituents and ±20% for minerals whose concentrations are less than 20% (Moore and Reynolds 1989).

Table A.25. Semi-quantitative XRD Results of Clay Minerals from Sediment Collected from Borehole 299-E33-46. Data are FIO. (Serne et al., 2008a)

Sample ID	Mineral Phase (wt%)				Normalization Factor
	Smectite	Illite	Chlorite	Kaolinite	
16A	30	48	12	9	0.87
26A	27	52	13	8	0.86
31B	23	56	12	9	0.67
42A	35	44	13	8	0.66
74A	22	53	18	8	1.01
84A	46	30	20	5	1.25
96A	32	44	16	9	1.10
109A	28	49	17	6	0.88
110A	50	38	6	6	0.75
113A	32	46	13	9	0.84
120B	39	40	15	6	2.26

A.4 Pit 30 and IDF Excavation (200 East Area) Sediments

Some near-surface Hanford formation sediments from the side walls of Pit 30 located west of the 200 East Area and from the large IDF excavation have been characterized. More details are found in Um et al. (2009). Figure A.13 shows the location of Pit 30 and the IDF excavation. All the sediment samples were obtained from the sidewalls using shovels and constitute disturbed grab samples from the Hanford formation. Individual samples vary in particle size from gravel-dominated H1a to sand-dominated H1 and fine sand silt lenses within the H1 sands.

A.4.1 Sediment Characterization

The Pit 30 and IDF grab samples were characterized for particle size (see Table A.26), total oxide composition (Table A.27), surface area (Table A.28, carbon content (Table A.29), and hydrous iron and manganese oxide content (Table A.30 and Table A.31, respectively).

Total elemental composition of these sediments shows that Si and Al are the major elements (74-83 wt% of total) and Ca and Fe make up the next most abundant elements (6-10 wt%). Although Al and Si contents between the bulk and less than 2 mm fractions are similar or slightly higher in less than 2 mm fraction in Pit 30-1, 30-3, and 30-4 sediments, elemental Fe and Ca contents show noticeably higher values in the bulk fraction for those sediments (Table A.27). Higher Fe and Ca contents in the bulk fraction of Pit 30 sediments indicate that there are more gravel fractions containing high calcium carbonate and Fe oxide coatings on the gravel surfaces. The highest elemental Fe content (8.2 wt%) was found in Pit 30-4 sediment, which has the highest gravel fraction (88 wt%) among the selected sediments, indicating presence of potential reactive sorbents (e.g., Fe oxides) in the gravel fraction. However, because this elemental analysis was conducted through total fusion process, some of Fe content could be from dissolution of clays, which also can coat the gravel surfaces, containing Fe in mineral structure.

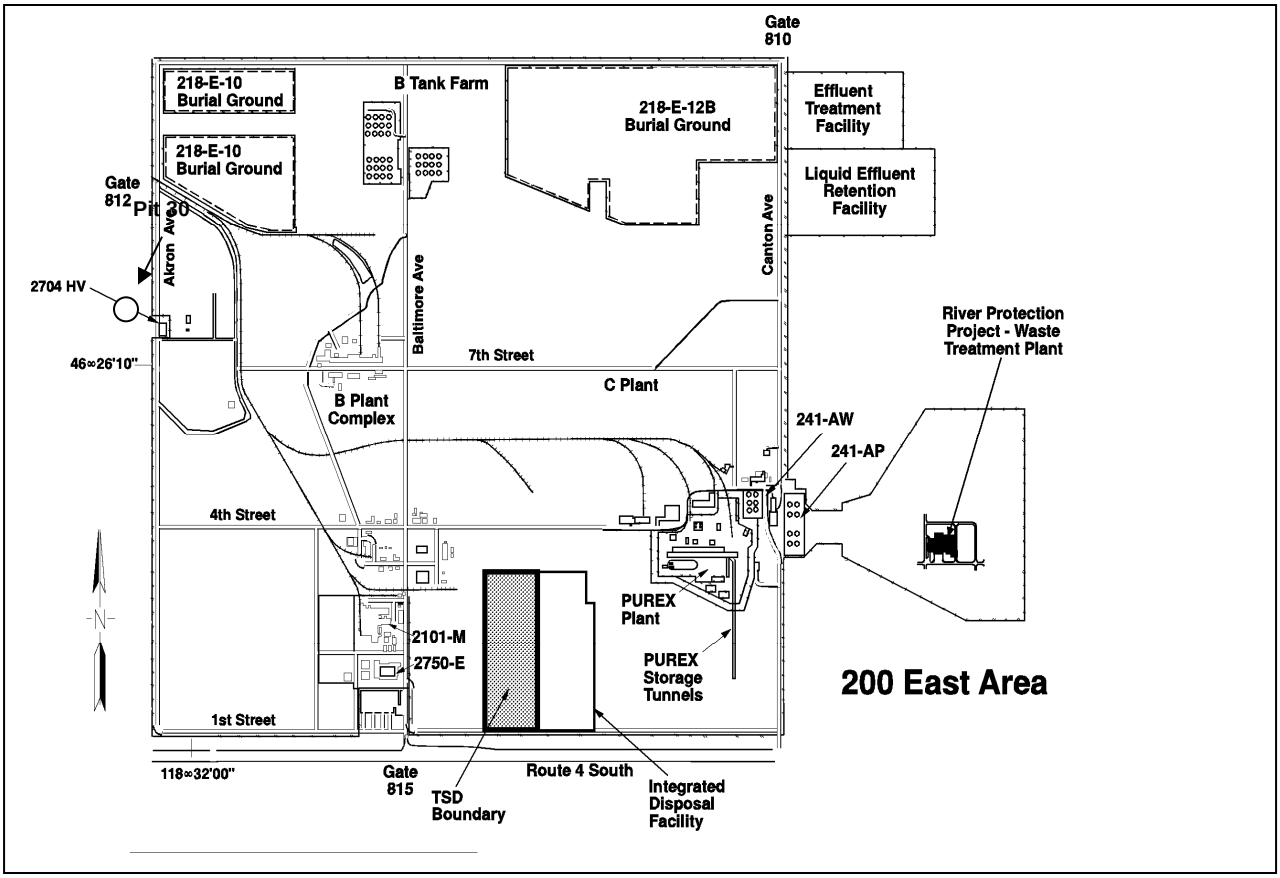

Figure A.13. Location of the Pit 30 and IDF Facility Excavations where Sediments Were Obtained.

Although the BET surface area was measured for both bulk and less than 2 mm fractions, because of the small diameter neck (~ 1 cm) of the surface analyzer sampling tubes, particles larger than 1 cm could not be included in the samples on which surface area was measured. However, the measured specific surface areas of less than 2 mm fraction for Pit 30-3 and Pit 30-4 were smaller than the surface areas measured for the bulk samples, despite the fact that the bulk sediment contains a significant portion of particles up to 1 cm in diameter. This is counter-intuitive since specific surface area is usually inversely correlated with particle size. This result may indicate the presence of high surface area materials such as Fe oxide coatings on the gravel surfaces.

Table A.26. Particle Size Distribution (wt%) of Hanford Formation Sediments. Data are FIO. (Um et al., 2009)

	Gravel	Sand	Silt	Clay
Sample ID	> 2 mm	53 µm – 2 mm	2 µm – 53 µm	< 2 µm
IDF-1 (bulk) H1	0.62	97.6	1.49	0.33
IDF-2A (bulk) silt lens	0.39	70.9	26.3	2.46
IDF-2B (bulk) silt lens	0.06	70.8	26.9	2.30
Pit 30-1 (bulk) H1	18.4	80.3	0.64	0.69
Pit 30-2 (bulk) H1a	30.1	60.1	7.11	2.64
Pit 30-3 (bulk) H1a	38.6	60.6	0.46	0.37
Pit 30-4 (bulk) H1a	88.4	11.0	0.41	0.21

Table A.27. Total Elemental Composition (wt%) of the Hanford formation Sediments.[(a)] Data are FIO. (Um et al., 2009)

Sample ID	Na_2O	MgO	Al_2O_3	SiO_2	K_2O	CaO	TiO_2	Fe_2O_3	LOI[#]	Total
Pit 30-1 (<2 mm)	2.81	1.63	12.6	69.2	2.35	3.39	0.61	4.51	2.3	99.8
Pit 30-3 (<2 mm)	2.69	1.55	12.4	69.7	2.53	3.16	0.54	3.84	2.5	99.2
Pit 30-4 (<2 mm)	2.61	1.63	12.8	69.8	2.56	3.07	0.63	4.48	2.3	100
IDF-1 (bulk)	2.74	1.48	12.5	70.7	2.51	3.17	0.52	3.75	2.2	99.8
IDF-2A (bulk)	2.14	1.57	11.7	71.1	2.59	2.94	0.58	3.98	3.1	100
IDF-2B (bulk)	1.90	1.61	11.6	71.3	2.62	2.87	0.57	3.82	3.6	100
Pit 30-1 (bulk)	2.76	1.84	12.6	68.2	2.22	3.87	0.77	5.17	2.3	100
Pit 30-2 (bulk)	2.19	1.80	12.4	68.3	2.60	3.34	0.70	4.68	3.4	99.8
Pit 30-3 (bulk)	2.74	2.16	12.7	66.5	2.20	4.31	0.89	6.01	2.0	99.9
Pit 30-4 (bulk)	2.78	3.16	13.6	60.0	1.56	6.49	1.32	8.23	1.7	99.4

(a) Minor amounts of elements (P_2O_5, V_2O_5, Cr_2O_3, MnO, ZnO, SrO, and BaO) are not shown in the table.
LOI = Loss on ignition.

Table A.28. Surface Area of Hanford formation Sediments from Pit 30 and IDF Excavation. Data are FIO. (Um et al., 2009)

Sediments	Surface area (m^2/g)
IDF-1 (< 2 mm)	ND
IDF-2A (< 2 mm)	ND
IDF-2B (< 2 mm)	ND
Pit 30-1 (< 2 mm)	3.93 ± 0.01
Pit 30-2 (< 2 mm)	ND
Pit 30-3 (< 2 mm)	4.38 ± 0.03
Pit 30-4 (< 2 mm)	5.39 ± 0.01
IDF-1 (bulk)	3.34 ± 0.02
IDF-2A (bulk)	5.57 ± 0.02
IDF-2B (bulk)	6.49 ± 0.02
Pit 30-1 (Bulk)	3.97 ± 0.01
Pit 30-2 (Bulk)	5.90 ± 0.02
Pit 30-3 (Bulk)	7.27 ± 0.02
Pit 30-4 (Bulk)	7.81 ± 0.02

Table A.29. Inorganic Carbon Content (as $CaCO_3$) in IDF and Pit 30 Sediments. Data are FIO. (Um et al., 2009)

Sediments	Inorganic Carbon as $CaCO_3$ (wt%)
IDF-1 (< 2mm)	ND
IDF-2A (< 2mm)	ND
IDF-2B (< 2mm)	ND
Pit 30-1 (< 2mm)	1.75 ± 0.06
Pit 30-2 (< 2mm)	ND
Pit 30-3 (< 2mm)	0.94 ± 0.02
Pit 30-4 (< 2mm)	1.29 ± 0.12
IDF-1 (bulk)	1.61 ± 0.32
IDF-2A (bulk)	2.70 ± 0.11
IDF-2B (bulk)	2.96 ± 0.29
Pit 30-1 (Bulk)	1.26 ± 0.10
Pit 30-2 (Bulk)	1.39 ± 0.04
Pit 30-3 (Bulk)	2.28 ± 0.08
Pit 30-4 (Bulk)	0.95 ± 0.01

ND = not determined

None of the sediments are significantly rich in calcium carbonate and the measured values are quite similar to uncontaminated Hanford formation sediments (Horton et al. 2003).

As mentioned, the surface area data suggested that iron oxide coatings might explain the unexpected results in which higher surface areas were found on bulk as opposed to the <2 mm fraction of several of the Pit 30 sediments. Therefore, more detailed characterization using chemical extractions was performed to measure hydrous oxide contents in the sediments.

The Tamm's and dithionite-citrate-bicarbonate (DCB) methods were used to determine the content of amorphous Fe oxide (ferrihydrite) and total free Fe including crystalline Fe oxides (hematite and goethite), respectively. Because the IDF sediments contained very low amounts of gravel, the amount of Fe extracted by Tamm's and DCB methods were very similar between the bulk and less than 2 mm fractions (Table A.30). However, both Tamm's and DCB extraction showed slightly higher Fe content in the less than 2 mm fraction of Pit 30 sediments, except Pit-30-3 sediment. Only Pit 30-3 sediment showed higher Fe oxide contents in the bulk fraction than sediment less than 2 mm fraction (Table A.30), indicative of more Fe oxides present on gravel fraction in Pit 30-3 sediment.

Table A.30. Extractable Fe µmol/g and % of total Fe in Sediment. Data are FIO. (Um et al., 2009)

	Extracted Fe (µmol/g)		% Fe Extracted	
Sediments	Tamm's	DCB	Tamm's	DCB
IDF-1 (< 2mm)	6.02 ± 0.53	12.9 ± 3.19	1.28%	2.75%
IDF-2A (< 2mm)	12.1 ± 0.07	40.9 ± 0.25	2.43%	8.21%
IDF-2B (< 2mm)	13.1 ± 1.16	49.7 ± 0.70	2.63%	9.97%
Pit 30-1 (< 2mm)	5.53 ± 1.09	14.1 ± 0.06	0.98%	2.50%
Pit 30-2 (< 2mm)	9.75 ± 0.09	65.2 ± 0.54	1.66%	11.12%
Pit 30-3 (< 2mm)	3.74 ± 0.33	11.4 ± 1.92	0.78%	2.37%
Pit 30-4 (< 2mm)	5.09 ± 0.26	23.3 ± 1.44	0.91%	4.15%
IDF-1 (bulk)	6.10 ± 0.82	12.1 ± 0.65	1.30%	2.58%
IDF-2A (bulk)	11.9 ± 0.57	40.2 ± 1.20	2.39%	8.06%
IDF-2B (bulk)	13.8 ± 2.16	50.6 ± 0.59	2.88%	10.58%
Pit 30-1 (Bulk)	5.07 ± 2.02	14.5 ± 0.78	0.78%	2.24%
Pit 30-2 (Bulk)	9.37 ± 2.40	56.3 ± 2.17	1.60%	9.61%
Pit 30-3 (Bulk)	4.30 ± 0.40	15.9 ± 0.90	0.57%	2.11%
Pit 30-4 (Bulk)	4.55 ± 0.29	22.1 ± 0.70	0.44%	2.14%

The DCB extraction removed more iron than the less aggressive Tamm's extraction, which dissolves both amorphous and crystalline iron oxides. Table A.31 shows the amount on manganese that was dissolved from the sediments. The manganese values in the table bracketed with parentheses are very close to the detection limit of the analytical instrument, inductively coupled plasma optical emission spectrometry, used to measure the extracts and are considered less than values.

Table A.31. Extractable Mn µmol/g and % of total Mn in Sediment. Data are FIO. (Um et al., 2009)

	Extracted Mn (µmol/g)		% Mn Extracted	
Sediments	Tamm's	DCB	Tamm's	DCB
IDF-1 (< 2mm)	(1.16E+00)	9.83E-01	<13.7%	11.6%
IDF-2A (< 2mm)	(2.14E+00)	2.34E+00	<25.4%	27.7%
IDF-2B (< 2mm)	(2.54E+00)	2.66E+00	<30.0%	31.4%
Pit 30-1 (< 2mm)	(1.09E+00)	1.14E+00	<11.0%	11.5%
Pit 30-2 (< 2mm)	(3.37E+00)	3.02E+00	<29.9%	26.8%
Pit 30-3 (< 2mm)	(6.13E-01)	1.05E+00	<7.2%	12.4%
Pit 30-4 (< 2mm)	(1.47E+00)	1.62E+00	<14.8%	16.4%
IDF-1 (bulk)	(8.12E-01)	9.77E-01	<9.6%	11.5%
IDF-2A (bulk)	(2.25E+00)	2.14E+00	<26.6%	25.3%
IDF-2B (bulk)	(2.49E+00)	2.72E+00	<29.4%	32.1%
Pit 30-1 (Bulk)	(7.45E-01)	1.17E+00	<6.6%	10.4%
Pit 30-2 (Bulk)	(2.58E+00)	2.52E+00	<22.9%	22.3%
Pit 30-3 (Bulk)	(5.90E-01)	8.03E-01	<4.6%	6.3%
Pit 30-4 (Bulk)	(1.11E+00)	1.41E+00	<6.1%	7.7%

A.5 Borehole 299-E33-338

Borehole 299-E33-338 is located near the southeast corner of the 241-B Tank Farm in the 200 East Area. The vadose zone portion of this borehole was drilled using the drive-barrel cable tool technique wherever possible. The borehole was drilled without the aid of drilling fluids such as water or mud, unless noted in the geology logs, to minimize the introduction of artificial moisture into the sediment cores. The borehole

was drilled to a total depth of 80.05 m (275.75 ft) bgs (Horton 2002). The water table was contacted at 77.5 m (254.2 ft) bgs and the top of basalt at 82.6 m (271 ft) bgs. Samples to the top of basalt were collected via a drive barrel/split spoon, before switching to a hard tool to drill 5 ft into the basalt.

Nearly continuous core was obtained down to a depth of ~78.6 m (258 ft) bgs. A total of 202 1-ft-long by 4-in.-diameter cores were retrieved, which accounts for ~75% the total length of the borehole. Each 2-ft splits poon contained two 1-ft lexan-lined core segments. Sediment cores were collected by driving a 10-cm (4-in.)-diameter 76-cm (2.5 in.)-long split spoon sampling device ahead of the drilled borehole. The borehole was then cleaned to the bottom of the cored interval prior to the next sampling interval. Field borehole logs indicate that hard tool drilling began at ~271 ft at the top of the basalt and continued to a final depth of ~275.5 ft bgs. The split spoon cores were contained in 30-cm (1-ft)-long, transparent, lexan core barrel liners (core sleeves). Core recovery was generally 100%; however, in some intervals of higher gravel content (~65%) within the first 15 ft, recovery was as low as 40%. In addition to lexan-lined core samples, sediment grab samples were collected in the field from cuttings recovered during drilling and/or from the split spoon drive shoe.

A.5.1 Characterization of Sediments from Borehole 299-E33-338

The characterization data for borehole 299-E33-338 have been previously published in Lindenmeier et al. (2003). Table A.32 lists the characterization samples and reports on particle size distribution, total and inorganic carbon content, total chemical composition, and mineralogy.

Table A.32. 299-E33-338 Cores Analyzed for Mineralogy and Geochemistry Details (depth and lithology). Data are FIO. (Lindenmeier et al., 2003)

Core Sample ID	Depth Interval (ft)	Top Depth (ft)	Bottom Depth (ft)	Mid-Depth (ft)	Lithology	Strati-graphic Unit	Comments
C3391-15.5	15.5-16.5	15.5	16.5	16.0	Silty sandy gravel	H1	
C3391-17.5	17.5-18.5	17.5	18.5	18.0	Gravelly sand	H1	
C3391-51.05	51.05-52.05	51.1	52.1	51.6	Silty sandy gravel/silty sand	H1/H2	
C3391-77.3	77.3-78.3	77.3	78.3	77.8	Gravelly sand	H2	
C3391-90.75	90.75-91.75	90.8	91.8	91.3	Sand	H2	
C3391-107.3	107.3-108.3	107.3	108.3	107.8	Sand	H2	
C3391-115.4	115.4-116.4	115.4	116.4	115.9	Sand	H2	
C3391-133	133-134	133.0	134.0	133.5	Sand	H2	
C3391-160.3	160.3-161.3	160.3	161.3	160.8	Sand	H2	
C3391-161.35	161.35-162.35	161.4	162.4	161.9	Silty sand	H2	
C3391-171.45	171.45-172.45	171.5	172.5	172.0	Sand	H2	
C3391-173.05	173.05-174.05	173.1	174.1	173.6	Sand/silt	H2	
C3391-198.1	198.1-199.1	198.1	199.1	198.6	Gravelly sand	H3	
C3391-200.1	200.1-201.1	200.1	201.1	200.6	Silty sand	H3	Organic matter and tephra present; paleosol?
C3391-213.8	213.8-214.8	213.8	214.8	214.3	Sand	CCUz	
C3391-218.7	218.7-219.7	218.7	219.7	219.2	Silt	CCUz	
C3391-219.7	219.7-220.7	219.7	220.7	220.2	Silt	CCUz	
C3391-220.65	220.65-221.65	220.7	221.7	221.2	Sandy silt	CCUz	
C3391-221.65	221.65-222.65	221.7	222.7	222.2	Sandy silt	CCUz	
C3391-239.8	239.8-240.8	239.8	240.8	240.3	Silty sandy gravel	CCUg	

A.5.2 Particle Size Distribution for Sediments from Borehole 299-E33-338

Figure A.14 is a bar chart showing the particle size distribution of the sediment samples. The figure shows that the Hanford formation sediments are predominantly sand with some gravel and silt/clay. At about 220 ft bgs, the silt dominated Cold Creek Unit silt (CCU_z) layer is found. This layer is about 20 ft thick at this location and overlies the gravel-dominated Cold Creek Unit gravel (CCU_g), also often called CCU_c, when encountered in the 200 West Area representing calcium carbonate or caliche rich sediments.

A.5.3 Carbon Content in Sediments from 299-E33-338

Table A.33 shows the total, inorganic, and organic carbon content of the sediments, with the latter simply calculated as the difference between total and inorganic carbon. As shown, the calcium carbonate content of the CCU_g sample from ~240 ft bgs does not contain elevated concentrations of caliche.

A.5.4 Total Oxide Content in Sediments from 299-E33-338

Table A.34 lists the total oxide content of the major constituents of the sediments from borehole 299-E33-338 and Table A.35 shows the total elemental concentration of minor and trace metals in the sediment as measured on sediment fused using lithium metaborate.

A.5.5 Mineralogy of Sediments from 299-E33-338

XRD analysis was conducted on sediment collected from borehole 299-E33-338, which was represented by two stratigraphic units: the Hanford formation and the Cold Creek unit. The Hanford formation is divided into three facies, with the shallowest being identified as H1 coarse sand, followed by the H2 facies, and the deepest being the H3 facies. Samples examined from H1 facies (15.5 to 51.05 ft) were dominated by quartz, with lesser amounts of feldspar. Mica and chlorite appeared as trace amounts, with the relative concentrations of both clay minerals increasing with depth. Hornblende also appeared in detectable amounts, with concentrations following the mica and chlorite abundance profile. Samples collected from the H2 facies (77.3 ft to 171.45 ft) appeared to be similar to the above facies, with perhaps more of a weathered profile. Clay minerals such as micas and chlorites are more abundant in this facies and are easily detected by XRD. Samples examined from the H3 facies also exhibited similar characteristics as the two earlier facies (i.e., H1 and H2). Sediment from the Cold Creek mud unit and Cold Creek gravel unit contain quartz and feldspars, along with significant amounts of clay material, predominantly mica and chlorite. Additionally, these samples contain hornblende in minor to trace concentrations, along with trace amounts of laumontite. For example, the XRD tracing of a typical sediment sample at 198.1-ft (CCU_z) mud unit is provided in Figure A.15, along with quartz and plagioclase reference patterns. The main reflection for quartz is 26.63° 2θ, followed by less intense reflections at 20.86, 36.53, 39.46, 42.43, 50.12, 59.92° 2θ. The primary reflections associated with feldspar minerals are found between 27.34° 2θ and 27.92° 2θ, with the higher 2θ values belonging to the plagioclase series. Chlorite and mica minerals were identified on the X-ray tracings by the reflections at 6.3° 2θ and 8.8° 2θ, respectively. The presence of hornblende was established by the characteristic 100% reflection at 10.5° 2θ. Additionally, trace amounts of the zeolite, laumontite, were identified in most of the samples by a diffraction peak positioned at 9.36° 2θ.

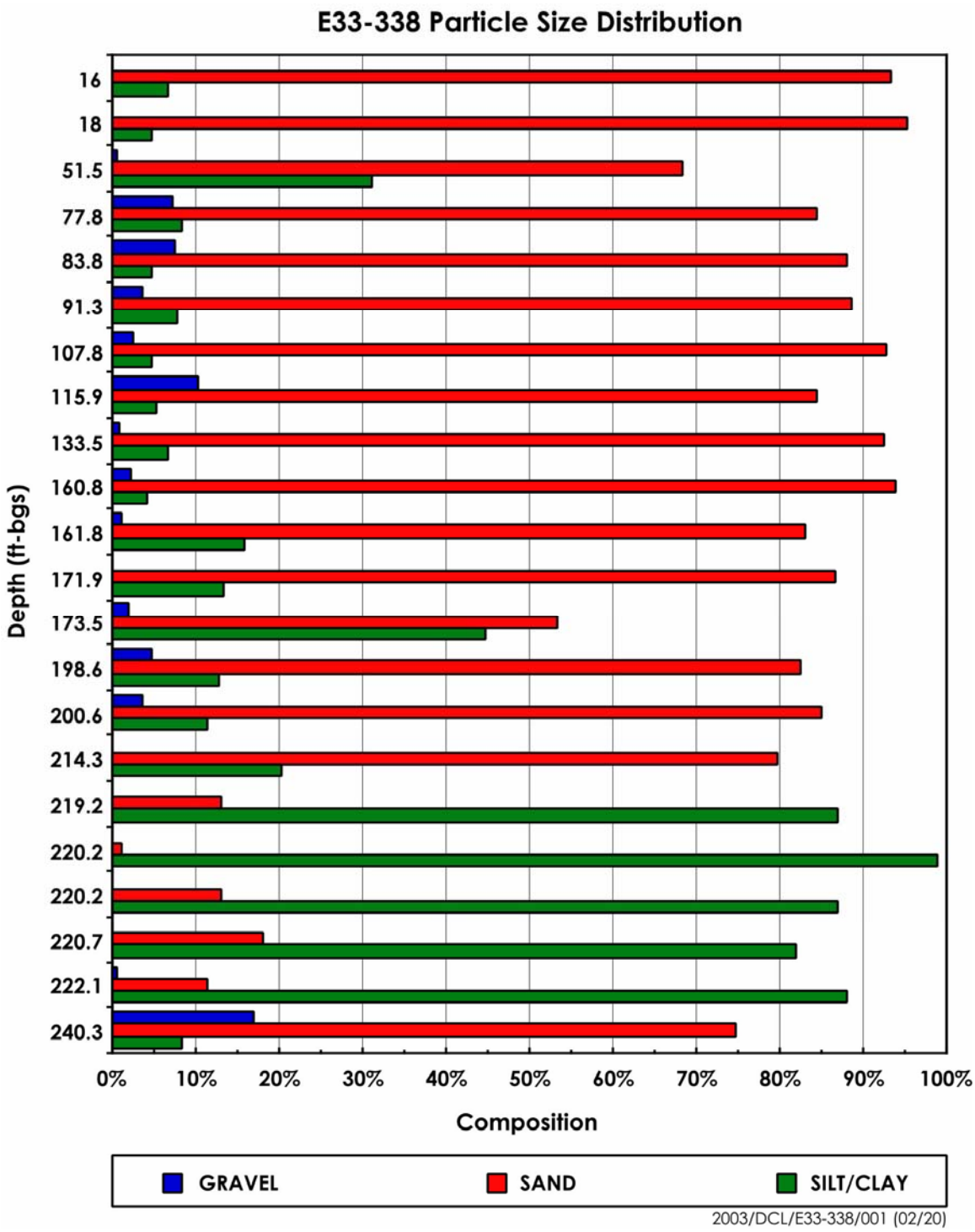

Figure A.14. Gravel, Sand and Silt/Clay (Mud) Content of the 299-E33-338 Sediments. Data are FIO. (Lindenmeier et al., 2003)

Table A.33. Calcium Carbonate and Organic Carbon Content. Data are FIO. (Lindenmeier et al., 2003)

Sample ID	Depth (ft-bgs)	Total Carbon (%)	Inorganic Carbon (%)	Inorganic Carbon as $CaCO_3$ (%)	Organic Carbon (by difference)
H1 Coarse Sand					
C3391_15.5	16.0	0.19	0.14	1.20	0.04
C3391_17.5	18.0	0.15	0.12	0.98	0.04
H2 Hanford Formation H2 Unit — Upper Sequence					
C3391_51.05	51.6	0.19	0.14	1.21	0.04
C3391_77.3	77.8	0.18	0.17	1.43	0.01
C3391_83.3	83.8	0.16	0.13	1.07	0.03
C3391_90.75	91.3	0.19	0.16	1.33	0.03
C3391_107.3	107.8	0.20	0.16	1.36	0.03
C3391_115.4	115.9	0.14	0.12	1.02	0.02
C3391_133	133.5	0.15	0.12	1.02	0.03
C3391_160.3	160.8	0.25	0.11	0.91	0.14
C3391_161.35	161.9	0.26	0.14	1.17	0.12
C3391_171.45	172.0	0.22	0.16	1.35	0.06
C3391_173.05	173.6	0.29	0.20	1.65	0.09
Hanford Formation H3 Unit					
C3391_198.1	198.6	0.15	0.08	0.66	0.07
C3391_200.1	200.6	0.13	0.08	0.67	0.05
Cold Creek Fine-Grained Mud Unit (CCUz)					
C3391_213.8	214.3	0.17	0.13	1.10	0.03
C3391_218.7	219.2	0.28	0.18	1.47	0.11
C3391_219_Below	220.2	0.28	0.22	1.84	0.05
C3391_219_Above	220.2	0.30	0.24	2.00	0.06
C3391_220.65	221.2	0.30	0.21	1.79	0.08
C3391_220.65 Dup	221.2	0.28	0.20	1.69	0.08
C3391_221.65	222.2	0.27	0.22	1.79	0.06
Cold Creek Gravely Sand Unit (CCUg)					
C3391_239.8	240.3	0.11	0.09	0.72	0.02

Table A.34. Element Constituents from Soil Fusion Method. Data are FIO (2 pages). (Lindenmeier et al., 2003)

Sample Id	Mid Depth (ft)	SiO_2 (%)	Al_2O3 (%)	Fe_2O_3 (%)	MnO (%)	MgO (%)	CaO (%)	Na_2O (%)	K_2O (%)	TiO_2 (%)	P_2O_5 (%)	LOI (%)	TOTAL (%)
H1 Coarse Sand													
C3391-15.5	16.00	64.24	12.92	6.75	0.114	2.23	4.80	3.01	1.82	1.211	0.25	2.75	100.09
C3391-17.5	18.00	63.42	12.86	7.01	0.107	2.17	4.77	3.04	1.70	1.145	0.24	2.85	99.30
C3391-51.05	51.55	61.82	13.11	7.92	0.116	2.73	5.28	2.97	1.94	1.391	0.30	2.64	100.21
H2 Hanford Formation H2 Unit — Upper Sequence													
C3391-77.3	77.80	68.20	12.72	4.78	0.076	1.93	3.67	2.88	2.33	0.711	0.17	2.19	99.65
C3391-83.3	83.80	68.37	13.14	4.85	0.076	1.86	3.67	2.95	2.27	0.722	0.17	2.31	100.39
C3391-90.75	91.25	70.33	12.70	3.93	0.066	1.64	3.18	2.73	2.49	0.543	0.13	2.22	99.95
C3391-107.3	107.80	69.96	12.96	4.21	0.070	1.69	3.32	2.87	2.45	0.593	0.14	2.13	100.40
C3391-115.4	115.90	65.68	13.30	6.09	0.098	2.27	4.30	3.05	2.10	0.925	0.19	2.20	100.20
C3391-133	133.50	69.41	12.66	4.03	0.069	1.59	3.25	2.86	2.53	0.568	0.14	2.06	99.17
C3391-160.3	160.80	69.00	13.24	4.41	0.073	1.79	3.50	3.22	2.22	0.630	0.15	1.83	100.06
C3391-161.35	161.85	69.56	12.94	4.29	0.071	1.74	3.36	3.20	2.17	0.611	0.15	1.91	99.99
C3391-171.45	171.95	68.65	13.03	4.54	0.080	1.87	3.70	3.24	2.21	0.636	0.17	2.11	100.23
C3391-173.05	173.55	66.76	12.98	4.67	0.084	1.94	3.91	3.26	2.10	0.665	0.20	2.65	99.21
Hanford Formation H3 Unit													
C3391-198.1	198.60	65.67	13.05	6.09	0.095	2.22	4.35	3.21	2.02	0.919	0.23	2.31	100.16
C3391-200.1	200.60	65.90	13.02	5.67	0.091	2.14	4.10	3.21	2.07	0.859	0.19	2.14	99.38
Cold Creek Mud Unit (CCUz)													
C3391-213.8	214.30	70.27	13.34	3.74	0.068	1.67	3.27	3.19	2.15	0.509	0.13	1.89	100.23
C3391-218.7	219.20	64.39	14.83	5.24	0.073	2.35	3.45	2.53	2.42	0.767	0.21	3.88	100.14
C3391-219.7 Below sand	220.20	65.24	14.81	5.09	0.073	2.10	3.22	2.41	2.43	0.771	0.22	3.96	100.33
C3391-219.7 Above sand	220.20	62.55	15.73	5.96	0.075	2.32	3.09	2.18	2.65	0.848	0.24	4.73	100.38

Table A.34. Element Constituents from Soil Fusion Method. Data are FIO (2 pages). (Lindenmeier et al., 2003)

Sample Id	Mid Depth (ft)	SiO_2 (%)	Al_2O3 (%)	Fe_2O_3 (%)	MnO (%)	MgO (%)	CaO (%)	Na_2O (%)	K_2O (%)	TiO_2 (%)	P_2O_5 (%)	LOI (%)	TOTAL (%)
C3391-220.65	221.15	58.91	15.01	5.89	0.076	2.26	3.02	2.05	2.56	0.806	0.21	4.76	95.55
C3391-220.65 /R	221.15	58.77	15.02	5.86	0.078	2.33	3.04	2.13	2.57	0.791	0.22	4.76	95.56
C3391-221.65	222.15	63.79	14.54	5.15	0.072	2.23	3.46	2.53	2.43	0.772	0.22	4.00	99.21
Cold Creek Gravely Sand Unit (CCUg)													
C3391-239.8	240.30	63.05	13.71	7.16	0.113	2.51	4.98	3.23	2.08	1.086	0.25	1.69	99.85

LOI = loss on ignition

Table A.35. Minor and Trace Element Constituents for 299-E33-338 Sediments. Data are FIO (8 pages). (Lindenmeier et al., 2003)

Sample ID	Mid Depth (ft)	Ba (ug/g)	Sr (ug/g)	Y (ug/g)	Sc (ug/g)	Zr (ug/g)	Be (ug/g)	V (ug/g)	Cr (ug/g)	Co (ug/g)	Ni (ug/g)	Cu (ug/g)	Zn (ug/g)
H1 Coarse Sand													
C3391-15.5	16	737	419	23	18	150	2	180	62	20	-20	27	55
C3391-17.5	18	739	419	22	17	139	2	176	41	23	-20	27	93
C3391-5105	51.55	695	355	26	20	182	2	213	53	27	-20	32	103
H2 Hanford Formation H2 Unit — Upper Sequence													
C3391-77.3	77.8	795	360	19	13	137	2	110	53	14	-20	32	64
C3391-83.3	83.8	843	383	20	11	128	2	109	43	14	-20	24	57
C3391-90.75	91.25	826	377	17	10	126	2	80	73	11	-20	28	67
C3391-107.3	107.8	873	394	18	10	118	2	89	66	12	-20	20	56
C3391-115.4	115.9	812	386	21	15	128	2	144	76	20	-20	28	81
C3391-133	133.5	871	389	16	10	115	2	80	38	10	21	17	50
C3391-160.3	160.8	857	415	17	12	110	2	98	61	12	-20	23	95
C3391-161.35	161.85	850	405	16	11	112	2	90	65	12	-20	23	68
C3391-171.45	171.95	852	423	19	11	168	2	100	80	13	26	27	70
C3391-173.05	173.55	842	425	21	11	200	2	99	86	14	32	30	80
Hanford Formation H3 Unit													
C3391-198.1	198.6	817	397	19	15	109	2	141	52	19	-20	27	107
C3391-200.1	200.6	814	401	19	15	115	2	127	59	17	27	26	78
C3391-200.1 Rep	200.6	Duplicate not Run							79	17	25	26	82
Cold Creek Mud Unit (CCUz)													
C3391-213.8	214.3	866	459	15	6	106	2	55	75	10	25	175	55
C3391-218.7	219.2	823	359	25	12	203	2	102	94	16	46	37	89
C3391-219.7 Below sand	220.2	830	352	28	12	245	2	94	87	17	46	40	92
C3391-219.7 Above sand	220.2	1022	305	30	15	235	2	124	109	20	55	49	121
C3391-220.65	221.15	1021	296	26	14	215	2	120	112	19	73	70	100
C3391-220.65 /R	221.15	1022	299	24	14	206	3	118	93	16	50	38	97
C3391-221.65	222.15	841	364	26	13	246	2	105	90	14	50	33	90
Cold Creek Gravely Sand Unit (CCUg)													
C3391-239.8	240.3	750	436	22	19	138	2	163	71	21	44	35	94

Table A.35. Minor and Trace Element Constituents for 299-E33-338 Sediments. Data are FIO (8 pages).

Sample ID	Depth (ft)	Ga (µg/g)	Ge (µg/g)	As (µg/g)	Rb (µg/g)	Sr (µg/g)	Y (µg/g)	Zr (µg/g)	Nb (µg/g)	Sn (µg/g)	Sb (µg/g)	Cs (µg/g)	Ba (µg/g)
H1 Coarse Sand													
C3391-15.5	16	18	1.4	-5	56	403	23.7	149	9.7	2	0.3	1.7	726
C3391-17.5	18	19	1.6	-5	56	405	24.9	145	10.9	11	0.3	1.7	747
C3391-5105	51.55	20	1.6	-5	63	345	29.0	185	11.6	2	0.3	2.0	693
H2 Hanford Formation H2 Unit — Upper Sequence													
C3391-77.3	77.8	17	1.6	-5	75	336	19.3	132	8.8	1	0.5	2.5	759
C3391-83.3	83.8	17	1.4	-5	77	364	19.3	133	8.4	5	0.6	2.3	801
C3391-90.75	91.25	16	1.5	-5	85	348	18.7	126	8.9	2	1.5	2.8	760
C3391-107.3	107.8	16	1.6	5	81	373	19.5	123	8.9	1	0.5	2.6	833
C3391-115.4	115.9	19	1.7	-5	71	387	22.3	134	9.5	2	0.4	2.1	803
C3391-133	133.5	16	1.4	5	79	382	17.6	113	7.6	1	0.5	2.7	828
C3391-160.3	160.8	16	1.4	-5	73	394	17.4	109	8.0	5	0.5	2.1	806
C3391-161.35	161.85	16	1.4	-5	71	394	17.6	113	8.2	2	0.4	2.1	831
C3391-171.45	171.95	17	1.6	5	73	412	20.8	169	10.5	1	0.5	2.2	830
C3391-173.05	173.55	16	1.5	-5	67	405	21.8	195	10.9	3	0.4	2.1	811
Hanford Formation H3 Unit													
C3391-198.1	198.6	18	1.6	-5	64	379	22.0	126	9.0	6	0.4	1.7	792
C3391-200.1	200.6	18	1.6	-5	62	388	21.6	125	9.0	2	0.3	1.7	800
C3391-200.1 Rep	200.6	18	1.7	-5	66	395	21.7	124	9.1	2	0.4	1.8	797
Cold Creek Fine-Grained Mud Unit (CCUz)													
C3391-213.8	214.3	16	1.3	-5	70	454	16.5	135	8.8	8	0.4	2.1	842
C3391-218.7	219.2	19	1.6	9	84	348	25.3	206	13.3	3	1.0	3.9	820
C3391-219.7 Below sand	220.2	21	1.7	8	101	344	31.3	254	16.2	3	0.8	5.0	809
C3391-219.7 Above sand	220.2	23	1.9	18	110	303	31.9	239	18.6	3	1.2	5.4	1,020
C3391-220.65	221.15	22	1.5	10	101	287	27.2	213	17.5	5	0.9	4.6	1,010
C3391-220.65 /R	221.15	20	1.7	8	84	357	29.0	242	14.9	2	0.9	3.9	827
C3391-221.65	222.15	20	1.6	8	82	361	28.7	244	14.8	2	0.9	4.1	925
Cold Creek Gravely Sand Unit (CCUg)													
C3391-239.8	240.3	20	1.5	-5	55	429	23.5	133	9.8	3	0.4	1.5	745

Table A.35. Minor and Trace Element Constituents for 299-E33-338 Sediments. Data are FIO (8 pages).

Sample ID	Depth (ft)	La (µg/g)	Ce (µg/g)	Pr (µg/g)	Nd (µg/g)	Sm (µg/g)	Eu (µg/g)	Gd (µg/g)	Tb (µg/g)	Dy (µg/g)	Ho (µg/g)	Er (µg/g)
H1 Coarse Sand												
C3391-15.5	16	29.1	58.5	6.70	26.4	5.62	1.66	5.15	0.81	4.65	0.89	2.59
C3391-17.5	18	26.5	54.5	6.42	25.8	5.72	1.66	5.12	0.85	4.71	0.93	2.76
C3391-5105	51.55	31.6	66.9	7.69	31.4	6.78	1.95	6.10	0.98	5.53	1.07	3.14
H2 Hanford Formation H2 Unit — Upper Sequence												
C3391-77.3	77.8	26.0	52.2	5.95	23.3	4.84	1.37	4.12	0.67	3.74	0.72	2.18
C3391-83.3	83.8	24.3	48.7	5.63	22.3	4.83	1.35	4.08	0.65	3.70	0.71	2.14
C3391-90.75	91.25	29.4	60.8	6.72	25.7	5.11	1.29	4.11	0.65	3.72	0.71	2.16
C3391-107.3	107.8	29.7	59.9	6.59	25.1	5.02	1.35	4.08	0.66	3.76	0.72	2.16
C3391-115.4	115.9	28.8	59.0	6.70	26.4	5.47	1.54	4.64	0.77	4.29	0.83	2.41
C3391-133	133.5	25.4	51.1	5.78	22.1	4.48	1.24	3.77	0.60	3.36	0.65	1.93
C3391-160.3	160.8	24.1	48.9	5.54	21.9	4.41	1.25	3.77	0.60	3.43	0.68	1.98
C3391-161.35	161.85	24.7	48.9	5.49	21.3	4.27	1.24	3.53	0.59	3.31	0.65	1.90
C3391-171.45	171.95	32.2	64.2	7.26	27.9	5.53	1.42	4.62	0.70	3.96	0.76	2.30
C3391-173.05	173.55	30.8	62.9	7.13	27.8	5.57	1.50	4.65	0.72	4.14	0.78	2.40
Hanford Formation H3 Unit												
C3391-198.1	198.6	24.6	49.3	5.77	23.5	4.92	1.47	4.39	0.71	4.08	0.80	2.34
C3391-200.1	200.6	24.4	49.5	5.80	23.2	5.01	1.47	4.44	0.73	4.18	0.80	2.40
C3391-200.1 Rep	200.6	24.6	51.1	6.03	23.9	5.17	1.50	4.58	0.72	4.16	0.82	2.42
Cold Creek Fine-Grained Mud Unit (CCUz)												
C3391-213.8	214.3	25.3	50.8	5.68	22.1	4.38	1.19	3.37	0.53	3.02	0.58	1.77
C3391-218.7	219.2	40.0	80.5	9.23	35.4	6.86	1.63	5.48	0.85	4.78	0.92	2.75
C3391-219.7 Below sand	220.2	47.0	95.6	10.8	41.0	7.93	1.83	6.42	0.99	5.60	1.09	3.28
C3391-219.7 Above sand	220.2	45.3	93.2	10.5	39.9	7.98	1.82	6.38	0.99	5.65	1.10	3.29
C3391-220.65	221.15	9.5	81.2	9.03	34.6	6.81	1.63	5.61	0.88	4.77	0.92	2.76
C3391-220.65 /R	221.15	41.0	83.2	9.36	36.0	7.20	1.64	5.82	0.90	5.09	0.99	2.97
C3391-221.65	222.15	41.5	77.8	9.40	34.9	6.96	1.54	6.02	0.92	5.07	0.98	2.98
Cold Creek Gravely Sand Unit (CCUg)												
C3391-239.8	240.3	21.4	44.4	5.35	22.3	4.97	1.49	4.65	0.75	4.25	0.84	2.45

Table A.35. Minor and Trace Element Constituents for 299-E33-338 Sediments. Data are FIO (8 pages).

Sample ID	Depth (ft)	Tm (µg/g)	Yb (µg/g)	Lu (µg/g)	Hf (µg/g)	Ta (µg/g)	W (µg/g)	Tl (µg/g)	Pb (µg/g)	Bi (µg/g)	Th (µg/g)	U (µg/g)
H1 Coarse Sand												
C3391-15.5	16	0.391	2.46	0.352	4.2	0.64	0.6	0.29	-5	-0.1	4.35	1.09
C3391-17.5	18	0.411	2.55	0.364	4.2	0.64	0.6	0.42	8	0.1	3.96	1.05
C3391-5105	51.55	0.457	2.87	0.417	5.3	0.68	0.7	0.74	7	0.1	5.23	1.36
H2 Hanford Formation H2 Unit — Upper Sequence												
C3391-77.3	77.8	0.315	2.02	0.291	3.9	0.54	0.8	0.61	9	0.2	4.69	1.21
C3391-83.3	83.8	0.327	2.08	0.292	3.9	0.52	0.7	0.48	8	0.1	4.48	1.18
C3391-90.75	91.25	0.329	2.09	0.293	3.8	0.56	1.0	0.53	11	0.3	6.12	1.45
C3391-107.3	107.8	0.318	2.04	0.288	3.5	0.57	0.9	0.59	10	0.1	5.53	1.34
C3391-115.4	115.9	0.365	2.33	0.327	3.8	0.58	0.7	0.54	9	0.2	5.15	1.23
C3391-133	133.5	0.286	1.79	0.260	3.3	0.48	0.9	0.45	6	0.1	4.71	1.18
C3391-160.3	160.8	0.291	1.81	0.266	3.2	0.49	0.7	0.49	7	0.1	4.23	1.09
C3391-161.35	161.85	0.286	1.81	0.259	3.3	0.50	0.7	0.50	7	0.1	4.45	1.21
C3391-171.45	171.95	0.347	2.20	0.323	4.9	0.73	1.0	0.56	10	0.2	5.91	1.54
C3391-173.05	173.55	0.362	2.34	0.341	5.8	0.75	1.2	0.45	7	0.1	5.67	1.58
Hanford Formation H3 Unit												
C3391-198.1	198.6	0.343	2.16	0.313	3.6	0.52	0.6	0.44	7	0.1	4.39	1.16
C3391-200.1	200.6	0.363	2.18	0.316	3.6	0.55	1.4	0.48	8	0.1	4.34	1.32
C3391-200.1 Rep	200.6	0.358	2.23	0.327	3.7	0.60	0.6	0.52	9	0.2	4.45	1.17
Cold Creek Fine-Grained Mud Unit (CCUz)												
C3391-213.8	214.3	0.262	1.65	0.249	3.8	0.51	0.9	0.43	7	0.1	4.72	1.30
C3391-218.7	219.2	0.410	2.56	0.373	5.9	0.84	1.4	0.67	12	0.2	8.16	2.19
C3391-219.7 Below sand	220.2	0.516	3.18	0.464	7.6	1.04	1.8	0.77	15	0.5	10.6	2.81
C3391-219.7 Above sand	220.2	0.504	3.14	0.462	7.2	1.23	1.7	0.97	20	0.7	11.1	2.97
C3391-220.65	221.15	0.427	2.67	0.392	6.3	1.07	1.6	0.66	12	0.3	10.1	2.63
C3391-220.65 /R	221.15	0.463	2.90	0.421	7.2	0.85	1.7	0.67	14	0.3	9.80	2.59
C3391-221.65	222.15	0.445	2.81	0.413	7.4	1.13	1.4	0.67	14	0.3	10.1	2.77
Cold Creek Gravely Sand Unit (CCUg)												
C3391-239.8	240.3	0.371	2.31	0.339	3.9	0.50	0.5	0.42	7	0.1	4.62	1.27

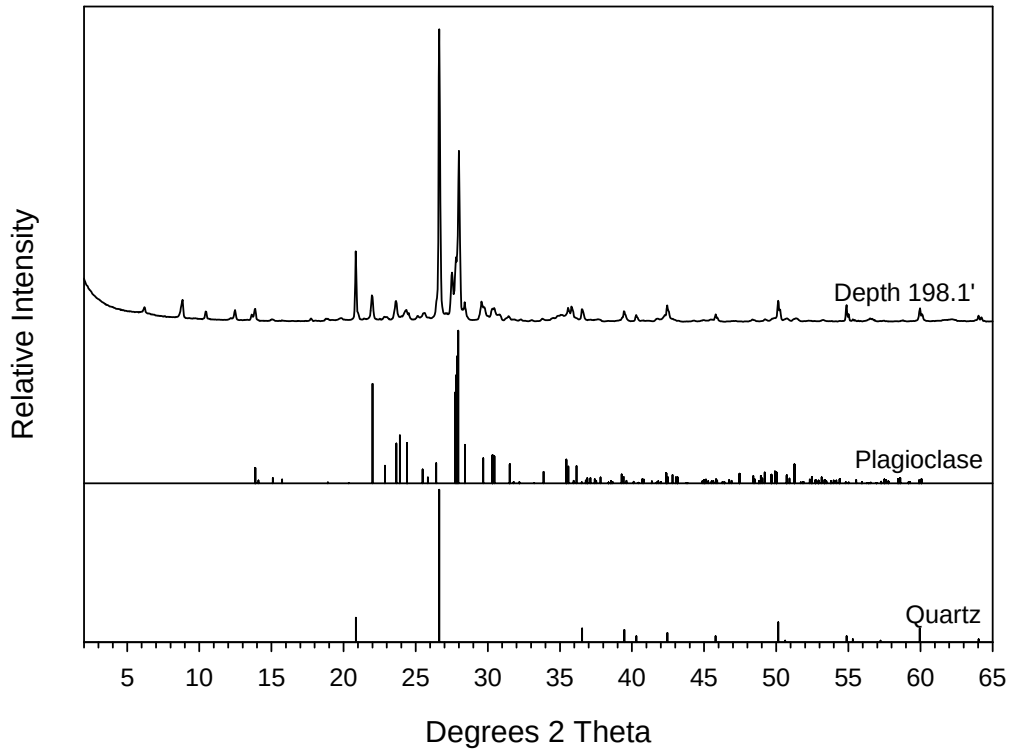

Figure A.15. XRD Tracing of Sediment Collected from 198.1 ft, along with the Standard Reference Patterns for Quartz and Plagioclase. (Lindenmeier et al., 2003)

Results for the bulk samples are provided in Table A.36. Quartz concentrations ranged from 22 wt% at 219.17 ft to 48.5 wt% at 51.05 ft. The borehole sediment contained plagioclase feldspar concentrations from 10.6 to 39.5 wt% and potassium feldspar content measured between 9.0 to 37.9 wt%. Plagioclase feldspar was more abundant than potassium feldspar, with the exception of the three samples in the H1 Hanford coarse sand and one sample in the lower portion of the CCUz unit. The amphibole phase comprised <10 wt% at most, with the majority of samples having concentrations in the 2 to 5 wt% range.

Table A.36. Semi-quantitative XRD Results of Minerals from Borehole 299-E33-338. Data are FIO. (Lindenmeier et al., 2003)

Sample ID	Mineral Phase (wt%) Quartz	Amphibole	Plagioclase	K-Spar	Mica	Chlorite	Goodness of Fit[a]
H1 Hanford Coarse Sand							
C3391-15.5	30.7	10	21.0	37.9	Tr	Tr	0.39
C3391-17.5	31.6	3.0	26.1	39.3	Tr	Tr	0.29
C3391-51.05	48.5	5.3	17.9	28.4	Tr	Tr	0.29
H2 Hanford Formation Unit--upper sequence							
C3391-77.3	44.0	3.8	23.7	28.5	Tr	Tr	0.48
C3391-83.3	30.3	3.3	31.0	15.7	18.0	2.3	0.23
C3391-90.75	38.1	2.6	22.3	15.2	19.7	2.1	0.49
C3391-107.3	37.8	3.0	26.3	12.8	17.3	2.7	0.41
C3391-115.4	28.0	4.9	32.0	10.9	21.5	2.8	0.26
C3391-133	35.5	3.5	26.3	11.9	20.1	2.7	0.46
C3391-160.3	32.0	4.7	27.1	12.3	20.7	3.1	0.35
C3391-161.35	38.4	2.8	27.0	12.0	16.9	2.6	0.50
C3391-171.45	29.0	7.8	29.9	9.0	21.2	3.2	0.24
C3391-173.05	ND	ND	ND	ND	ND	ND	ND
H3 Hanford Formation Unit							
C3391-198.1	24.8	3.3	39.5	11.2	18.0	3.2	0.26
C3391-200.1	29.8	4.1	31.7	13.1	18.1	2.8	0.40
Cold Creek Fine-Grained Mud Unit (CCUz)							
C3391-213.8	31.5	7.3	30.8	10.7	17.1	2.6	0.23
C3391-218.7	30.3	7.2	25.2	12.1	21.7	3.4	0.30
C3391-219.7 below sand	ND	ND	ND	ND	ND	ND	ND
C3391-219.7 above sand	30.8	4.7	16.9	17.4	25.6	4.6	0.45
Cold Creek Gravel Sand Unit (CCUg)							
C3391-220.65	31.8	6.0	27.3	13.6	17.9	3.4	0.44
C3391-221.65	38.1	5.8	18.9	15.8	26.3	5.0	0.38
C3391-239.8	27.4	3.3	33.8	9.3	23.3	2.9	0.32

(a) 1.0 represents ideal goodness of fit
ND = not determined

Clay minerals identified in the whole rock sediment included mica and chlorite. Mica concentrations ranged from trace amounts in the H1 Hanford coarse sand unit to as high as high as 26% in the Cold Creek gravel sand unit. Chlorite concentrations were less than 5 wt% in all sediments analyzed with only trace amounts detected in the H1 unit. Smectite and kaolinite minerals were not identified in the whole rock sediment samples due in part to the sample preparation technique and the low overall concentration, respectively.

XRD analysis was performed on the <2 micron fraction of each sample. The clay fraction is dominated by four clay minerals (smectite, chlorite, illite and kaolinite) with minor amounts of quartz and feldspar. Figure A.16 provides XRD-tracings of a typical clay fraction (from sample 198.1 ft) following a treatment with of Mg-saturation and solvation with ethylene glycol. Smectites are considered the fraction of the Mg-saturated sub-sample that gives a basal reflection at 5.28° 2θ upon solvation with ethylene glycol. Illite is the simplest of the four clay mineral phases to identify in this sediment. The basal reflections are located at 8.88, 17.8, and 26.7° 2θ. The various treatments, including cation saturation, solvation with ethylene glycol, and heating, do not affect the structure of the illite.

Chlorites are identified by their basal series of diffraction peaks at 6.24, 12.5, 18.8, and 25.2° 2θ, which are unaffected by cation saturation or ethylene glycol solvation. Kaolinite is difficult to identify in the presence of a chlorite mineral. Basal reflections characteristic to kaolinite are positioned at 12.5 and 24.9° 2θ, which are super imposed on the even-order chlorite peaks. These kaolinite reflections are unaffected by cation saturation and ethylene glycol solvation. Positive identification of kaolinite in the presence of chlorite can be determined by examination of the 24.9 to 25.2° 2θ region of the XRD tracing. The kaolinite basal reflection at 24.9° 2θ can be distinguished from the chlorite 25.2° 2θ reflection in some situations. For example, XRD tracings of the clay fractions from depths 219.7A and 219.7B both show a bi-module peak from 24.9° 2θ to 25.2° 2θ.

Trace amounts of quartz are evident by the diffraction peak located at 20.85° 2θ. The 100% reflection for quartz (26.6° 2θ) is hidden by the third basal reflection of illite located at 26.6° 2θ. Plagioclase feldspar is also identified in the clay fraction by the minor diffraction peak at 27.8° 2θ as well as hornblende by the minor peak at 10.41° 2θ. Additionally, laumontite was detected in the clay fraction from several depths in the lower Cold Creek unit (220.65 ft and 221.65 ft), evident by the reflection at 9.36° 2θ.

Results for the clay minerals in the < 2 micron fraction are presented in Table A.37. Total recoveries were normalized to 100% and the normalization factor used for each sample is provided in the last column. Smectites ranged in concentrations from a low of 3 wt% (83.3 ft) to a high of 60 wt% (15.5 ft). Illite amounts varied from 28 to 61 wt% with the majority of samples having concentrations in the 40 to 55 wt% range. Chlorite and kaolinite were the least abundant of the clay minerals identified in the samples with concentrations equal to or less than 25 wt% and 14 wt%, respectively. Quartz and feldspar minerals were present as trace amounts in the clay fraction and therefore were not included in totals presented in Table A.37.

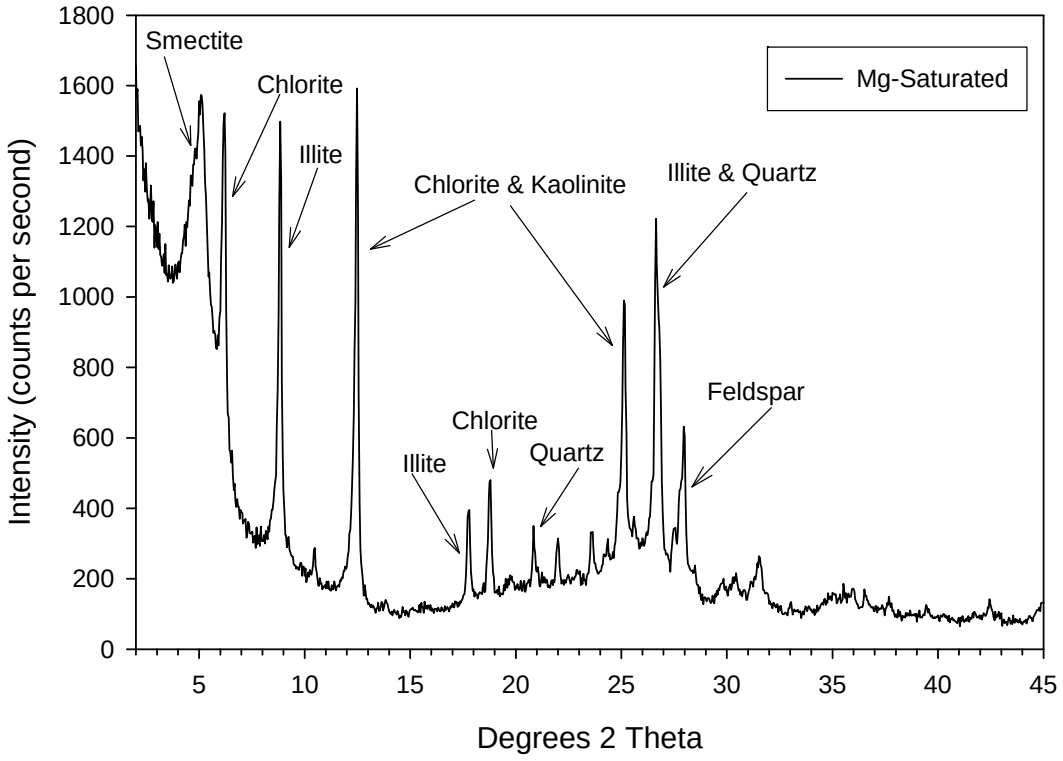

Figure A.16. XRD Tracings of Preferentially Oriented Clay Slide Taken from Borehole 299-E33-338 at a Depth of 198.1 ft. The scans were collected from 2 to 45° 2θ with a 0.04° step and 2-second

dwell time. The black line represents the Mg-saturated fraction. Data are FIO. (Lindenmeier et al., 2003)

Table A.37. Semi-quantitative XRD Results of Clay Minerals Separated from the Sediment Collected from Borehole 299-E33-338. Data are FIO. (Lindenmeier et al., 2003)

Sample Depth/ID	Mineral Phase (wt%)				Normalization Factor
	Smectite	Illite	Chlorite	Kaolinite	
15.5	60	28	7	5	0.73
17.5	53	31	10	6	0.92
51.05	25	52	13	10	0.49
77.3	31	44	15	9	0.64
83.3	3	61	22	14	0.81
90.75	10	61	19	9	0.49
107.3	22	51	14	13	1.96
115.4	18	53	21	8	0.61
133	23	53	18	6	0.51
160.3	25	48	19	8	0.55
161.35	19	54	20	7	0.56
171.45	27	42	23	8	0.50
173.05	28	37	25	10	0.54
198.1	35	42	18	5	0.79
200.1	18	53	21	8	0.61
213.8	23	53	18	6	0.51
218.7	25	48	19	8	0.55
219.7 below	19	54	20	7	0.56
219.7 above	25	52	13	10	0.49
220.65	31	44	15	9	0.64
221.65	35	42	18	5	0.79
239.8	31	44	19	6	0.74

Total clay recoveries were within ±25% of the “ideal” 100% for 4 of the 22 samples analyzed. The majority of clay recoveries were between 25% and 50%, with only one sample having a normalization factor of 1.96. This sample, 107.3 ft, cracked significantly during the analysis, which resulted in a poorly oriented sediment. Other factors affecting the semi-quantification procedure (i.e., preparation and condition of the clay filter cake) were generally controlled and are not thought to be a significant factor. Quantitative analysis is considered good if errors amount to ±10% of the amounts present for major constituents and ±20% for minerals whose concentrations are less than 20% (Moore and Reynolds 1989).

A.6 References

Amonette JA. 1991. *Soil Mineralogical Analysis by X-ray Diffraction*. Procedure JEA, Pacific Northwest National Laboratory, Richland, Washington.

Grim RE 1968. *Clay Mineralogy.* Second edition. McGraw-Hill book Company, New York.

Horton DG, HT Schaef, RJ Serne, CF Brown, MM Valenta, TS Vickerman, IV Kutnyakov, SR Baum, KN Geiszler, and KE Parker. 2003. *Geochemistry of Samples from Borehole C3177(299-E24-21)*. PNNL-14289, Pacific Northwest National Laboratory, Richland, Washington.

Horton DG. 2002. *Borehole Data Package for Calendar Year 2001 RCRA Wells at Single-Shell Tank Waste Management Area B-BX-BY*. PNNL-13827, Pacific Northwest National Laboratory, Richland, Washington.

Kaplan DI, KE Parker, and IV Kutynakov. 1998, 1. *Radionuclide Distribution coefficients for Sediments Collected from Borehole 299-E17-21: Final Report for Subtask 1a*. PNNL-11966, Pacific Northwest National Laboratory, Richland, Washington.

Lindenmeier CW, RJ Serne, BN Bjornstad, GW Gee, HT Schaef, DC Lanigan, MJ Lindberg, RE Clayton, VL LeGore, IV Kutnyakov, SR Baum, KN Geiszler, CF Brown, MM Valenta, TS Vickerman, and LJ Royack. 2003. *Characterization of Vadose Zone Sediment: RCRA Borehole 299-E33-338 Located Near the B-BX-BY Waste Management Area*. PNNL-14121, Pacific Northwest National Laboratory, Richland, Washington.

Meyer PD and RJ Serne. 1999. *Near-Field Hydrology Data Package for the Immobilized Low-Activity Waste2001 Performance Assessment*. PNNL-13035, Pacific Northwest National Laboratory, Richland, Washington.

Moore DM and RC Reynolds, Jr. 1989. *X-ray Diffraction and the Identification and Analysis of Clay Minerals*. Oxford University Press, New York.

Reidel SP and KD Reynolds. 1998. Characterization plan for the immobilized low-activity waste borehole. PNNL-11802, Pacific Northwest National Laboratory, Richland, Washington.

Reidel SP, DG Horton, and MM Valenta. 2001. *Geologic and Wireline Borehole Summary from the Second ILAW Borehole (299-E24-21)*. PNNL-13652, Pacific Northwest National Laboratory, Richland, Washington.

Reidel SP and DG Horton. 1999. *Geologic Data Package for 2001 Immobilized Low-Activity Waste Performance Assessment*. PNNL-12257, Rev. 1, Pacific Northwest National Laboratory, Richland, Washington.

Schramke, J., Rai, D., and R. Fulton. 1988. Determination of plutonium oxidation states by solvent extraction. Symposium on nuclear analytical chemistry and geochemistry, American Chemical Society, Conference-8806308.

Serne RJ, CF Brown, HT Schaef, EM Pierce, MJ Lindberg, Z Wang, PL Gassman, and JG Catalano. 2002. *300 Area Uranium Leach and Adsorption Project*. PNNL-14022, Pacific Northwest National Laboratory, Richland, Washington.

Um W, RJ Serne, GV Last, RE Clayton, and ET Glossbrenner. 2009. “The effect of gravel size fraction on the distribution coefficients of selected radionuclides.” *Journal of Contaminant Hydrology* 107(1-2):82-90.

Appendix B – Characterization Data for 200 West Area Sediments

This appendix contains detailed characterization data on vadose zone sediments from five boreholes drilled in the 200 West Area. Full details are found in the technical reports cited in the text. Since the goal of this report is to inform investigators of the existing data available for Remedial Investigation/Feasibility Study (RI/FS) tasks and provide a centralized location to support site evaluations, the data *have not* been reviewed for technical accuracy per NQA-1 guidelines, but have been reproduced from the original reports. Hence, the data provided here are *for information only* (FIO).

B.1 Borehole 299-W10-27 (C3125)

Well 299-W10-27 is a Resource Conservation and Recovery Act (RCRA) groundwater monitoring well located approximately 200 m northeast of the TX Tank Farm within the 200 West Area. Near continuous core sampling was performed between 50 to 132 ft bgs (Lindsey et al. 2001), for a total of 33 split spoon core runs. Two, 4-in.-diameter, 1-ft-long, lexan-lined core samples were recovered from each 2.5-ft split spoon in 299-W10-27. Upon recovery, any open spaces in the ends of the liners were stuffed with aluminum foil in the field and plastic end caps were secured with duct tape. The liners were sealed with plastic end caps and the outsides labeled with chain-of-custody or borehole ID number, an “up” arrow, and the letter “A” or “B”. The letter “A” was assigned to the deeper of the two cores in the core run. Borehole 299-W10-27 (C3125) was drilled using the cable-tool method between January 22 and March 13, 2001.

The total depth of the borehole is 268.7 ft (81.9 m) bgs; the hole terminated within the Ringold Formation Unit E gravels at 81 ft (25 m) below the groundwater table. Sampling above 50 ft was limited to core-barrel grab samples every 5 ft, while below 132 ft bgs grab samples were collected every 5 ft from the hard-tool drill cuttings. An additional three split spoon cores were collected between hard-tooled intervals from the saturated zone within Ringold Formation Unit E gravels.

Table B.1 presents a list of the cores analyzed from 299-W10-27. The data are discussed in more detail in Serne et al. (2004a).

B.1.1 Borehole 299-W10-27 Sediment Characterization

Sediments were characterized for particle size, total and inorganic carbon content, and total elemental composition. Results of these analyses are presented in the sections below.

Table B.1. Sample Locations for Borehole 299-W10-27. Data are FIO. (Serne et al., 2004a)

Core Sample ID	Discrete Sample Depth (ft)	Lithology	Stratigraphic Unit	Comments
C3125-52.5	53.3	Silty fine sand	H2	
C3125-53.5	54.2	Silty fine-medium sand	H2	
C3125-61	61.2	Silty fine-coarse sand	H2	
C3125-87.5	88.2	Silty fine sand	H2	
C3125-92.5	93.0	Silty fine sand	CCU_z	
C3125-100	100.5	Sandy caliche	CCU_c	
C3125-113.5	114.0	Fine-medium sand	R_{tf}	
C3125-117.5	118.5	Silt and sand	R_{tf}	Clastic dike within R_{tf}
C3125-130	130.2	Muddy sandy gravel	R_{wi}	

One physical and chemical characterization sample was collected from each of the depths indicated.

B.1.2 Particle Size Analyses for 299-W10-27 Sediments

The particle size data are shown in Table B.2 and Table B.3. The Hanford formation sediments (H2) are dominated by sand while the Cold Creek (CCU_c and CCU_z) sediments are dominated by silt. The two Ringold Formation Taylor Flats (R_{tf}) samples were distinct: one dominated by sand, the other by silt and clay. The sample from the Ringold Formation Wooden Island member (R_{wi}) was also dominated by sand, but had a large silt/clay fraction (~36%). The CCU_c sediments can be highly variable in particle size and in the 200 West Area often contain caliche, which acts as a cement binding the assorted particles together.

B.1.3 Carbon Content in 299-W10-27 Sediments

The carbon content of the sediments is shown in Table B.4. The Cold Creek unit sample from 100 ft bgs contains significant concentrations of calcium carbonate and one of the Ringold Formation Taylor Flat member sediments also contains elevated calcium carbonate.

B.1.4 Total Oxide Composition of 299-W10-27 Sediments

Table B.5 shows the major and minor element oxide composition of the sediments and Table B.6 lists the trace element concentrations in the sediments. No detailed mineralogical analysis was performed on the sediments from borehole 299-W10-27.

Table B.2. Wet Sieve Particle Size Results for Borehole 299-W10-27 Sediments. Data are FIO. (Serne et al., 2004a)

Depth (ft bgs)	Stratigraphic Unit	Weight Percent		
		Gravel	Sand	Silt/Clay
53.3	H2	0.61	83.94	15.45
53.5	H2	0.39	88.58	11.03
61	H2	4.16	73.86	21.98
88.3	H2	0.14	52.28	47.58
92.5	CCU_z	0.00	27.11	72.89
100	CCU_c	10.5	68.44	21.07
113.5	R_{tf}	0.00	88.78	11.22
117.5	R_{tf}	0.91	11.77	87.32
130	R_{wi}	15.68	48.23	36.09

Table B.3. Particle Size Data for Borehole 299-W10-27 Sediments Using Sieving and Hydrometer Techniques. Data are FIO. (Serne et al., 2004a)

Stratigraphic Unit	H2		H2		H2		H2
Sample	53.3		53.5		61		88.3
			Wet Sieve				
µm	% finer than	µm	% finer than	µm	% finer than	µm	% finer than
2000	99.39	2000	99.61	2000	95.84	2000	99.86
1000	97.79	1000	97.69	1000	89.18	1000	99.37
500	88.86	500	81.41	500	69.38	500	96.21
250	56.95	250	43.21	250	49.92	250	86.63
105	25.14	105	18.93	105	30.23	105	66.59
74	20.14	74	14.66	74	26.16	74	57.95
53	15.45	53	11.03	53	21.98	53	47.58
			Hydrometer				
86.65	47.19	80.98	11.88	83.79	20.63	85.30	43.24
59.83	35.86	56.76	8.91	58.64	17.41	59.35	35.00
33.41	20.76	32.55	6.68	33.35	12.89	33.55	24.71
18.06	15.10	17.75	5.20	18.11	10.31	18.14	16.47
10.33	9.44	10.22	4.45	10.41	9.03	10.38	12.35
7.27	6.61	7.23	4.45	7.31	7.09	7.31	9.27
5.94	5.66	5.90	4.45	5.96	6.45	5.97	8.24
5.14	5.66	5.11	4.45	5.16	6.45	5.17	8.24
1.48	5.66	1.47	2.97	1.48	3.87	1.48	6.18

Table B.3. (cont.)

Stratigraphic Unit	CCU_z		CCU_c		R_{tf}		R_{tf}		R_{wi}
Sample	92.5		100		113.5		117.5		130
Wet Sieve									
µm	% finer than	µm	% finer than	µm	% finer than	µm	% finer than	µm	% finer than
2000	100	2000	89.5	2000	100	2000	99.09	2000	84.32
1000	100	1000	83.36	1000	99.68	1000	99.09	1000	73.91
500	99.98	500	76.85	500	96.43	500	98.92	500	61.3
250	99.98	250	65.1	250	39	250	98.38	250	53.21
105	97.32	105	39.2	105	6.01	105	98.28	105	42.87
74	90.82	74	29.37	74	2.58	74	96.53	74	39.49
53	72.89	53	21.07	53	0.06	53	87.32	53	36.09
Hydrometer									
90.75	71.35	83.10	25.85	80.83	10.19	89.17	78.65	86.20	37.61
62.11	53.99	57.52	16.62	56.77	8.15	61.78	65.13	60.24	32.71
34.35	32.78	32.92	12.93	32.63	6.79	34.36	41.78	34.43	28.62
18.35	21.21	17.95	11.08	17.79	5.43	18.43	29.49	18.63	23.71
10.45	15.43	10.32	9.23	10.25	4.75	10.46	19.66	10.60	17.99
7.34	12.53	7.28	8.31	7.23	4.07	7.31	13.52	7.43	14.72
5.98	11.57	5.93	7.39	5.90	4.07	5.96	12.29	6.05	13.90
5.17	10.61	5.13	7.39	5.11	4.07	5.14	9.83	5.23	13.08
1.48	5.79	1.48	7.39	1.47	2.72	1.47	4.92	1.48	6.54

Table B.4. Total, Inorganic, and Organic Carbon Content of Vadose Zone Sediments from Borehole 299-W10-27. Data are FIO. (Serne et al., 2004a)

Depth (ft bgs)	Stratigraphic Unit	Total Carbon (%)	Inorganic Carbon (%)	IC as $CaCO_3$ (%)	Organic Carbon (by difference)
53.3	H2	0.26	0.22	1.84	0.04
53.5	H2	0.22	0.20	1.64	0.02
61	H2	0.22	0.21	1.75	0.01
88.3	H2	0.35	0.32	2.68	0.03
92.5	CCU_z	0.41	0.32	2.63	0.09
100	CCU_l	2.75	2.65	22.05	0.10
113.5	R_{tf}	0.08	0.06	0.48	0.02
113.5(dup)	R_{tf}	0.05	0.01	0.09	0.04
117.5	R_{tf}	1.16	1.05	8.79	0.11
130	R_{wi}	0.05	0.08	0.69	0.03

Table B.5. Total Chemical Composition of Borehole 299-W10-27 Sediments (as wt% oxides). Data are FIO. (Serne et al., 2004a)

Depth (ft bgs)	53.3	53.5	61	88.3	92.5	100	113.5	113.5 DUP	117.5	130
Unit	H2	H2	H2	H2	CCU_u	CCU_l	R_{tf}	R_{tf}	R_{tf}	R_{wi}
CO_2	0.81	0.73	0.77	1.17	1.17	9.71	0.22	0.04	3.85	0.29
Na_2O	2.56	2.60	2.52	2.42	2.02	1.97	2.56	2.60	2.16	2.95
MgO	1.82	1.54	1.87	1.66	1.79	2.85	1.36	1.35	1.53	2.70
Al_2O_3	12.40	12.17	12.37	11.83	11.58	9.74	12.08	12.21	11.13	12.28
SiO_2	66.32	68.41	66.59	66.53	66.39	48.91	69.59	69.27	63.73	60.08
P_2O_5	0.17	0.14	0.17	0.15	0.16	0.15	0.10	0.10	0.12	0.30
SO_3	NA	NA	NA	NA	NA	NA	NA	NA	NA	NA
Cl	NA	NA	NA	NA	NA	NA	NA	NA	NA	NA
K_2O	2.25	2.43	2.23	2.26	2.23	1.10	2.41	2.38	2.29	1.67
CaO	3.37	3.13	3.67	3.65	3.23	15.67	1.95	1.90	4.97	5.26
TiO_2	0.670	0.575	0.784	0.654	0.658	1.193	0.520	0.532	0.530	1.465
V_2O_5	1.67E-02	1.42E-02	2.01E-02	1.54E-02	1.32E-02	2.82E-02	1.29E-02	1.34E-02	1.36E-02	3.77E-02
Cr_2O_3	1.05E-02	7.60E-03	1.08E-02	1.23E-02	8.04E-03	6.72E-03	7.89E-03	7.45E-03	9.06E-03	1.08E-02
MnO	0.105	0.086	0.101	0.094	0.103	0.100	0.089	0.084	0.103	0.152
Fe_2O_3	8.92	6.11	8.13	7.38	9.15	7.14	8.94	8.69	11.05	12.75
CoO	1.53E-03	1.14E-03	1.65E-03	1.27E-03	1.27E-03	1.53E-03	1.14E-03	8.90E-04	1.27E-03	2.80E-03
NiO	4.20E-03	2.55E-03	1.86E-02	2.11E-02	3.82E-03	3.82E-03	3.18E-03	1.78E-03	4.07E-03	4.58E-03
ZnO	7.72E-03	7.22E-03	7.84E-03	7.84E-03	1.24E-03	8.59E-03	7.84E-03	-3.73E-03	6.72E-03	9.09E-03
Rb_2O	8.31E-03	8.42E-03	8.75E-03	8.75E-03	9.08E-03	3.17E-03	9.08E-03	8.75E-03	9.41E-03	4.81E-03
SrO	4.27E-02	4.28E-02	4.19E-02	4.27E-02	3.19E-02	4.93E-02	4.00E-02	4.12E-02	3.74E-02	3.98E-02
YO_2	3.21E-03	2.58E-03	3.05E-03	3.18E-03	3.82E-03	2.79E-03	2.50E-03	2.51E-03	2.94E-03	3.67E-03
ZrO_2	2.69E-02	2.02E-02	2.33E-02	3.41E-02	4.46E-02	2.33E-02	1.78E-02	1.76E-02	2.20E-02	2.38E-02
BaO	8.457E-02	8.932E-02	8.558E-02	8.284E-02	7.386E-02	5.387E-02	8.189E-02	8.245E-02	7.681E-02	8.898E-02
ThO_2	9.69E-04	8.45E-04	7.97E-04	9.61E-04	1.15E-03	7.08E-04	6.91E-04	6.60E-04	8.45E-04	6.76E-04
UO_3	3.00E-04	2.22E-04	2.61E-04	3.39E-04	3.82E-04	3.30E-04	2.03E-04	2.02E-04	3.37E-04	2.03E-04
Total	99.60	98.12	99.43	98.03	98.68	98.72	100.01	99.33	101.65	100.13

NA = not analyzed.

Table B.6. Trace Element Composition of Borehole 299-W10-27 Sediments (as µg per g dry sediment). Data are FIO. (Serne et al., 2004a)

Depth (ft bgs)	53.3	53.5	61	88.3	92.5	100	113.5	113.5 DUP	117.5	130
Unit	H2	H2	H2	H2	CCU_u	CCU_l	R_{tf}	R_{tf}	R_{tf}	R_{wi}
Be	2	2	2	2	2	1	2	2	2	2
Sc	11	10	12	10	10	15	8	8	9	22
Ga	15	14	16	15	15	12	14	13	14	17
Ge	1.6	1.2	1.5	1.3	1.4	1	1.4	1.2	1.6	0.9
As	9	6	8	7	7	6	7	<5	10	<5
Se	NA	NA	NA	NA	NA	NA	NA	NA	NA	NA
Nb	11.5	8.8	10.1	11.3	12.6	9.4	7.7	7.7	9.1	11.9
Mo	3	<2	2	3	<2	<2	3	<2	4	0
Ag	<0.5	<0.5	<0.5	<0.5	<0.5	<0.5	<0.5	<0.5	<0.5	<0.5
In	<0.1	<0.1	<0.1	<0.1	<0.1	<0.1	<0.1	<0.1	<0.1	<0.1
Sn	4	3	4	4	3	2	5	4	5	3
Sb	1.2	0.8	0.9	0.8	1	0.4	1.3	0.9	1.6	0.4
Cs	3.3	3	3.3	3.2	4.1	1	3.4	3.3	3.9	1.1
La	33.1	27.5	26.9	32.5	38.1	26.3	22.1	23.4	27.7	24.9
Ce	61.8	53.9	51.9	62.1	74.4	49.3	45.3	45.2	53.2	49.9
Pr	6.9	5.82	6.18	6.98	8.6	5.49	5.03	5.02	6.11	5.77
Nd	27.8	22	24.9	28.1	33.3	22.2	18.9	19.6	24.4	23.4
Sm	5.35	4.33	4.74	5.23	6.07	4.64	3.74	3.87	4.61	5.17
Eu	1.27	1.08	1.18	1.14	1.31	1.25	0.967	0.980	1.04	1.70
Gd	3.98	3.23	3.98	3.97	5.33	3.54	3.04	3.18	3.66	4.60
Tb	0.75	0.54	0.72	0.74	0.88	0.62	0.53	0.55	0.66	0.80
Dy	4.38	3.27	4.00	4.16	4.94	3.86	3.18	3.30	3.85	4.96
Ho	0.83	0.65	0.78	0.80	0.97	0.74	0.65	0.63	0.79	1.00
Er	2.52	1.87	2.44	2.54	2.98	2.08	1.92	1.89	2.35	2.86
Tm	0.373	0.275	0.353	0.374	0.457	0.306	0.282	0.281	0.356	0.419
Yb	2.53	1.86	2.30	2.44	2.89	2.02	1.80	1.89	2.26	2.65
Lu	0.373	0.289	0.350	0.371	0.460	0.304	0.288	0.282	0.335	0.407
Hf	5.5	3.8	4.6	6.6	8.2	4.4	3.4	3.3	4.5	4.4
Ta	0.96	0.71	0.78	0.94	1.03	0.70	0.59	0.64	0.77	0.79
W	1.5	1.0	1.1	1.9	1.6	0.6	1.2	1.2	1.6	0.1
Tl	0.48	0.46	0.42	0.46	0.32	0.19	0.49	0.29	0.51	0.26
Pb	13	13	11	12	2	8	10	<5	13	0
Bi	0.3	0.2	0.2	0.3	0.1	0.1	0.3	<0.1	0.4	<0.1

NA = not analyzed.

B.2 Boreholes In the Vicinity of the T Tank Farm in the 200 West Area

Two boreholes, 299-W11-39 and C4105, in the vicinity of the T Tank Farm have also been characterized for chemical, physical, and mineralogical properties. The location of these two boreholes is shown in Figure B.1. In 299-W11-39 two, 4-in.-diameter, 1-ft-long lexan-lined core samples were recovered from each 2-ft split spoon. Upon recovery, any open spaces in the ends of the liners were stuffed with aluminum foil in the field and plastic end caps secured with duct tape. Liners were sealed with plastic end caps and the outsides labeled with chain-of–custody or borehole ID number, up arrow, and the letter "A" or "B". The letter "A" was assigned to the deeper of the two cores in the 1-ft core run. Table B.7 lists the four sediment samples from borehole 299-W11-39 that were characterized in detail.

Borehole C4105 was drilled and sampled using a driven-probe technique (Reynolds 2003). The borehole is closest to single-shell tank 241-T-106, where it lies approximately 28.1 ft (8.6 m) southwest. Total depth of the borehole was 130.9 ft (39.9 m) bgs; the hole terminated within the vadose zone about 100 ft (30 m) above the groundwater table. During drilling, a total of 22, 1.25-ft long split spoon core samples were collected intermittently starting at a depth of about 14 ft bgs. In all, 30 ft of core was collected from C4105, which accounts for about 23% of the total length of the hole. No samples or drill cuttings were collected between the 22 core runs because the hole was advanced in a closed configuration using a solid, removable tip. Surface elevation of the since-abandoned borehole was 675.02 ft above mean sea level and geographic coordinates were N136720.758 m and E566761.692 m (Reynolds 2003). Probe hole C4105 was decommissioned between March 14-18, 2003, by back-pulling the casing while filling the hole with dry bentonite. Each split spoon in C4105 contained two 0.5-ft-long stainless-steel core liners. A separate subsample was collected from each of the two liners for physical, chemical, and radiological characterization, from most of the 22 split spoons collected. Two of the liners were empty; thus, a total of 42 samples were collected for physical, chemical, and radiological characterization from C4105 (Table B.8).

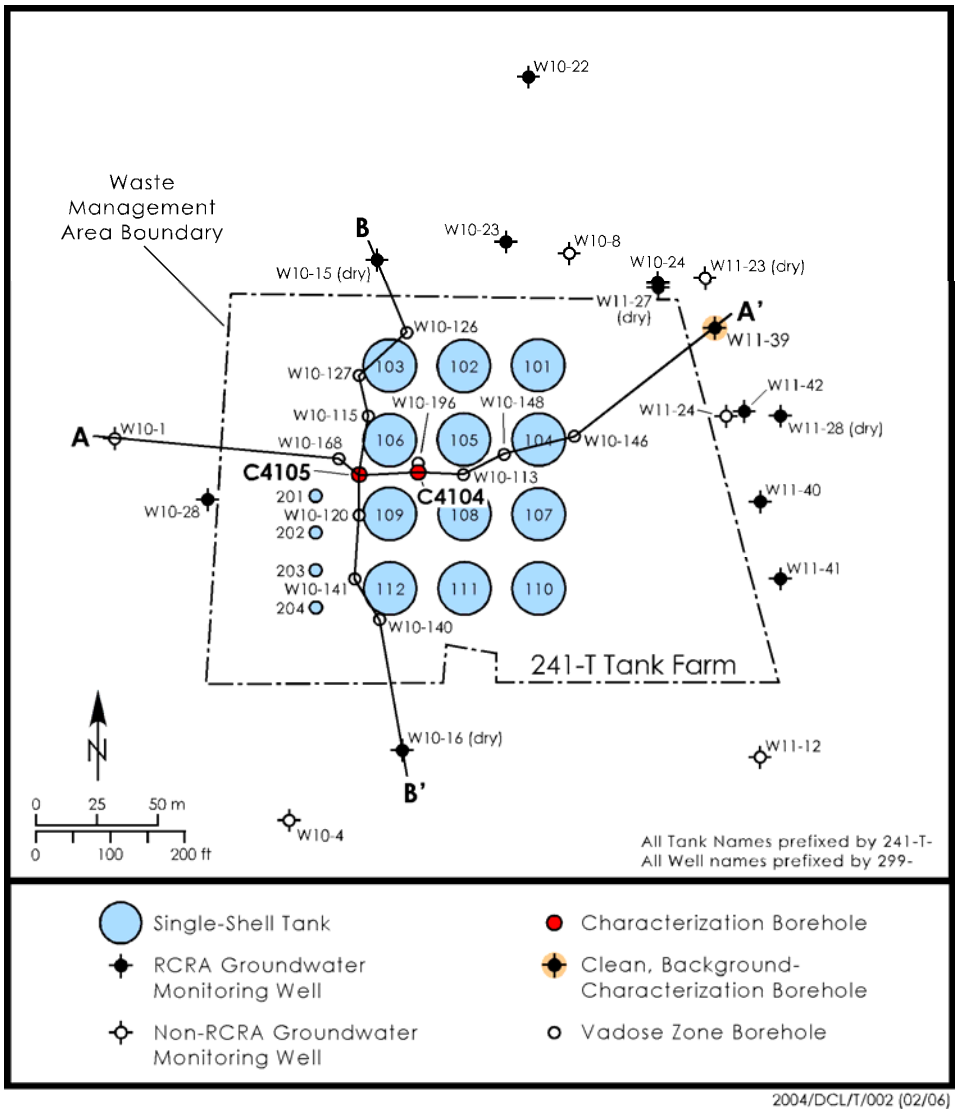

Figure B.1. Location of Boreholes 299-W11-39 and C4105. (Serne et al., 2004a)

Table B.7. Samples Locations for 299-W11-39. Data are FIO. (Serne et al., 2004a)

Core Sample ID	Discrete Sample Depth (ft)	Lithology	Stratigraphic Unit
C3117-49.5	49.5	Silty sand	H2
C3117-60.5	60.5	Silty sand	H2
C3117-78	78.0	Sandy silt	H2
C3117-92	92.0	Silty sand	CCU_z
One characterization sample was collected from each of the depths indicated.			

Table B.8. Split spoon Core Samples From C4105. Data are FIO. (Serne et al., 2004a)

Core Sample ID	COC#	Top Depth (ft)	Bottom Depth (ft)	Mid Depth (ft)	Lithology	Strati-Graphic Unit	Comments
C4105-14.16	S03044-01	14.16	15.66	14.91	Silty sandy gravel	backfill	
C4105-21.70	S03044-02	21.70	23.05	22.38	Silty sandy gravel	backfill	
C4105-35.74	S03044-03	35.74	37.14	36.44	Silty sandy gravel	backfill	Small-diameter (2") core – upper liner empty
C4105-39.18	S03044-04	39.18	40.53	39.86	Silty gravelly sand	backfill	Small-diameter (2") core – upper liner empty
C4105-47.30	S03044-05	47.30	48.03	51.69	Sand	H2	
C4105-54.98	S03044-06	54.98	56.53	55.76	Gravelly sand	H2	
C4105-68.95	S03044-07	68.95	70.45	69.70	Sand	H2	
C4105-80.18	S03044-08	80.18	81.58	80.88	Sand	H2	
C4105-85.36	S03044-09	85.36	87.11	86.24	Sandy silt	CCU_z	
C4105-87.22	S03044-10	87.22	88.52	87.87	Sand to silty sand	CCU_u	
C4105-92.24	S03044-11	92.24	93.59	92.92	Gravelly muddy sand	CCU_l	
C4105-96.01	S03044-12	96.01	97.46	96.74	Muddy sand	CCU_l	
C4105-99.33	S03044-13	99.33	100.68	100.00	Silty sand	CCU_l	
C4105-101.02	S03044-14	101.02	102.36	101.69	Sandy silt	CCU_l	
C4105-102.17	S03044-15	102.17	103.52	102.85	Gravelly sandy mud	CCU_l	
C4105-105.89	S03044-16	105.89	107.24	106.57	Sandy mud to silt	CCU_l	
C4105-109.07	S03044-17	109.07	110.37	109.72	Silt, sandy silt, to silty sand	CCU_l	
C4105-114.97	S03044-18	114.97	116.30	115.64	Sand to sandy silt	R_{tf}	
C4105-119.85	S03044-19	119.85	121.19	120.52	Sand, silty sand, and clayey silt	R_{tf}	
C4105-122.90	S03044-20	122.90	124.24	123.57	Sandy gravel	R_{wi}	
C4105-128.91	S03044-21	128.91	130.12	129.51	Silty sandy gravel	R_{wi}	
C4105-128.58	S03044-22	128.58	129.58	129.08	Silty sandy gravel	R_{wi}	Re-drill of #21?; mostly not analyzed

The stratigraphic contacts (ft bgs) for the various lithologies in the two boreholes are shown in Table B.9.

Table B.9. Depth of Contacts Between the Various Lithologies in Boreholes 299-W11-39 and C4105. Data are FIO. (Serne et al., 2004a)

		Well ID	
		299-W11-39	C4105
	Surface Elev. ft (amsl)	688.6	675.0
Depth (ft) bgs	Backfill	0	0
	H1	5	NP
	H2	33.5	40.6
	CCU_z	89.9	85.5
	CCU_c	98.0	92
	R_{tf}	120.0	111
	R_{wi}	130	122
Thickness (ft)	Backfill	5	40.6
	H1	28.5	NP
	H2	55.4	44.9
	CCU_z	8.1	6.5
	CCU_c	22	19
	R_{tf}	10	11
	R_{wi}	ND	ND
Elevation at top of unit (ft) above msl	Backfill	688.6	675.0
	H1	683.6	NP
	H2	655.1	634.4
	CCU_z	598.7	589.5
	CCU_c	590.6	583.0
	R_{tf}	568.6	564.0
	R_{wi}	558.6	553.0

Amsl = above mean sea level; ND = not determined; NP = not present.

B.2.1 Characterization Data for Boreholes 299-W11-39 and C4105

Particle size, total carbon content, and total elemental composition were analyzed for borehole 299-W11-39. The same measurements were performed on the sediments from borehole C4105. Mineralogical analysis was also carried out for borehole C4105.

B.2.2 Particle Size Data for Borehole 299-W11-39

Table B.10 provides particle size data for the four sediment samples from borehole 299-W11-39 that were characterized using wet sieve and hydrometer methods. Two of the Hanford formation (H2) sediment samples were predominantly sand, whereas the other sample was predominantly silt/clay. The Cold Creek sample (CCU_z) was nearly 90% silt/clay.

Table B.10. Wet Sieve Particle Size Results for Borehole 299-W11-39 Sediments. Data are FIO. (Serne et al., 2004a)

	Stratigraphic Unit	Weight Percent (wt%)		
		Gravel	Sand	Silt/Clay
49.5	H2	6.80	78.19	15.01
60.5	H2	5.53	57.89	36.58
78	H2	2.40	12.56	85.03
92	CCU_z	0.03	10.70	89.27

B.2.3 Carbon Content for Sediments in Borehole 299-W11-39

The carbon content of the same samples are shown in Table B.11 and show that all of the samples contain a low organic content. The two Cold Creek fine grained mud unit samples have slightly more calcium carbonate than two of the three Hanford formation sediments.

Table B.11. Total, Inorganic, and Organic Carbon Content of Vadose Zone Sediments from Borehole 299-W11-39. Data are FIO. (Serne et al., 2004a)

Depth (ft)	Stratigraphic Unit	Total Carbon (%)	Inorganic Carbon (%)	Inorganic Carbon as $CaCO_3$ (%)	Organic Carbon (by difference)
49.5	H2	0.25	0.22	1.83	0.03
60.5	H2	0.25	0.18	1.50	0.07
78	H2	0.52	0.48	4.00	0.04
92	CCU_Z	0.47	0.39	3.25	0.08
92(dup)	CCU_z	0.47	0.41	3.42	0.06

B.2.4 Total Oxide Composition of 299-W11-39 Sediments

Table B.12 and Table B.13 list the chemical composition of the major constituents (as oxides) and trace metals for the sediments from borehole 299-W11-39, respectively. The chemical composition of the sediments is similar among all four samples.

Table B.12. Total Chemical Composition of Borehole 299-W11-39 Sediments (as wt% oxides). Data are FIO. (Serne et al., 2004a)

Depth (ft bgs)	49.5	60.5	78	92	92 dup
Unit	H2	H2	H2	CCU_z	CCU_Z
CO_2	0.81	0.66	1.76	1.43	1.50
Na_2O	2.57	2.64	1.53	1.86	1.86
MgO	1.80	2.12	2.07	1.89	1.94
Al_2O_3	12.44	12.63	14.14	12.28	12.59
SiO_2	66.29	64.31	61.62	64.62	64.47
P_2O_5	0.15	0.24	0.15	0.15	0.16
SO_3	NA	NA	NA	NA	NA
Cl	NA	NA	NA	NA	NA
K_2O	2.33	2.10	2.97	2.54	2.59
CaO	3.56	4.06	3.09	3.19	3.14
TiO_2	0.706	1.005	0.701	0.669	0.667
V_2O_5	0.019	0.025	0.016	0.014	0.014
Cr_2O_3	0.007	0.009	0.009	0.008	0.010
MnO	0.092	0.109	0.097	0.100	0.103
Fe_2O_3	7.18	8.25	7.82	8.48	8.73
CoO	0.002	0.002	0.002	0.002	0.002
NiO	0.003	0.004	0.004	0.004	0.005
CuO	0.008	0.005	0.005	0.005	0.005
ZnO	0.007	0.010	0.010	0.007	0.009
Rb_2O	0.008	0.008	0.014	0.010	0.012
SrO	0.042	0.042	0.023	0.028	0.028
YO_2	0.003	0.004	0.005	0.004	0.005
ZrO_2	0.020	0.030	0.030	0.037	0.037
BaO	0.086	0.080	0.077	0.076	0.077
ThO_2	9.01E-04	1.11E-03	1.38E-03	1.24E-03	1.32E-03
UO_3	2.43E-04	3.18E-04	4.26E-04	3.94E-04	4.11E-04
LOI	2.12	1.89	4.90	3.22	3.14
Total (no LOI)	98.13	98.34	96.14	97.41	97.96
Total (with LOI)	99.44	99.58	99.28	99.20	99.59

NA = not analyzed; LOI = loss on ignition

Table B.13. Trace Element Composition of Borehole 299-W11-39 Sediments (as µg per gram dry sediment). Data are FIO. (Serne et al., 2004a)

Depth (ft bgs)	49.5	60.5	78	92	92
Unit	H2	H2	H2	CCU_Z	CCU_Z
Be	2	2	3	2	2
Sc	12	15	13	11	11
Ga	15	17	19	16	17
Ge	1.2	1.4	1.8	1.4	1.9
As	6	7	16	9	13
Se	NA	NA	NA	NA	NA
Nb	9.0	11.4	14.2	23.3	14.5
Mo	3	<2	2	2	3
Ag	<0.1	<0.1	<0.1	<0.1	<0.1
In	<0.1	<0.1	<0.1	<0.1	<0.1
Sn	3	3	7	4	5
Sb	0.7	0.7	1.5	1.4	1.9
Cs	3.2	3.1	8.1	5.1	6.0
La	31.2	37.8	43.2	40.2	42.5
Ce	61.2	69.3	82.9	77.0	80.8
Pr	6.49	8.09	9.17	8.89	9.21
Nd	24.5	32.0	36.5	35.5	37.0
Sm	4.90	6.13	7.23	6.67	6.93
Eu	1.25	1.43	1.47	1.36	1.43
Gd	3.81	5.24	5.36	5.05	5.46
Tb	0.65	0.89	1.02	0.95	1.01
Dy	3.97	4.90	6.09	5.40	5.72
Ho	0.78	0.96	1.16	1.04	1.10
Er	2.19	2.87	3.49	3.27	3.47
Tm	0.315	0.423	0.527	0.505	0.517
Yb	2.17	2.77	3.55	3.18	3.36
Lu	0.334	0.417	0.520	0.469	0.497
Hf	3.8	5.9	5.9	7.4	7.4
Ta	0.77	0.92	1.19	13.1	1.13
W	2.0	2.9	2.7	2.2	2.3
Tl	0.37	0.46	0.67	0.99	0.65
Pb	10	27	19	9	18
Bi	0.3	0.2	0.6	0.2	0.5

NA = not analyzed.

B.2.5 Particle Size Data for Sediments from Borehole C4105

One sediment sample from each of the major sedimentary lithologies in borehole C4105 was subjected to the hydrometer method to evaluate the fine sand and smaller particle size distribution. The larger particles present were not quantified in any detail but the results shown in Table B.14 are reported as % finer than for the bulk sediment. The sample of the Hanford unit H2 has the least silt and clay and is predominately sand and gravel. The sample from the Ringold Formation Wooden Island member (R_{wi}) is also coarse with little silt and clay. The two samples from the Cold Creek lower subunit (CCU_c) are fairly coarse also, especially at the top of the subunit, where less than 35% of the mass is <60 microns. At the bottom of the Cold Creek lower unit 60% of the mass is <60 microns. The Ringold Formation Taylor Flats member (R_{tf}) sample is fine grained with 75% of the mass being <60 microns in size. The Cold Creek upper subunit (CCU_Z) is the finest grained material characterized and had more than 80% of the mass <60 microns in size.

Table B.14. Particle Size Data for One Sample from Each Major Stratigraphic Unit in Borehole C4105 Sediments. Data are FIO. (Serne et al., 2004a)

Sample	7A	10A		11A		16A		19A		20A	
Depth (ft bgs)	Strat Unit	Depth (ft bgs)	Strat Unit	Depth (ft bgs)	Strat Unit	Depth (ft bgs)	Strat Unit	Depth (ft bgs)	Strat Unit	Depth (ft bgs)	Strat Unit
70.1	H2	88.2	CCU_Z	93.3	CCU_C	106.9	CCU_C	120.9	R_{tf}	123.9	R_{wi}
µm	% finer than	µm	% finer than	µm	% finer than	µm	% finer than	µm	% finer than	µm	% finer than
80.93	9.85	96.32	92.44	89.06	41.64	94.56	71.64	97.18	84.73	83.76	22.70
56.71	7.22	67.02	83.96	61.79	35.03	64.95	58.96	67.63	77.23	58.72	19.77
32.66	6.57	38.18	77.18	35.19	30.41	36.57	48.51	38.02	65.23	33.76	18.31
17.85	5.91	20.30	62.76	19.00	25.78	19.12	30.60	20.03	48.74	18.21	13.18
10.26	4.60	11.32	46.65	10.93	24.46	10.72	20.15	11.17	35.24	10.39	9.52
7.22	3.28	7.83	38.16	7.66	22.47	7.45	14.18	7.73	26.99	7.30	7.32
5.91	3.94	6.30	30.53	6.26	21.15	6.06	12.69	6.24	23.24	5.95	6.59
5.09	2.63	5.44	29.68	5.38	19.83	5.20	9.70	5.37	20.99	5.14	5.86
1.47	3.28	1.52	16.11	1.54	16.52	1.49	6.72	1.50	9.75	1.49	6.59

B.2.6 Carbon Content in Sediments from Borehole C4105

The carbon content of the C4105 sediments are shown in Table B.15. Of particular interest is the large variation of calcium carbonate equivalent concentration in the lower subunit of the Cold Creek (CCU_c). Several depths show significant caliche while other nearby depths, especially at the bottom of the unit, show low caliche concentrations.

Table B.15. Carbon Content of Vadose Zone Sediments in Borehole C4105. Data are FIO. (Serne et al., 2004a)

Sample No.	Depth (ft bgs)	Stratigraphic Unit	Total Carbon (%)	Inorganic Carbon (%)	Inorganic Carbon as $CaCO_3$ (%)	Organic Carbon (by difference)
1A	15.3	Bkfl	0.12	0.08	0.67	0.04
2A	22.7	Bkfl	0.15	0.07	0.58	0.08
3A	36.8	Bkfl	0.16	0.06	0.50	0.10
4A	40.2	Bkfl	0.29	0.10	0.83	0.19
5A	48.4	H2	0.18	0.12	1.00	0.06
6A	56.1	H2	0.16	0.10	0.83	0.06
7A	70.1	H2	0.19	0.13	1.08	0.06
8A	81.2	H2	0.38	0.32	2.66	0.06
9A	86.7	CCU_z	0.49	0.37	3.10	0.12
10A	88.2	CCU_z	0.53	0.47	3.91	0.06
10A DUP	88.2	CCU_z	0.51	0.40	3.29	0.11
11A	93.3	CCU_c	5.41	5.22	43.47	0.19
12A	97.1	CCU_c	2.15	1.96	16.30	0.19
13A	100.3	CCU_c	0.86	0.81	6.76	0.05
14A	102.0	CCU_c	7.33	7.02	58.50	0.31
15A	103.2	CCU_c	5.80	5.68	47.34	0.12
16A	106.9	CCU_c	0.82	0.71	5.95	0.11
17A	110.0	CCU_c	0.13	0.12	1.00	0.01
17A DUP	110.0	CCU_c	0.10	0.07	0.56	0.03
18A	116.0	R_{tf}	0.24	0.20	1.70	0.04
19A	120.9	R_{tf}	0.45	0.37	3.07	0.08
20A	123.9	R_{wi}	0.21	0.18	1.50	0.03
21A	129.8	R_{wi}	0.05	0.03	0.22	0.02

Samples with values in red contain significant amounts of caliche.

B.2.7 Mineralogy of Sediments from Borehole C4105

X-ray diffraction (XRD) analysis of C4105 borehole samples 7A, 10A, 16A, 19A, and 20A shows that most all sediments are mineralogically similar despite having wide ranging particle size distributions. The samples are dominated by quartz and feldspar (both plagioclase and alkali-feldspar), with lesser amounts of clay, calcite, and amphibole. Figure B.2 is an example background subtracted XRD pattern of sample 10A (88.2 ft bgs). Intensity for the primary quartz reflection (26.6° 2θ) was truncated to increase the pattern detail. The main reflections associated with feldspar minerals are between 27.34° 2θ and 27.92° 2θ, with the higher 2θ values belonging to the plagioclase series. Clay minerals were identified on the X-ray tracings by the reflections at 6.3° 2θ and 8.8° 2θ. The presence of an amphibole was established by the characteristic 100% reflection at 10.5° 2θ. In addition, minor amounts of calcite were identified in these samples by a diffraction peak positioned at 29.45° 2θ.

By contrast, XRD results from sample 11A indicate the sediment is dominated by calcite. The major reflection for calcite (29.40° 2θ) dominates the pattern as shown in Figure B.3. Lesser amounts of quartz, feldspar, amphibole, and clays were also identified by XRD, but at much lower concentrations than in the

previously described sediments. The calcite domination is corroborated by the data shown in Table B.15 for sample 11A. Results from the semi quantification of the minerals in the bulk samples from C4105 are provided in Table B.16.

Quartz concentrations range from 27 to 54 wt% (excluding 11A), with an average quartz concentration of 38 ± 10 wt%. Plagioclase feldspar is present at concentrations between 12 to 43 wt% and potassium feldspar concentrations are between 4 to 15 wt%. Plagioclase feldspar was more abundant than potassium feldspar in all C4105 samples. The amphibole phase comprised <5 wt%. Calcite concentrations measured 55 wt% in sample 11A, with all other samples having <4 wt%. Clay minerals, consisting primarily of a 6.3 ° 2θ reflection (chlorite and smectite) as well as the 8.8° 2θ reflection (mica), make up between 8 and 32 wt% of the sediment samples. Detailed XRD examination of the clay fraction from each sediment sample (except 11A) was conducted. The clay fraction is dominated by four clay minerals: smectite, chlorite, illite, and kaolinite with minor amounts of quartz and feldspar.

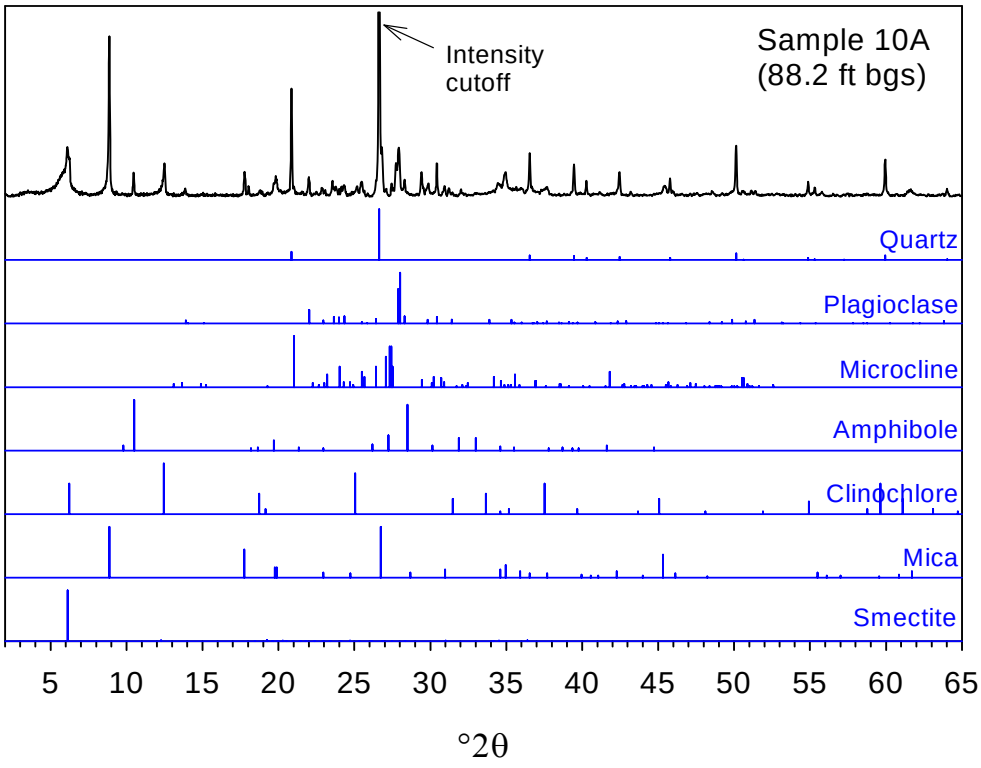

Figure B.2. XRD Tracing for Sediment Sample 10A (88.2 ft bgs) Collected from Borehole C4105, with Matching PDF™ Files. Data are FIO. (Serne et al., 2004a)

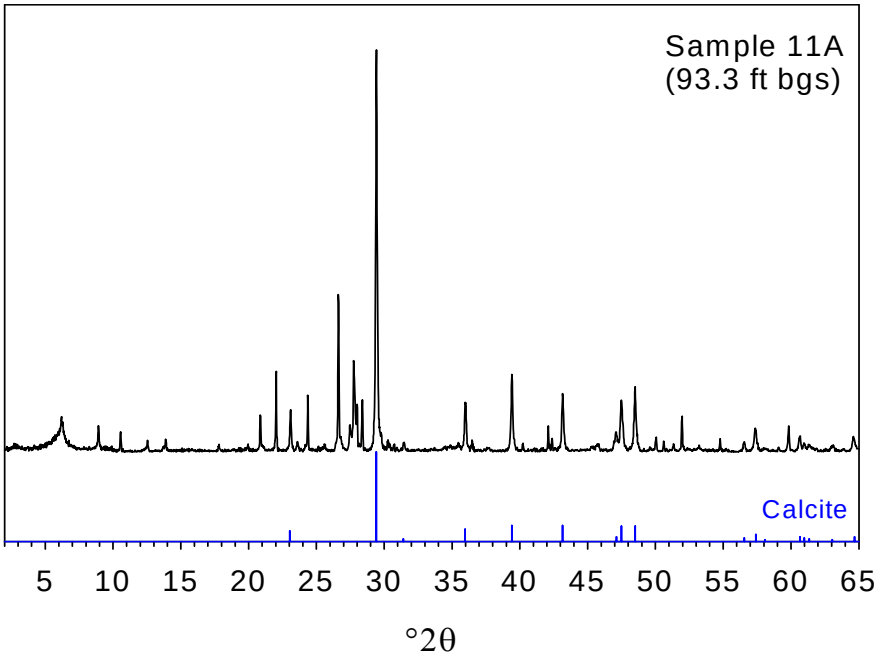

Figure B.3. XRD Tracing for Sediment Sample 11A (93.3 ft bgs) Collected from Borehole C4105, with Calcite PDF™ File. Data are FIO. (Serne et al., 2004a)

Table B.16. Whole Rock Quantitative XRD Results Determined by JADE Whole Pattern Fitting on Sediment Samples Collected from Borehole C4105. Results are given in wt%. Data are FIO. (Serne et al., 2004a)

Sample ID	Depth (ft bgs)	Quartz	Plagioclase	Microcline	Amphibole	Calcite	Clay Minerals
7A	70.1	34	39	15	2	1	8
10A	88.2	41	17	6	4	2	29
11A	93.3	11	18	7	<1	55	10
16A	106.9	35	19	6	5	3	33
19A	120.9	54	12	4	<1	2	28
20A	123.9	27	43	12	4	4	11

Figure B.4 provides an example XRD pattern of a typical clay assemblage (sample 19A) following two different treatments. Smectite is the fraction of the Mg-saturated sub-sample that gives a basal reflection at 5.85° 2θ and expands to 5.28° 2θ after solvation with ethylene glycol. Glycerol solvation treatments on two Mg-saturated clay slides (10A and 19A) were used to confirm the absence of vermiculite in the clay fraction. Vermiculite clay produces a basal reflection at 5.00° 2θ in the presence of glycol; however, in the presence of glycerol, vermiculite retains a basal reflection of 6.10° 2θ. A significant change in intensity of the basal reflection at 6.10° 2θ between the two treatments would indicate the presence of vermiculite. No observable intensity changes occurred on the basal reflection positioned at 6.10° 2θ in either of the two clay samples examined.

Illite is the easiest of the four clay minerals to identify in these sediments. The basal reflections for illite are at 8.88, 17.8, and 26.7° 2θ. The various treatments, including cation saturation and solvation with ethylene glycol, do not affect the position of these reflections. Chlorite is identified by a basal series of diffraction peaks at 6.24, 12.5, 18.8, and 25.2° 2θ, which are unaffected by cation saturation or ethylene

glycol solvation. Kaolinite is difficult to identify in the presence of chlorite. Basal reflections characteristic of kaolinite are at 12.5 and 24.9° 2θ and are superimposed on the even-ordered chlorite reflections. Kaolinite reflections are unaffected by cation saturation and ethylene glycol solvation. Positive identification of kaolinite in the presence of chlorite can be determined by differentiating kaolinite basal reflection at 24.9° 2θ from the chlorite reflection at 25.2° 2θ (Figure B.4). Published reports characterizing clay fractions of Hanford formation sand-dominated sediment from other studies (Serne et al. 2002a,b, 2004a,b,c, 2008a,b,c,d; Lindenmeier et al. 2003) identified kaolinite using electron microscopy.

Trace amounts of quartz in the <2.0 μm fractions are evident by the diffraction peak located at 20.85° 2θ. The 100% reflection for quartz (26.6° 2θ) is hidden by the third-order basal reflection of illite located at 26.6° 2θ. Plagioclase feldspar is also identified in the clay fractions by the minor diffraction peak at 27.8° 2θ. Semi-quantitative results of clay minerals in the <2.0 μm fractions are presented in Table B.17. Total recoveries were normalized to 100%. Smectite concentrations range from 26 to 56 wt% with an average of 41 wt%. Illite concentration varies from 33 to 50 wt% with an average concentration of 42 wt%. Chlorite and kaolinite are the least abundant of the clay minerals identified in the samples with concentrations equal to or less than 20 and 7 wt%, respectively. Quartz and feldspar minerals were present as trace amounts in the clay fraction and therefore were not included in totals in Table B.17.

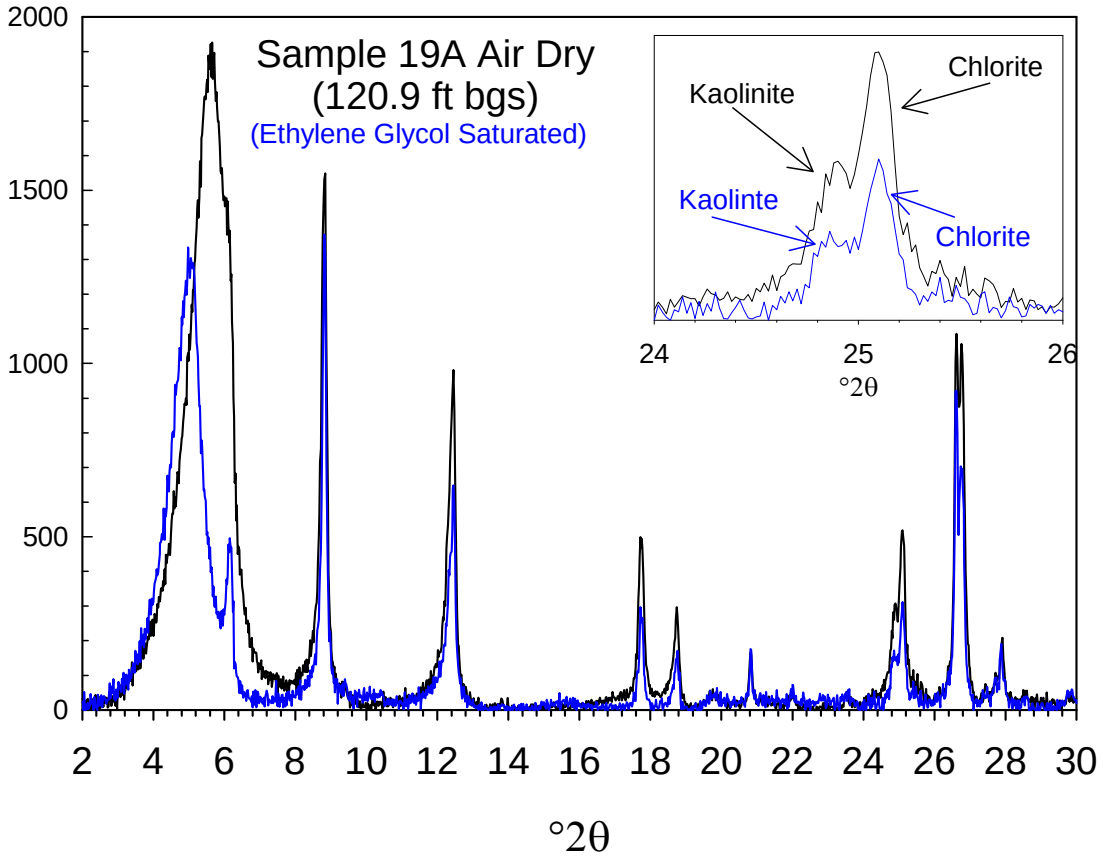

Figure B.4. XRD Tracing of Clay Fraction from Sediment Sample 19A (120.9 ft bgs) Collected from Borehole C4105, with Matching PDF™ Files. Data are FIO. (Serne et al., 2004a)

Table B.17. Semi Quantitative XRD Results of Clay Minerals in <2 um Fraction of Sediment Samples Collected from Borehole C4105. Results are given in wt%. Data are FIO. (Serne et al., 2004a)

Sample ID	Depth (ft bgs)	Smectite	Illite	Chlorite	Kaolinite
7A	70.1	26	47	20	7
10A	88.2	35	50	10	5
16A	106.9	48	42	6	5
19A	120.9	56	33	7	5
20A	123.9	40	40	13	7

B.3 Boreholes Near SX Tank Farm

Boreholes were drilled into uncontaminated sediments west of the SX Tank Farm in the late 1990s. The boreholes were drilled to increase the groundwater monitoring well coverage of the tank farm. The boreholes B8812 (well 299-W22-48) and B8814 (well 299-W22-50) (see Figure B.5 for location) were drilled as part of an integrated effort to 1) collect intact subsurface core samples for detailed vadose zone characterization, and 2) construct down gradient RCRA groundwater monitoring wells in the uppermost-unconfined aquifer. Additional well completion, aquifer testing, and water sampling information and results are reported in Horton and Johnson (2000).

The vadose zone portions of the boreholes were drilled using the drive-barrel cable tool technique wherever possible. The boreholes were drilled without the aid of drilling fluids such as water or mud, unless noted in the logs, to minimize the introduction of artificial moisture into the sediment samples and core. The lower portion of borehole B8814, i.e., below the water table, was drilled with an air rotary technique. Borehole sampling consisted of near continuous split spoon coring and/or sediment grab sampling throughout the borehole. Each borehole was cored by driving a 4-in.-diameter by 2.5-ft-long split spoon sampling device ahead of the drilled borehole. Each borehole was then cleaned out to the bottom of the cored interval prior to sampling the next interval.

Split spoon core refusal was reached at the Ringold Formation silty sandy gravel in both wells; cable tool drilling continued to at least the water table with a hard tool bit. The split spoon cores are contained in either 6-in.-long or 1-ft-long lexan core barrel liners (core sleeves). Continuous core recovery was nearly 100%. Sediment grab samples were collected by hand or scoop from the drill cuttings recovered during drilling and/or from the split spoon drive shoe. The split spoon cores provide the most representative intact samples available and the core depth intervals are believed to be accurate to within 0.5 ft of true depth. Fine sediment structure and subtle facies variations are usually well preserved in the split spoon cores. The lexan liners were cut with a saw and the core split into two slabs or halves along the long axis. Sub-sampling for geochemical characterization was from the middle (inside) of the core slab.

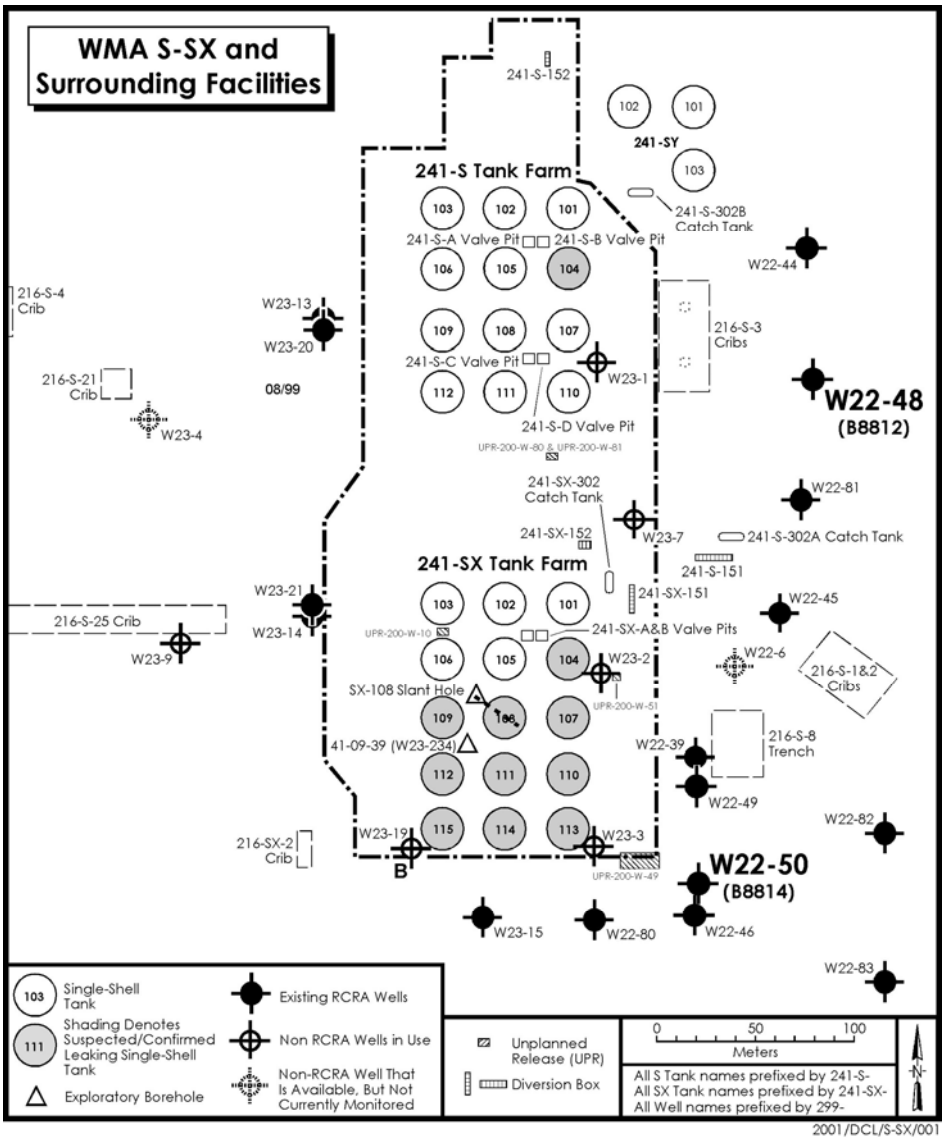

Figure B.5. Location Map for 299-W22-48 and 299-W22-50 Boreholes. (Horton and Johnson, 2000)

B.3.1 Borehole 299-W22-48

Well 299-W22-48 is located approximately 135 meters east of tank S-110 and approximately 100 meters north of the SX Tank Farm (Figure B.5). Well coordinates are 566,996.641 meters east and 134,425.096 meters north [datum is NAD83 (91)]. Land surface elevation is 207.132 meters above mean sea level. Total depth (TD) of the borehole is 249 ft bgs. The water table was encountered at approximately 226 ft bgs. The borehole was composed of a 4-in.-diameter well casing with a 15-ft.-long sampling screen placed at the water table (see also Horton and Johnson 2000).

B.3.1.1 Characterization of Sediments from 299-W22-48

Particle size distribution, particle density, total and inorganic carbon content, major element oxide content, minor element content, cation exchange capacity (CEC), and detailed mineralogical measurements were performed.

B.3.1.2 Particle Size Analyses of Sediments from 299-W22-48

Both dry sieve and wet sieve methods were applied to identify the particle size distribution. The dry sieve data shown in Table B.18 are coarser than the wet sieve data shown in Table B.19. Table B.20 shows a comparison between the wet and the dry sieve data. The most significant difference occurs for the Cold Creek fine-grained sample at 136 ft bgs, where the sand content drops from 60% to 18% upon wet sieving. There is a complementary increase in the silt and clay content when wet sieved. This implies that the Cold Creek fine-grained facies sediments are more aggregated and individual particles tend to cling to each other through static electrical forces generated via dry sieving but disperse upon being wetted with sodium hexametaphosphate dispersing agent.

Table B.18. Dry Sieve Results from Borehole 299-W22-48. Data are FIO. (Horton and Johnson, 2000)

Depth (ft bgs)	Strat. Unit	Percent Gravel	Percent Sand	Percent Silt/Clay
37	H1a	0.60	91.40	7.74
39.5	H1a	1.42	89.80	8.78
42.5	H1	63.17	36.83	
44.5	H1	63.26	36.74	
47	H1	73.38	22.98	3.64
50	H1	19.46	76.70	3.84
53.5	H1	21.22	77.71	1.07
56	H1	9.46	88.02	2.52
57.5	H1	2.96	92.39	4.66
62	H2	0.29	94.52	5.19
64.5	H2	0.06	95.38	4.56
67	H2	0.99	96.06	2.95
70	H2	0.96	99.04	2.89
69.5	H2	1.58	94.26	4.17
74.5	H2	1.74	86.46	11.81
77	H2	0.02	89.77	10.21
91.5	H2	0.39	94.60	5.01
101.5	H2	0.01	98.11	1.88
136	CCUz	1.06	60.33	38.56
163.5	Rtf	0.00	94.18	5.79

Table B.19. Particle Size Distribution Determined by Wet Sieving/Hydrometer Method. Data are FIO. (Horton and Johnson, 2000)

Sample (ft bgs)	Unit	% Gravel	% Sand	% Silt	% Clay
39.5	H1a	0.16	77.59	20.58	1.68
47	H1a	64.64	18.69	15.13	1.55
91.5	H2	0.25	70.65	26.99	2.11
101.5	H2	0	78.71	18.82	2.47
136	CCUz	0.01	18.45	75.89	5.65
146	CCUc	52.36	27.11	15.23	5.3
148.5	CCUc	26.31	59.86	10.32	3.5

163.5	Rtf	0.01	89.00	9.67	1.32

Wet sieving samples with high % of $CaCO_3$ dissolves several % of the starting mass, which may affect reported values.

Table B.20. Comparison of Particle Size Distributions for Dry vs. Wet Sieving. Data are FIO. (Horton and Johnson, 2000)

Depth ft bgs	Unit	Type	wt% Gravel	wt% Sand	wt% Silt/Clay
39.5	H1a	Dry	1.42	89.8	8.78
		Wet	0.16	77.6	22.24
47	H1	Dry	73.4	23.0	3.6
		Wet	64.6	18.7	16.7
91.5	H2	Dry	0.39	94.6	5.01
		Wet	0.25	70.6	29.2
101.5	H2	Dry	0.01	98.11	1.88
		Wet	0	78.7	21.3
136	CCUz	Dry	1.06	60.33	38.56
		Wet	0.01	18.4	81.6
163.5	Rtf	Dry	0	94.18	5.79
		Wet	0.01	89.0	11.0

The Hanford Unit H1 is much coarser than the units above and directly below it. The Cold Creek upper subunit CCUz is fine-grained and well sorted compared to the other units below it. Determining the true particle size of the Cold Creek unit caliche layer is problematic, because it is usually moderately to strongly cemented. As result, the sieving method only measures calcareous aggregates of gravel, sand, silt, and/or clay broken up during drilling and sampling. To obtain an accurate particle size distribution of the caliche, a petrographic analysis is required. Alternatively, the sieving method could be used if carbonate is first dissolved before analysis.

B.3.1.3 Particle Density Data for Sediments from 299-W22-48

The particle density of bulk sediment was determined for selected aliquots from the borehole 299-W22-48 using pycnometers. The results are shown in Table B.21. The particle densities in Table B.21 reflect the mineral composition of the Hanford formation and the Cold Creek unit, which are both predominantly composed of quartz, plagioclase, and potassium feldspar.

Table B.21. Particle Densities for Selected Samples of W22-48 Sediments. (Horton and Johnson, 2000)

Depth (ft bgs)	Stratigraphic Unit	Density (g/cm^3)	Std. Dev. (3 trials)
39.5	H1a	2.682	0.005
47	H1	2.762	0.003
91.5	H2	2.667	0.034
101.5	H2	2.620	0.016
136	CCUz	2.661	0.003
140	CCUz	2.680	0.007
146	CCUc	2.535	0.011
148	CCUc	2.604	0.012
163.5	Rtf	2.651	0.011

B.3.1.4 Carbon Content in Sediments from 299-W22-48

Measured carbon for borehole 299-W22-48 are shown in Table B.22. The calcium carbonate equivalent (in terms of grams of calcite per gram of oven dry sediment) appears typical of Hanford formation sediments, which range between about 1 and 5 wt% $CaCO_3$ (Last et al. 1989).

Samples from depths of 146 and 148.5 ft bgs for borehole 299-W22-48 have high (~38%) $CaCO_3$ associated with the Cold Creek lower subunit (CCU_g or CCU_c) carbonate facies. The $CaCO_3$ content decreases again in the underlying non-pedogenically altered Ringold Formation. The caliche rich sediment at borehole 299-W22-48 contains higher calcium carbonate than the caliche-rich sediment at borehole 299-W22-50. If the caliche in 299-W22-50 is within a finer-grained sediment facies than the caliche at 299-W22-48, finer grained material may not concentrate as much calcite by evaporative processes during the near surface wetting and drying cycles.

The method used to measure the organic carbon relies upon subtracting the inorganic carbon from the total carbon in the sample and for such low C values is not accurate. The low values for organic carbon are within the ranges generally reported for Hanford sediments.

Table B.22. Calcium Carbonate and Organic Carbon Content (wt%) for Sediments from Borehole 299-W22-48. Data are FIO. (Horton and Johnson, 2000)

Depth (ft bgs)	Strat. Unit	Total Carbon (%)	Inorganic Carbon (%)	Inorganic Carbon as $CaCO_3$ (%)	Organic Carbon (%)
29.5	H1a	0.18	0.16	1.33	0.02
32	H1a	0.14	0.10	0.83	0.04
39.5	H1a	0.24	0.21	1.75	0.03
47	H1	0.20	0.15	1.25	0.05
56	H1	0.28	0.22	1.83	0.06
74.5	H2	0.29	0.24	2.00	0.05
74.5	H2	0.31	0.26	2.17	0.05
91.5	H2	0.26	0.22	1.83	0.04
101.5	H2	0.43	0.39	3.25	0.04
106.5	H2	0.25	0.22	1.83	0.03
115.5	H2	0.27	0.26	2.17	0.01
136	CCUz	0.40	0.35	2.92	0.05
143.5	CCUz	0.52	0.44	3.67	0.08
146	CCUc	4.78	4.60	38.37	0.17
148.5	CCUc	4.64	4.56	38.00	0.08
151	Rtf	0.16	0.13	1.08	0.03
163.5	Rtf	0.12	0.09	0.75	0.03
170	Rtf	0.15	0.13	1.08	0.02
172.5	Rtf	0.15	0.14	1.17	0.01
187	Rtf	0.02	0.01	0.08	0.01
192	Rwi(e)	0.02	0.01	0.08	0.01

B.3.1.5 Elemental Composition of the Sediments from 299-W22-48

The elemental composition of the 299-W22-48 bulk sediment was determined by a combination of energy and wavelength dispersion X-ray fluorescence (XRF) and converted to oxides (Table B.23). It was

assumed that the Fe present in the sediments is all Fe_2O_3, although there may be some reduced (ferrous oxides) iron also present. The presence of calcium carbonate has been accounted for by converting the calcium carbonate in Table B.22 back to percent CO_2, and adding it to the XRF totals.

The data in Table B.23 suggest two trends in major element composition that reflect lithology. The most evident trend is the substantial increase in CaO and CO_2 in the caliche samples from 146 and 148.5 ft depths. Less evident is a decrease in K_2O and increases in CaO and Fe_2O_3 in the gravel sample at 47 ft depth compared to the overlying and underlying sandy samples. There also appears to be a decrease in Na_2O and an increase in MgO in the CCUz fine-grained sample (136 ft depth) relative to the overlying sediments from the Hanford formation. These same trends are noted in samples from borehole 299-W22-50 (to be discussed below) and probably represent differences in the mineral composition of the various lithologies. The calculated mass balances range between 98% and 105% with a mean of 101 ± 2 wt% for the 14 samples. Table B.24 presents the oxide composition of the clay fraction of the 299-W22-48 sediments.

Table B.23. Bulk Chemical Composition of 299-W22-48 Sediments (wt% as oxides). Data are FIO. (Horton and Johnson, 2000)

Depth (ft bgs)	39.5	47	91.5	101.5	136	146	148.5	163.5
Strat. Unit	H1a	H1	H2	H2	CCUz	CCUc	CCUc	Rtf
Oxides								
Na_2O	2.25	2.68	2.26	2.25	1.62	0.63	1.06	2.01
MgO	3.32	4.23	3.00	3.35	4.14	7.24	4.16	2.97
CO_2	0.84	0.60	0.88	1.56	1.40	18.39	18.24	0.36
Al_2O_3	14.19	14.55	13.13	13.36	13.21	6.24	8.03	13.11
SiO_2	70.17	62.15	72.20	72.31	67.39	36.43	43.47	73.91
P_2O_5	<0.21	<0.25	<0.20	<0.21	<0.20	<0.32	<0.32	<0.19
SO_3	0.08	0.12	0.06	0.09	0.06	0.39	0.32	0.06
Cl	0.04	<0.02	0.04	0.04	0.03	<0.02	<0.02	0.04
K_2O	2.52	1.49	2.61	2.52	2.31	0.97	1.52	2.90
CaO	3.16	7.72	3.16	3.24	3.37	24.08	20.90	2.08
TiO_2	0.61	1.53	0.52	0.59	0.64	0.55	0.39	0.54
V_2O_5	0.01	0.05	0.01	0.01	0.01	0.02	0.01	0.01
Cr_2O_3	0.00	0.01	0.01	0.01	0.01	0.00	0.01	0.00
MnO	0.07	0.14	0.06	0.06	0.06	0.25	0.05	0.05
Fe_2O_3	4.00	9.64	3.46	3.89	4.13	3.41	3.06	3.36
SrO	0.04	0.04	0.04	0.04	0.03	0.04	0.04	0.03
BaO	0.09	0.07	0.09	0.09	0.07	0.04	0.05	0.08
Total	101.61	105.28	101.75	103.63	98.67	99.01	101.65	101.70

Table B.24. XRF Analysis of Clay Fraction from Borehole 299-W22-48 (wt%). Data are FIO. (Horton and Johnson, 2000)

	Sample Depth (ft bgs)						
Oxide	39.4	47	91.5	101.5	136	146	163.5
Na_2O	NM	NM	NM	NM	NM	NM	NM
MgO	NM	NM	NM	NM	NM	NM	NM
CO_2	NM	NM	NM	NM	NM	NM	NM
Al_2O_3	13.74	13.57	16.66	15.23	17.43	5.61	13.90
SiO_2	42.50	50.38	48.78	46.00	51.24	25.62	45.89
P_2O_5	0.47	0.75	0.67	0.71	0.58	0.82	0.49
SO_3	0.16	0.19	0.22	0.21	0.21	0.35	0.18
Cl	1.31	0.35	1.00	2.50	0.13	0.44	1.54
K_2O	2.09	1.60	2.76	2.42	2.61	0.57	2.44
CaO	2.98	4.46	1.94	1.15	1.95	29.05	1.19
TiO_2	0.76	1.07	0.80	0.81	0.76	0.17	0.72
V_2O_5	0.03	0.02	0.02	0.02	0.02	0.01	0.02
Cr_2O_3	0.01	0.01	0.01	0.01	0.01	0.00	0.01
MnO	0.18	0.15	0.17	0.18	0.11	0.30	0.31
Fe_2O_3	10.78	12.01	10.24	10.19	10.10	2.98	10.20
SrO	0.02	0.03	0.02	0.01	0.01	0.03	0.02
BaO	0.03	0.05	0.04	0.04	0.04	0.01	0.05

NM = not measured

B.3.1.6 Cation Exchange Capacity for Sediments from 299-W22-48

The CEC of sediment from selected depths in borehole 299-W22-48 was determined using two different procedures (Polemio and Rhoades 1977; Amrhein and Suarez 1990) for calcareous sediments. Five grams of each sample was used in triplicate determinations using both methods. The cation exchange capacities for the 299-W22-48 sediment from various depths are shown in Table B.25.

Table B.25. Comparison of Cation Exchange Capacity of Core Samples from 299-W22-48 (meq/100 g) Using Two Different Methods. Data are FIO. (Horton and Johnson, 2000)

Depth (ft bgs)	Stratigraphic Unit	Polemio and Rhoades	Amrhein and Suarez
39.5	H1a	16.5 ± 3.9	6.1 ± 0.2
91.5	H2	13.3 ± 7.0	4.8 ± 0.4
101.5	H2	16.3 ± 1.0	6.0 ± 0.4
136	CCUz	25.2 ± 3.0	8.9 ± 2.5
146	CCUc	39.6 ±5.6	19.4 ± 2.2
148.5	CCUc	26.7 ± 0.8	13.2 ± 5.1
163.5	Rtf	15.7 ± 1.7	5.2 ±0.2

The largest CEC is associated with the Cold Creek unit caliche samples (146 to 148.5 ft depths) even though the XRD results presented below indicate significantly fewer clay minerals than the other

sediments. However, the caliche likely contains significant quantities of clay particles cemented with $CaCO_3$ that do not disaggregate when sieved.

The method of Polemio and Rhoades (1977) consistently yields higher measures of CEC than the method of Amrhein and Suarez (1990). It could be that the Polemio and Rhoades (1977) method does not correct for calcium carbonate dissolution, or a less likely possibility is that the Amrhein and Suarez (1990) method overcorrects. A third method was used to determine the exchangeable base cations (Na, K, Mg, Ca, Sr, Ba), similar to the ammonium acetate procedure in Ciesielski and others (1997). The comparison of the ammonium acetate extraction to the two CEC method results are shown in Table B.26. The ammonium acetate extraction results in general agreement with the CEC as determined using the Amrhein and Suarez (1990) method.

Table B.26. Comparison of the Base Cation Sum and CEC Measurements in meq/100 g. Data are FIO. (Horton and Johnson, 2000)

W22-48 Depth (bgs)	Ammonium Acetate Sum	Polemio and Rhoades (1977)	Amrhein and Suarez (1990)
B8812-39.5 [H1a]	7.66	16.5 ± 3.9	6.1 ± 0.2
B8812-47 [H1]	10.99	not done	not done
B8812-91.5 [H2]	10.36	13.3 ± 7.0	4.8 ± 0.4
B8812-101.5 [H2]	11.68	16.3 ± 1.0	6.0 ± 0.4
B8812-136 [CCUz]	11.22	25.2 ± 3.0	8.9 ± 2.5
B8812-146 [CCUc]	14.85	39.6 ±5.6	19.4 ± 2.2
B8812-148.5 [CCUc]	12.06	26.7 ± 0.8	13.2 ± 5.1
B8812-163.5 [Rtf]	7.94	15.7 ± 1.7	5.2 ±0.2
B8812-192 [Rwi(e)]	5.57	not done	not done

B.3.1.7 Mineralogy of Sediments from Borehole 299-W22-48

The mineralogy of bulk sediment samples and the clay fractions (<2 um) from borehole 299-W22-48 depths were characterized by XRD. Table B.27 shows the semi-quantitative % mass mineralogy distribution for the bulk sediments and the clay-sized fraction for borehole 299-W22-48.

Table B.27. Semi-Quantitative Mineral Content for Borehole 299-W22-48 (wt%). Data are FIO. (Horton and Johnson, 2000)

Bulk Sediment	Quartz	K-Feldspar	Na-Feldspar	Calcite	Total
39.5’ (H1a)	60	<5	20	ND	~85
47’ (H1)	20	<5	15	10	~50
91.5’ (H2)	45	40	15	ND	~100
101.5’ (H2)	95	<5	20	ND	~115
136’ (CCUz)	80	30	10	ND	~120
146’ (CCUc)	25	<5	10	40	~80
148.5’ (CCUc)	25	10	20	40	~95
163.5’ (Rtf)	65	20	10	ND	~95

Clay Sized Fraction Depth (ft)	Quartz	Feldspar	Calcite	Smectite	Illite	Chlorite	Kaolinite	Total
39.5’ (H1a)	<5	<5	Tr	25	20	15	<5	~75
47’* (H1)	<5	<5	5	10	10	10	<5	~50
91.5’ (H2)	<5	<5	Tr	20	35	20	<5	~90
101.5’ (H2)	10	<5	Tr	25	35	35	10	~120
136’ (CCUz)	10	<5	Tr	20	30	20	10	~95
146’* (CCUc)	<5	<5	40	15	10	10	<5	~90
148.5’* (CCUc)	<5	<5	40	<5	10	<5	<5	~85
163.5’ (Rtf)	10	<5	ND	30	50	30	<5	~130

ND = not detected; Tr = trace amount detected <5%

B.3.2 Borehole 299-W22-50

Well 299-W22-50 is located approximately 25 meters southeast of the southeast corner of the S-SX Tank Farm fence (Figure B.5). Well coordinates are 566,904.261 meters east and 134,139.756 meters north [datum is NAD83 (91)]. Land surface elevation is 669.75 ft amsl [204.142 meters]. This borehole was drilled from the surface to approximately 241 ft bgs using the core-barrel cable tool technique and from 241 ft to 547.5 ft bgs (TD) using the air rotary technique. The water table was encountered at approximately 219 ft bgs. The borehole was composed of a 4-in.-diameter well casing with a 15-ft.-long sampling screen placed at the water table.

Borehole sampling consisted of near continuous split spoon coring from approximately 20 ft bgs to a depth of 177.5 ft bgs and sediment grab samples collected at approximately 5-ft intervals throughout the drilling and coring of the borehole. Split spoon core refusal occurred at 177.5 ft bgs; cable tool drilling continued below this depth with a hard tool bit to approximately 243 ft bgs. Drilling continued with air rotary to total depth. During coring, 124 core sleeves (12-in. liners) were recovered. Archive grab samples were collected at approximately 5-ft intervals from surface to 20 ft bgs and below the cored interval, from 180.5 ft to TD.

B.3.2.1 Borehole 299-W22-50 Characterization

Particle size distribution, particle density, total and inorganic carbon content, major element oxide content, minor element content, CEC, and detailed mineralogical measurements were performed.

B.3.2.2 Particle Size of Sediments in Borehole 299-W22-50

Both dry sieving and the wet sieving/hydrometer methods were used to determine the total particle size range for vadose zone sediments from selected depths in 299-W22-50. The dry sieving samples were used to help locate the upper and lower contacts for the coarse-grained Hanford H1 unit. The dry sieving data

were used along with the moisture content and geophysical logging to help differentiate the boundary for a H1 unit within the Hanford formation.

For the dry sieving, an aliquot of the oven dry sediment was sieved through the following sequence of sieves: 4, 2, 1, 0.5, 0.25, 0.212, 0.125, 0.063 mm, and pan. The second particle size measurement used the hydrometer method and concentrated on quantifying the silt and clay distribution. The silt and clay separates were saved for mineralogical analyses. The dry sieving results for core samples collected from 299-W22-50 sediments are shown in Table B.28. The wet sieving results are presented in Table B.29.

Table B.28. Particle Size Distributions (determined by dry sieving) for 299-W22-50. Data are FIO. (Horton and Johnson, 2000)

Depth (ft bgs)	Strat. Unit	Percent Gravel	Percent Sand	Percent Silt/Clay
47.5	H1a	0.99	96.00	3.01
48.5	H1a	0.01	92.45	7.55
50-51	H1a	0.56	90.11	9.33
51	H1a	0.23	90.81	8.95
52.5	H1a	4.82	90.55	4.63
53.5	H1	6.06	92.09	1.85
54.5	H1	3.95	96.05	0.00
56	H1	10.69	85.34	3.97
57	H1	4.55	93.95	1.50
58	H1	48.62	49.38	2.01
60	H1	86.63	12.04	1.33
61	H1	50.91	45.67	3.42
62.5	H2	0.99	96.00	3.01
63.5	H2	1.70	96.75	1.56
65	H2	0.26	94.51	5.23
66	H2	1.35	96.69	1.97
68.5	H2	0.00	92.23	7.77
70-71	H2	2.28	92.22	5.51

Table B.29. Particle Size Distributions Determined by Wet Sieving/Hydrometer Method for Borehole 299-W22-50. Data are FIO. (Horton and Johnson, 2000)

Sample ft bgs	Stratigraphic Unit	% Gravel	% Sand	% Silt	% Clay
51	H1a	0.03	81.84	15.42	2.71
60	H1	35.93	43.84	17.33	2.9
116	H2	0.00	63.84	33.86	2.29
135	CCUz	0.00	8.76	80.79	10.46
140	CCUc	0.00	11.91	83.7	4.38
160.5	Rtf	5.17	82.88	9.64	2.31

The wet sieving/hydrometer data show a finer particle size distribution than the dry sieving data. This trend is often found for Hanford Site sediments. Table B.30 shows a comparison between the wet sieving/hydrometer data and the dry sieving data for two samples that were analyzed with both methods. The biggest difference in particle size distribution occurs for the Hanford formation H1 unit gravel. The wet sieving data suggest that more than half of the gravel disaggregates and becomes sand and finer

particles. Alternatively, the two measurements were performed on different aliquots from the 6-in.-long core and there may have been a large difference in the gravel content in the two aliquots.

Table B.30. Comparison of Particle Size Distributions Using the Dry Versus Wet Sieving/ Hydrometer Methods for Borehole 299-W22-50. Data are FIO. (Horton and Johnson, 2000)

Depth	Unit	Type	wt% Gravel	wt% Sand	wt% Silt/Clay
51	H1a	Dry	0.23	90.81	8.95
		Wet	0.03	81.84	18.13
60	H1	Dry	86.63	12.04	1.33
		Wet	35.93	43.84	20.23

Gravelly sand of the Hanford Unit H1 is much coarser than the other Hanford formation units. The Cold Creek subunits, CCUz and CCUc, are both relatively fine-grained and similar compared to the Ringold Formation sample below it. However, because the Cold Creek caliche is moderately to strongly cemented with $CaCO_3$, there is usually a problem with completely disaggregating the sample; therefore, the particle size distribution for the caliche using either method is probably not representative of the grain size of individual particles in this unit.

B.3.2.3 Particle Density of Sediments from Borehole 299-W22-50

The particle density of bulk grains was determined for selected core samples from the 299 W22-50 using pycnometers. The results are shown in Table B.31. The particle density values are slightly lower than previous Hanford measurements that have ranged from 2.70 to 2.82 g/cm^3 (see Serne et al. 1993).

Table B.31. Particle Densities for Borehole 299-W22-50 Core Samples. Data are FIO. (Horton and Johnson, 2000)

Sample Name	Stratigraphic Unit	Density (g/cm^3)	Std. Dev. (3 trials)
51	H1a	2.626	0.014
60	H1	2.735	0.016
116	H2	2.694	0.017
135	H2	2.652	0.007
140	CCUc	2.680	0.007
160.5	Rtf	2.656	0.011

B.3.2.4 Carbon Content of Sediments from Borehole 299-W22-50

The calcium carbonate equivalent and organic carbon content of the bulk sediments for selected depths from borehole 299 W22-50 are shown in Table B.32. The calcium carbonate equivalent (in terms of grams of calcite per gram of oven dry sediment) are low for all samples except for depths 135 through 141 ft bgs, which has been identified as a caliche rich zone.

The method used to measure the organic carbon relies on subtracting the inorganic carbon from the total carbon in the sample. For low carbon contents, this method is not accurate. The low values for organic carbon are within the ranges generally reported for Hanford sediments, but a more sensitive method is required to increase the accuracy.

Table B.32. Calcium Carbonate and Organic Carbon Content (wt%) for Core Samples from Borehole 299-W22-50. Data are FIO. (Horton and Johnson, 2000)

W22-50 Depth (bgs)	Total Carbon (%)	Inorganic Carbon (%)	Inorganic Carbon as $CaCO_3$ (%)	Organic Carbon (%)
20	0.28	0.23	1.92	0.05
22.5	0.29	0.25	2.08	0.04
25	0.21	0.14	1.17	0.07
27.5	0.21	0.17	1.42	0.04
30	0.23	0.19	1.58	0.04
32.5	0.18	0.13	1.08	0.05
35	0.23	0.18	1.50	0.05
37.5	0.23	0.19	1.58	0.04
40	0.22	0.19	1.58	0.03
42.5	0.26	0.21	1.75	0.05
45	0.28	0.22	1.83	0.06
47.5	0.29	0.24	2.00	0.05
51	0.27	0.23	1.92	0.04
52.5	0.21	0.18	1.50	0.03
55	0.26	0.2	1.67	0.06
56	0.25	0.23	1.92	0.02
60	0.32	0.29	2.42	0.03
67.5	0.27	0.22	1.83	0.05
76	0.23	0.21	1.75	0.02
96	0.26	0.24	2.00	0.02
111	0.36	0.31	2.58	0.05
115	0.31	0.25	2.08	0.06
116	0.26	0.22	1.83	0.04
130	0.43	0.35	2.92	0.08
135	0.49	0.4	3.33	0.09
140	0.28	0.23	1.92	0.05
141	1	0.92	7.67	0.08
150.5	0.1	0.07	0.58	0.03
160.5	0.08	0.04	0.33	0.04
174	0.03	0	0.00	0.03

B.3.2.5 Cation Exchange Capacity of Sediments from Borehole 299-W22-50

The exchangeable base cations (Na, K, Mg, Ca, Sr, Ba) for selected sediments from 299-W22-50 were determined using the ammonium acetate procedure in Ciesielski and others (1997). The sum of extractable cations are shown in Table B.33. All the uncontaminated sediments from the Hanford Reservation show that Ca and Mg dominate (>90% of total displaceable cations) the exchange sites. The sum of the base cations does not align with the particle size measurements, since the coarse H1 unit shows a relatively high sum, whereas the finer-grained CCUz shows a lower sum.

Table B.33. Base Cation Composition of Sediments from W22-50. Data are FIO. (Horton and Johnson, 2000)

	Ammonium Acetate						
W22-50 Depth (bgs)	meq/100 g						
	Ba	Ca	K	Mg	Sr	Na	Sum
B8814-51 [H1a]	0.017	12.207	0.733	2.467	0.030	0.359	15.81
B8814-60 [H1]	0.015	10.745	0.483	1.469	0.015	0.327	13.05
B8814-116 [H2]	0.030	7.469	0.154	0.946	0.015	0.200	8.81
B8814-116 Dup	0.028	6.965	0.139	0.903	0.014	0.186	8.23
B8814-135 [CCUz]	0.040	10.005	0.379	2.632	0.022	0.300	13.38
B8814-140 [CCUc]	0.028	7.742	0.266	1.777	0.015	0.215	10.04
B8814-160.5 [Rtf]	0.013	5.872	0.272	1.127	0.014	0.153	7.45

B.3.2.6 Elemental Composition of Sediments from Borehole 299-W22-50

The elemental composition of the bulk sediment from borehole 299-W22-50 was determined by a combination of energy and wavelength dispersion XRF and converted to oxides. Results are shown in Table B.34. The Fe present in the sediments has been assumed to be Fe_2O_3, even though there may be some reduced (ferrous oxides) iron also present. The total content has been adjusted to reflect the presence of calcium carbonate by converting the calcium carbonate in Table B.32 to percent CO_2, and adding it to the XRF totals.

The major-oxide chemical composition of the bulk sediments from various depths from borehole 299-W22-50 show that silica predominates, and that alumina is second in abundance. Iron, magnesium, calcium, sodium, potassium, carbonate, and titanium make up most of the rest of the oxides. The calculated mass balances range between 96.95% and 101.76% with a mean of 99.95% ± 1.75% for the six samples.

Table B.34. Bulk Chemical Composition of 299-W22-50 Core Samples (% as oxides). Data are FIO. (Horton and Johnson, 2000)

Oxides	51 ft	60 ft	116 ft	135 ft	140 ft	160.5 ft
	H1a	H1	H2	CCUz	CCUc	Rtf
Na_2O	2.09	2.56	2.37	1.47	1.85	3.02
MgO	3.55	3.33	3.80	4.31	3.80	2.67
CO_2	0.92	1.16	0.88	1.60	0.92	0.16
Al_2O_3	12.09	13.08	13.70	14.30	13.26	11.41
SiO_2	63.86	64.61	69.42	66.00	68.46	68.89
P_2O_5	<0.22	<0.27	<0.21	<0.20	<0.21	<0.20
SO_3	0.11	0.15	0.08	0.06	0.06	0.06
Cl	<0.016	<0.016	0.046	0.044	0.035	0.020
K_2O	1.79	1.77	2.46	2.63	2.33	1.71
CaO	5.30	5.96	3.78	3.76	3.38	3.37
TiO_2	1.24	1.10	0.65	0.73	0.81	0.70
V_2O_5	0.04	0.03	0.01	0.01	0.01	0.02
Cr_2O_3	0.01	0.01	0.01	0.01	0.01	0.00
MnO	0.12	0.10	0.07	0.08	0.07	0.08
Fe_2O_3	8.00	7.33	4.13	4.78	4.52	4.51
SrO	0.04	0.04	0.05	0.03	0.04	0.05
BaO	0.07	0.08	0.09	0.07	0.08	0.07
Total	99.46	101.59	101.76	100.10	99.83	96.95

The major elemental oxide composition of the clay fraction in selected sediments from borehole 299-W22-50 is shown in Table B.35.

Table B.35. Major Constituent Oxide Content of Clay Fraction from Borehole 299-W22-50 (wt%). Data are FIO. (Horton and Johnson, 2000)

	Sample Depth (ft bgs)			
Oxide	51	60	135	140
NaO	NM	NM	NM	NM
MgO	NM	NM	NM	NM
CO_2	NM	NM	NM	NM
Al_2O_3	12.90	11.55	17.69	14.98
SiO_2	46.96	43.54	48.46	45.14
P_2O_5	0.58	0.71	0.60	0.55
SO_3	0.22	0.27	0.21	0.19
Cl	0.20	0.14	1.14	0.44
K_2O	1.36	1.62	2.30	2.02
CaO	5.51	12.76	2.10	3.02
TiO_2	0.82	0.85	0.67	0.68
V_2O5	0.02	0.02	0.02	0.02
Cr_2O_3	0.01	0.01	0.01	0.01
MnO	0.15	0.14	0.12	0.10
Fe_2O_3	11.79	9.78	9.39	10.67
SrO	0.02	0.04	0.01	0.02
BaO	0.03	0.06	0.03	0.04

	Sample Depth (ft bgs)			
Oxide	51	60	135	140
NM = not measured				

B.3.2.7 Mineralogy of Sediments from Borehole 299-W22-50

Bulk sediment and clay fractions (<2 um) mineralogy from borehole 299-W22-50 depths (51 ft, 60 ft, 116 ft, 135 ft, 140 ft, and 160.5 ft) were characterized by XRD. The semi-quantitative mass percentages for the bulk sediment and the clay sized separate are shown in Table B.36. The mineralogy of both the bulk sediment and the clay size fraction is quite similar to the samples from the same lithologies at borehole 299-W22-48.

Table B.36. Wt% Mass Mineralogy Distribution for the Bulk Sediments and the Clay-Sized Samples for Borehole 299-W22-50. Data are FIO. (Horton and Johnson, 2000)

Bulk Sediment	Quartz	K-Feldspar	Na-Feldspar	Calcite	Total
50’ (H1a)	60	10	25	ND	~95
60’ (H1)	45	10	25	ND	~80
116’ (H2)	45	15	30	ND	~90
135’ (CCUz)	60	5	15	ND	~80
140’ (CCUc)	60	10	15	ND	~85
160.5’ (Rtf)	50	10	30	ND	~90

Clay Sized Fraction	Quartz	Feldspar	Calcite	Smectite	Illite	Chlorite	Kaolinite	Total
Depth (ft)								
50’ (H1a)	5	<5	10	30	15	10	10	~85
60’ (H1)	5	5	25	5	15	10	10	~75
116’ (H2)	10	<5	Tr	30	30	35	10	~120
135’ (CCUz)	5	<5	<5	30	30	30	10	~115
140’ (CCUc)	10	<5	<5	15	10	10	5	~60
160.5’ (Rtf)	5	5	Tr	10	15	15	10	~60
ND = not detected; Tr = trace amount detected ~1-4%								

B.3.2.8 Clay Mineralogy for Boreholes 299-W22-48 and 299-W22-50

The mineralogy of the bulk size fraction and the silt and clay size fractions of 299-W22-48 sediments from selected depths is very similar to the mineralogy of sediments from 299-W22-50 from equivalent geologic strata. Sediments in both boreholes were largely dominated by quartz (~45% to 95%) and feldspars, plagioclase feldspar (~10% to 20%) and alkali feldspar (~20% to 40%). Minor amounts of mica, chlorite, and amphibole were also detected in the samples. Depths 146 ft and 148.5 ft from borehole 299-W22-48 were rich in calcite (~40%), with lesser amounts of quartz (~20% to 25%), plagioclase feldspar (~10% to 20%) and potassium feldspar (<10%). Chlorite and mica were detected at trace amounts in the calcite rich sediments.

The clay fraction of both boreholes is dominated by four major clay minerals: smectite (17.0 Å), illite (10.0 Å), chlorite (14.1 Å), and kaolinite (7.0 Å). XRD patterns of Mg^{2+} saturated, ethylene glycol solvated clay fractions are presented below. The smectite (001) basal reflection expanded to 17 Å when saturated with ethylene glycol. Illite had a (001) basal reflection of 10.0 Å and an (002) basal reflection of 5.0 Å. Presence of chlorite was confirmed by the (001) basal reflection at 14.1 Å, in addition to the (003) and (004) reflections at 4.74 Å and 3.52 Å, respectively. The identification of kaolinite is based on the (002) reflection. The first two basal reflections for kaolinite, (001) and (002), have d-spacing of 7.1 Å and

3.58 Å, which overlap the chlorite (002) and (004) basal reflections, making identification difficult. Careful examination of the XRD patterns from both boreholes showed a kaolinite (002) reflection on the shoulder of the chlorite (004) reflection. Minor amounts of quartz, feldspar, calcite, and amphibole were detected in the clay fraction of both boreholes, along with substantial amounts of calcite in depths 146 ft and 148.5 ft from borehole 299-W22-48. Additionally, transmission electron microscopy (TEM) analysis of the clay fractions confirmed the presence of kaolinite and identified trace amounts of minerals such as Fe-oxide, anatase, apatite, and sepiolite.

The XRD semi-quantitative measurements of minerals in the clay fraction suggest that smectite (17.1 Å) ranged in concentration from 10 to 30 wt%. Illite (10 Å) concentrations ranged from ~10% to 50% and chlorite (14.1 Å) concentrations were a little less (~5 to 35 wt%). Minor amounts of kaolinite (~5% to 10%) were also detected. Quartz, feldspar, and amphiboles made up less than ~15 wt% of the clay fraction. Significant amounts of calcite were detected in the clay fraction from borehole B8812 depths 146 ft (~40 wt%) and 148.5 ft (~40 wt%) and from borehole 299-W22-50 at depth 60 ft (~25 wt%), with lesser amounts (~ 5 to 10 wt%) in borehole 299-W22-48 (depth 47 ft) and borehole 299-W22-50 (depths 51 ft, 135 ft, and 140 ft).

Total mass balance for the clay fraction ranged from a low of 45 wt% to a high of 130 wt%. Recoveries ranging from 80% to 120% are considered acceptable for XRD analysis (Newman 1987). Low recoveries for semi-quantitative measurements by XRD can be attributed to several factors. The clay fractions having a significant amount of calcite removed during treatment generally produced low recoveries. The <2 micron fractions in borehole 299-W22-48, depth 47 ft, and borehole 299-W22-50, depths 50 ft, 60 ft, and 140 ft had calcite concentrations between 5 to 25 wt%. After treatment to remove calcite from these depths, the amount of clay remaining was not adequate to prepare a sample valid for semi quantitative measurements. Sample degradation (peeling, curling clay substrates) also added to the problem.

The only significant trend in the mineral content of samples from borehole 299-W22-48 is the substantial increase in calcite relative to the other minerals in the caliche at 146 to 148.5 ft depth. This difference is noted in both the whole rock and the ≤ 2 μm fraction.

Analysis of illites by TEM from borehole 299-W22-48 (39 ft, 91.5 ft, and 163.5 ft) and 299-W22-48 (51 ft and 116 ft) showed large angular platy particles. Figure B.6 is an example of a typical illite particle with minor amounts of Fe from depth 163.5 ft (borehole 299-W22-48). Using data from TEM analysis and assuming all iron as Fe^{3+}, the following structural formula was calculated from data collected from 10 illites in sample 163.5 ft (borehole 299-W22-48):

$$[K_{0.74}Ca_{0.02}Na_{0.02}]^{+0.80}[(Al_{1.62}Mg_{0.29}Fe_{0.16}Ti_{0.02})^{+0.0}(Si_{3.19}Al_{0.81})^{-0.81}]^{-0.81}O_{10}(OH)_2$$

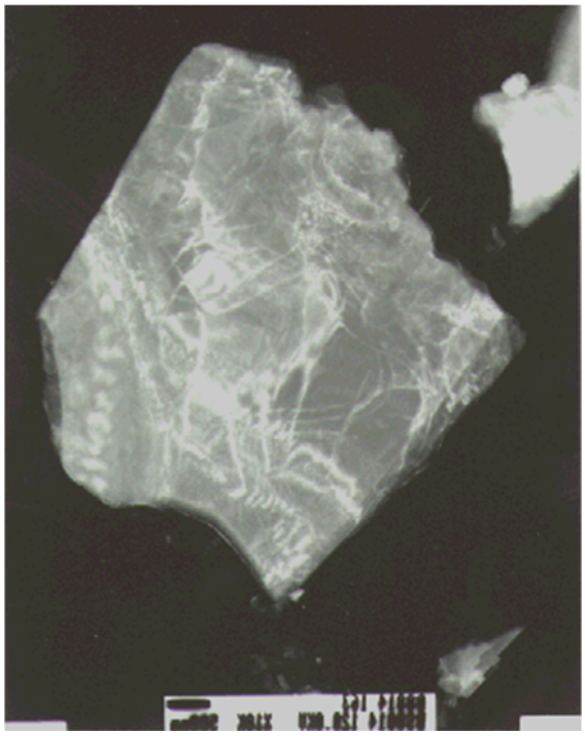

Figure B.6. Typical Illite Particle From Borehole 299-W22-48, 163.5 Depth. (Horton and Johnson, 2000)

As in muscovite, the layer charge in illite originates from the substitution of Al^{3+} for Si^{4+} in the tetrahedral sheet. No excess layer charge is created with the minor substitutions of Mg^{2+}, Fe^{3+}, and Ti^{4+} for Al^{3+} in the octahedral sheet. The interlayer charge of +0.80 balances the charge on the 2:1 silicate structure. Iron content varied from a low of 0.04 to a high of 0.26 atoms per $O_{10}(OH)_2$. Examination of illites from four other depths showed similar chemistry and morphology to the illites in 163.5 ft depth sample.

Chlorite particles were typically found at all depths in both boreholes. The particles were characterized as large platy particles shaped by angular edges. Figure B.7 is an example of a chlorite from borehole 299-W22-48, (91.5 ft depth), positioned closely to illites (top of Figure B.6). Chemistry of the chlorites ranged between Mg-rich and Fe-rich varieties. Assuming all the iron is Fe^{+2}, a structural formula was developed from similar chlorites examined from depth 91.5 ft:

$$[(Ca_{0.03}]^{+0.06}[(Al_{1.54}Mg_{2.44}Fe_{1.51}Ti_{0.02})^{+0.60}(Si_{3.31}Al_{0.69})^{-0.69}]O_{10}(OH)_8$$

The layer charge of –0.69 resulting from the Al^{+3} substituting for Si^{+4} in the tetrahedral sheet is compensated by the charge derived from substitution in the octahedral sheet. Fe^{+2} content varied from a low of 1.22 to a high of 1.57 atoms per $O_{10}(OH)_8$ whereas Mg^{+2} ranged from a low of 1.72 to a high of 3.38 atoms per $O_{10}(OH)_8$. Minor amounts of Ti^{+4} were routinely detected in chlorite particles along with trace amounts of Ca^{+2}, Na^{+1}, and K^{+1}.

Smectite clays examined by TEM were mostly limited to the smaller size particles (<0.5 microns) in the sample. Figure B.8 is an example of fine delicate smectite flakes with thin curled edges common to Borehole 299-W22-48, 163.5 ft depth.

Chemical composition of the smectites was hard to establish, due in part to the difficulty of isolating the aggregates from other minerals in the sample during TEM analysis. Considering this limitation, a

structural formula was developed using data collected from an average smectite in borehole 299-W22-48, 163.5 ft depth:

$$[(Ca_{0.05}Mg_{0.10})]^{+0.30}[(Al_{0.54}Mg_{0.56}Fe_{1.07}Ti_{0.01})^{-0.01}(Si_{3.72}Al_{0.28})^{-0.28}]^{-0.29}O_{10}(OH)_4$$

Substitution of Al^{3+} into the tetrahedral site for Si^{4+} causes a layer charge of –0.28, which is balanced by the interlayer cations, Mg^{2+} and Ca^{2+}. Occupying octahedral sites are trivalent cations (Al^{3+}, Fe^{3+}) and, in lesser amounts the divalent cation (Mg^{2+}). Trace amounts of Ti^{4+} were also detected in the octahedral sites of most smectites. Although only a few smectites were examined from each depth, minor variations in chemistry were limited to the proportions of individual cations occupying octahedral sites. Smectites had Fe^{3+} ranging between 0.24 and 1.07, atoms per $O_{10}(OH)_4$, which caused variations in the octahedral Al^{3+} content.

Figure B.7. Chlorite Particle From Borehole 299-W22-48, 91.5 ft. (Horton and Johnson, 2000)

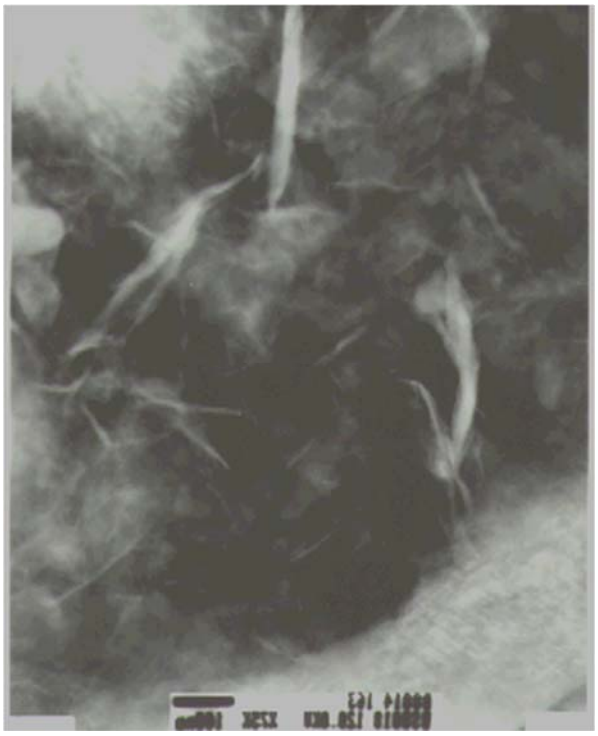

Figure B.8. Thin Smectite Flakes From Borehole 299-W22-48, 163.5 ft Depth. (Horton and Johnson, 2000)

Kaolinite particles were platy in habit, and often consisted of aggregates of smaller individual particles. Figure B.9 is a very well-defined kaolinite particle with the characteristic hexagonal morphology.

Most kaolinites examined in the borehole samples did not have such a well-defined morphology, and thus were not easily identified by appearance. The structural formula developed from TEM data collected from kaolinites in borehole 299-W22-48, 91.5 ft depth is:

$$(Al_{3.99}Fe_{0.02})(Si_{3.96}Al_{0.04})O_{10}(OH)_8$$

All kaolinites examined by TEM from both boreholes had some degree of Fe^{3+} substitution for Al^{3+} in the octahedral layer.

Figure B.9. Kaolinite Particle From Borehole 299-W22-48, 91.5 ft Depth. (Horton and Johnson, 2000)

B.3.3 Composite Sediments from 299-W22-50 Sediments

"Borehole Fine Sand" is a composite of all the sediment from the 299-W22-50 borehole core sleeves between the depths of 62.5 and 97 ft, excepting one 1-ft-long sleeve between 85 and 86 ft reserved for hydraulic measurements. The contents of 27 four-inch-diameter sleeves were composited. Based on a cursory visual inspection, the 27 cores showed fairly uniform lithologic consistency, although thin stringers and bedding planes were frequently observed. The Borehole Fine Sand represents the laminated, slightly silty medium- to fine-grained, sand unit in the Hanford formation H2 subunit. The H2 subunit lies below the backfill and a gravelly zone directly underlying the S-SX WMA and under the SX Tank Farm. These strata contain much of the contamination currently found in the vadose zone sediments, and is representative of the Hanford formation in the vicinity of tank leaks.

B.3.3.1 Particle Size Distribution for the Borehole Fine Sand

Both dry sieving and the hydrometer methods were used to determine the particle size distributions. The dry sieving results are shown in Table B.37 and the hydrometer/wet sieve results are shown in Table B.38.

Table B.37. Particle Size Distribution Determined by Dry Sieve Method. Data are FIO. (Horton and Johnson, 2000)

	Weight % Retained on Each Sieve								
Composite Name	4.00 mm	2.00 mm	1.00 mm	500 um	250 um	212 um	125 um	63 um	< 63 um
Borehole Fine Sand	0.00	0.02	1.99	5.95	18.97	7.14	23.47	29.25	13.21

Composite Name	% Gravel	% Coarse Sand	% Med. And Fine Sand	% Silt+Clay	Classification

Borehole Fine Sand	0.02	7.94	78.83	13.21	Slightly muddy sand

Table B.38. Particle Size Distribution Determined by Wet Sieving/Hydrometer Method (Horton and Johnson, 2000)

Composite Name	% Gravel	% Sand	% Silt	% Clay	Classification (Folk 1968)
Borehole Fine Sand	0.00	77.43	18.19	4.38	Muddy sand

B.3.3.2 Particle Density for the Borehole Fine Sand

The particle density of bulk grains for the composite 299-W22-50 sample was determined using pycnometers and yielded a value of 2.675 g/cm^3 with a standard deviation of 0.011 g/cm^3. This range compares favorably with particle density measurements made on discrete samples from boreholes 299-W22-48 and 299-W22-50. The currently measured particle densities for Hanford formation sediments from 299-W22-48 and -50 are slightly lower than values reported by Serne et al. (1993) (2.70 to 2.82 g/cm^3), possibly due to differences in analyst technique.

B.3.3.3 Carbon Content for the Borehole Fine Sand

The carbon results for the composite sediment from 299-W22-50 are shown in Table B.39. In general, the measurements were made on triplicate aliquots. The calcium carbonate equivalent (in terms of grams of calcite per gram of oven dry sediment) are low but within the normal range for non-pedogenically altered Hanford formation sediments. The amount of $CaCO_3$ is a function of (1) how much soil development has taken place or (2) how much carbonate-cemented detrital material has been transported and redeposited. The Hanford formation generally contains more detrital $CaCO_3$ than the Ringold, because the floods were more effective at ripping apart cemented calcic paleosols and redistributing the material.

Table B.39. Calcium Carbonate and Organic Carbon Content (wt%). Data are FIO. (Horton and Johnson, 2000)

Sample Name	Total Carbon	Std. Dev.	$CaCO_3$ equivalent	Std. Dev.	Organic C (by difference)	Std. Dev.
Borehole Fine Sand	0.28	0.007	1.92	0.06	0.05	0.01

B.3.3.4 Cation Exchange Capacity for the Borehole Fine Sand

The CEC of the composite sediments was determined using procedures developed for calcareous sediments (Polemio and Rhoades 1977; Amrhein and Suarez 1990). The CEC results as determined by the two methods vary significantly (see Table B.40). Not only does the method of Amrhein and Suarez method yield lower CEC estimates, but the Polemio and Rhoades technique also resulted in larger variability of estimated CEC. To date, the accuracy of these methods has not yet been determined for the low CEC of Hanford sediments with low calcite contents.

Table B.40. Results of Cation Exchange Capacity of Composite Sediments (meq/100 g) Using Three Different Techniques. Data are FIO. (Horton and Johnson, 2000)

Composite Name	Polemio and Rhoades (1977)	Amrhein and Suarez (1990)	Ammonium Acetate Sum
Borehole Fine Sand	9.2 ± 8.9	2.9 ± 0.6	8.32

Table B.40 also compares a third method of estimating CEC using high ionic strength ammonium acetate that measures several base cations. The sum of all the major exchanged cations is the estimate of the CEC.

B.3.3.5 Elemental Composition for the Borehole Fine Sand

The elemental compositions of the bulk sediments, as determined by XRF and converted to oxides are shown in Table B.41. All iron is assumed to be Fe_2O_3, although a large proportion of the iron may be associated with the FeO basaltic component of the sediment.

Table B.41. Bulk Chemical Composition of Composite Sediments (% as oxides). Data are FIO. (Horton and Johnson, 2000)

Oxide	Borehole Fine Sand
Na_2O	2.37
MgO	3.12
CO_3	1.15
Al_2O_3	13.25
SiO_2	71.03
P_2O_5	<0.20
SO_3	0.06
Cl	0.04
K_2O	2.39
CaO	3.13
TiO_2	0.55
V_2O_5	0.01
Cr_2O_3	0.01
MnO	0.06
Fe_2O_3	3.54
SrO	0.04
BaO	0.08
Total	101.58

The mineralogy of the bulk, and silt and clay size fractions of the composite sediments was determined by XRD. The XRD analyses show the Hanford Formation composite sample is dominated by quartz (30-80%), and plagioclase feldspar (5-20%), with minor amounts (<10%) of potassium feldspar, and amphibole (Table B.42).

Table B.42. Semi-quantitative Mineral Content of Composite Sediments. Data are FIO. (Horton and Johnson, 2000)

Quartz		K-Feldspar	Na-Feldspar		Calcite
Bulk Sediment (wt%)					
50		10	20		nd
Clay Fraction (wt%)					
Quartz	Feldspar	Smectite	Illite	Chlorite	Kaolinite
5	<5	30	40	20	5

The clay fraction (<2 micron) of the borehole fine sand is dominated by four clay minerals: illite (10Å), smectite (15Å), chlorite (14.1Å), and kaolinite (7Å) with minor amounts of quartz (3.34Å), feldspar (3.18Å), and amphibole (8.4Å). Additionally, trace amounts of apatite, Fe-oxides, and sepiolite, were detected in the clay fraction during the TEM analysis of the borehole fine sand.

B.4 References

Amrhein C and DL Suarez. 1990. “Procedure for Determining Sodium-Calcium Selectivity in Calcareous and Gypsiferous Soils.” *Soil Sci. Soc. Am. J.* 54:999-1007.

Ciesielski, H. T. Sterckeman, M. Santerne, J. Willery. 1997. "A comparison between three methods for the determination of cation exchange capacity and exchangeable cations in soils." Agronomie, 17, 9-16.

Horton DG and VG Johnson. 2000. *Borehole Data Package for Wells 299-W22-48, 299-W22-49, and 299-W22-50 at Single-Shell Tank Waste Management Area S-SX*. PNNL-13200, Pacific Northwest National Laboratory, Richland, Washington.

Last GV, BN Bjornstad, MP Bergeron, DW Wallace, DR Newcomer, JA Schramke, MA Chamness, CS Cline, SP Airhart, and JS Wilbur. 1989. *Hydrogeology of the 200 Areas Low-Level Burial Grounds - An Interim Report*. PNL-6820, 2 Volumes. Pacific Northwest Laboratory, Richland, Washington

Lindenmeier CW, RJ Serne, BN Bjornstad, GW Gee, HT Schaef, DC Lanigan, MJ Lindberg, RE Clayton, VL LeGore, IV Kutnyakov, SR Baum, KN Geiszler, CF Brown, MM Valenta, TS Vickerman, and LJ Royack. 2003. *Characterization of Vadose Zone Sediment: RCRA Borehole 299-E33-338 Located Near the B-BX-BY Waste Management Area*. PNNL-14121, Pacific Northwest National Laboratory, Richland, Washington.

Lindsey KA, SE Kos, and KD Reynolds. 2001. *Vadose Zone Geology of Boreholes 299-W10-27 and 299-W11-39 T-TX-TY Waste Management Area Hanford Site, South-Central Washington*. RPP-8531, Rev. 0, CH2M Hill Hanford Group, Inc., Richland, Washington.

Newman ACD (ed.). 1987. *Chemistry of Clays and Clay Minerals*: Monograph No. 6, Mineralogical Society, London.

Polemio M and JD Rhoades. 1977. “Determining Cation Exchange Capacity: A New Procedure for Calcareous and Gypsiferous Soils.” *Soil Sci. Soc. Am. J.* 41:524-528.

Reynolds KD. 2003. *Completion Report for Probe Hole C4105 (T-106) T Tank Farm Drilling and Sampling*. RPP-16340, Rev. 0, Prepared for the Office of River Protection, CH2M Hill Hanford Group, Inc., Richland, Washington.

Serne RJ, CW Lindenmeier, JL Conca, JA Campbell, VL LeGore, JE Amonette, KJ Cantrell, and MI Wood. 1993. *Solid-Waste Leach Characteristics and Contaminant-Sediment Interactions. Vol. 1: Batch Leach and Adsorption Tests and Sediment Characterization.* PNL-8889, Pacific Northwest Laboratory, Richland, Washington

Serne RJ, HT Schaef, BN Bjornstad, BA Williams, DC Lanigan, DG Horton, RE Clayton, VL LeGore, MJ O'Hara, CF Brown, KE Parker, IV Kutnyakov, JN Serne, AV Mitroshkov, GV Last, SC Smith, CW Lindenmeier, JM Zachara, and DB Burke. 2002a. *Characterization of Uncontaminated Vadose Zone Sediment from the Hanford Reservation - RCRA Borehole Core Samples and Composite Samples*. PNNL-13757-1, Rev. 1, Pacific Northwest National Laboratory, Richland, Washington.

Serne RJ, CF Brown, HT Schaef, EM Pierce, MJ Lindberg, Z Wang, PL Gassman, and JG Catalano. 2002b. *300 Area Uranium Leach and Adsorption Project*. PNNL-14022, Pacific Northwest National Laboratory, Richland, Washington.

Serne RJ, GV Last, HT Schaef, DC Lanigan, CW Lindenmeier, CC Ainsworth, RE Clayton, VL Legore, MJ O'Hara, CF Brown, RD Orr, IV Kutnyakov, TC Wilson, KB Wagnon, BA Williams, and DS Burke. 2008a. *Characterization of Vadose Zone Sediment: Borehole 41-09-39 in the S-SX Waste Management Area*. PNNL-13757-3, Rev. 1, Pacific Northwest National Laboratory, Richland, Washington.

Serne RJ, HT Schaef, BN Bjornstad, DC Lanigan, GW Gee, CW Lindenmeier, RE Clayton, VL Legore, RD Orr, MJ O'Hara, CF Brown, GV Last, IV Kutnyakov, DS Burke, TC Wilson, and BA Williams. 2008b. *Characterization of Vadose Zone Sediment: Borehole 299-W23-19 [SX -115] in the S-SX Waste Management Area*. PNNL-13757-2, Rev. 1, Pacific Northwest National Laboratory, Richland, Washington.

Serne RJ, GV Last, GW Gee, HT Schaef, DC Lanigan, CW Lindenmeier, MJ Lindberg, RE Clayton, VL Legore, RD Orr, IV Kutnyakov, SR Baum, KN Geiszler, CF Brown, MM Valenta, and TS Vickerman. 2008c. *Characterization of Vadose Zone Sediment: Borehole 299-E33-45 Near BX-102 in the B-BX-BY Waste Management Area*. PNNL-14083, Rev 1Pacific Northwest National Laboratory, Richland, Washington.

Serne RJ, BN Bjornstad, GW Gee, HT Schaef, DC Lanigan, RG Mccain, CW Lindenmeier, RD Orr, VL Legore, RE Clayton, MJ Lindberg, IV Kutnyakov, SR Baum, KN Geiszler, MM Valenta, TS Vickerman, and LJ Royack. 2008d. *Characterization of Vadose Zone Sediment: Borehole 299-E33-46 Near Tank B-110 in the B-BX-BY Waste Management Area*. PNNL-14119, Rev. 1, Pacific Northwest National Laboratory, Richland, Washington.

Serne RJ, BN Bjornstad, DG Horton, DC Lanigan, CW Lindenmeier, MJ Lindberg, RE Clayton, VL LeGore, RD Orr, IV Kutnyakov, SR Baum, KN Geiszler, MM Valenta, and TS Vickerman. 2004a. *Characterization of Vadose Zone Sediments Below the TX Tank Farm: Boreholes C3830, C3831, C3832 and RCRA Borehole 299-W10-27*. PNNL-14594, Pacific Northwest National Laboratory, Richland, Washington.

Serne RJ, BN Bjornstad, DG Horton, DC Lanigan, CW Lindenmeier, MJ Lindberg, RE Clayton, VL LeGore, RD Orr, IV Kutnyakov, SR Baum, KN Geiszler, MM Valenta, TS Vickerman, and HT Schaef. 2004b. *Characterization of Vadose Zone Sediments Below the T Tank Farm: Boreholes C4104, C4105, 299-W10-196 and RCRA Borehole 299-W11-39*. PNNL-14849, Pacific Northwest National Laboratory, Richland, Washington.

Serne RJ, BN Bjornstad, DG Horton, DC Lanigan, CW Lindenmeier, MJ Lindberg, RE Clayton, VL LeGore, RD Orr, IV Kutnyakov, SR Baum, KN Geiszler, MM Valenta, and TS Vickerman. 2004c. *Characterization of Vadose Zone Sediments Below the TX Tank Farm: Boreholes C3830, C3831, C3832 and RCRA Borehole 299-W10-27*. PNNL-14594, Pacific Northwest National Laboratory, Richland, Washington.

Appendix C – Aquifer Sediments

Characterization work has also been performed on sediments obtained for pump-and-treat wells in the 200 West Area. These sediments, received in 4-in.-diameter by 6-in.-long core sleeves, represent sediments from the Ringold Formation unit E (gravel dominated) or Ringold Formation lower mud unit. Since the goal of this report is to inform investigators of the existing data available for Remedial Investigation/Feasibility Study (RI/FS) tasks and provide a centralized location to support site evaluations, the data *have not* been reviewed for technical accuracy per NQA-1 guidelines. The data have been reproduced from the original reports and the data provided here *for information only* (FIO).

A description of the sediments is found in Table C.1 and more details on the characterization data can be found in Um and Serne (2006) and Um et al. (2005, 2009).

Table C.1. Description of Core Liners. Data are FIO. (Um et al., 2005)

Borehole	HEIS #	Liner #	Depth Interval	Formation	Intact Core?
C4298 Well "R"(699-30-66) depth to water table =254.45 ft bgs					
C4298	B192K1	1	279-279.5	Ringold Unit E	No - slough
C4298	B192K2	1	314-314.5	Ringold Unit E	No - slough
C4298	B192K3	1	347-347.5	Ringold Unit E	No - slough
C4298	B192K4	1	386.5-387	Ringold Unit E	No - slough
C4299 Well "P" (699-36-70B) depth to water table = 264.84 ft bgs					
C4299	*B19136*	*1*	*271.5-272*	*Ringold Unit E*	*Yes*
C4299	*B19137*	*2*	*308.5-309*	*Ringold Unit E*	*Yes*
C4299	B19138	1	344-344.5	Ringold Unit E	No - slough
C4299	B19139	2	373.5-374	Ringold Unit E	No - slough
C4299	*B19140*	*1*	*419-419.5*	*Ringold Unit E*	*Yes*
C4300 Well "K" (299-W19-48) depth to water table = 258.20 ft bgs					
C4300	B19373	1	289-289.5	Ringold Unit E	No - slough
C4300	B19374	1	341-341.5	Ringold Unit E	No - slough
C4300	B19375	1	406-406.5	Ringold Unit E	No - slough
C4300	*B19377*	*2*	*427.5-428*	*Ringold Lower Mud*	*Yes*
C4971 Well 299-W22-86 depth to water table = 233.5 ft bgs					
C4971	NA	NA	261.5-262.0	Ringold Unit E	No - slough
C4977 Well 299-W22-87 depth to water table = 232.2 ft bgs					
C4977	*NA*	*NA*	*258.5-259.0*	Ringold Unit E	*Yes*
C4990 Well 299-W11-47 depth to water table = 242.8 ft bgs					
C4990	*NA*	*1,2,3,4*	*404.7-406.7*	*Ringold Lower Mud*	*Yes*

Liner # = split spoon sampling consisted of 4 sleeves each 6 in. long in each push; #1 is closest to the shoe (deepest), and #4 is the shallowest. Usually liners #1 and #2 represent "virgin" sediment not impacted by slough falling back in the hole.

The sediments in many of the core liners were dominated by slough from the coarse-grained Ringold Unit E strata. Boreholes in the 200-UP-1 and 200-ZP-1 operable units within the 200 West Area are prone to sediment “cave in” below the water table prior to split spoon sampling. Photographs of four of the intact sediments (Figure C.1 through Figure C.4) show that the Ringold Unit E sediments are predominantly gravel and many contain cobbles. The Ringold lower mud unit contains no gravel is dominated by silt and clay sized particles.

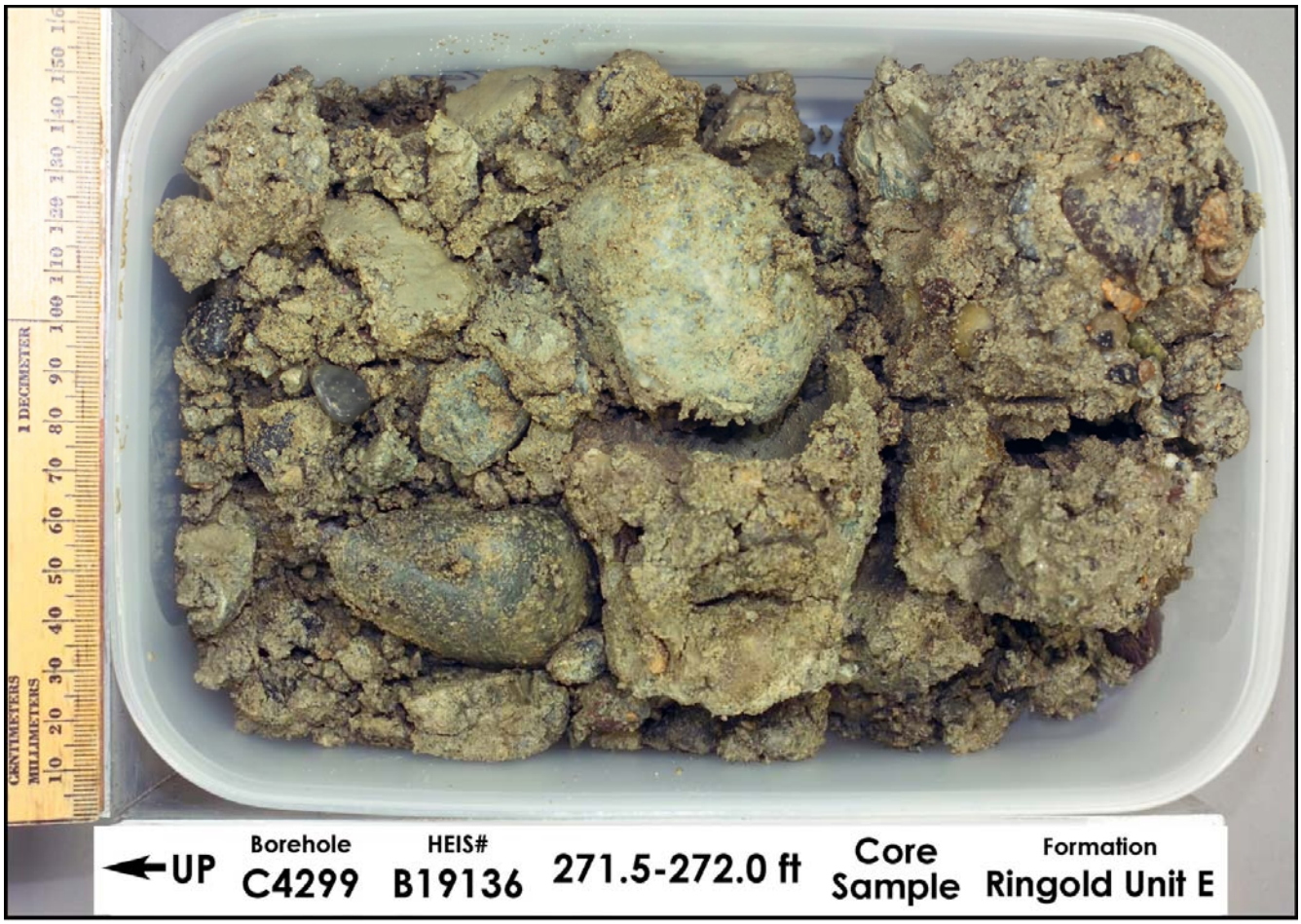

Figure C.1. Sediment in Core Liner B19136 from Borehole C4299 (Um et al., 2005)

Figure C.2. Sediment in Core Liner B19137 from Borehole C4299 (Um et al., 2005)

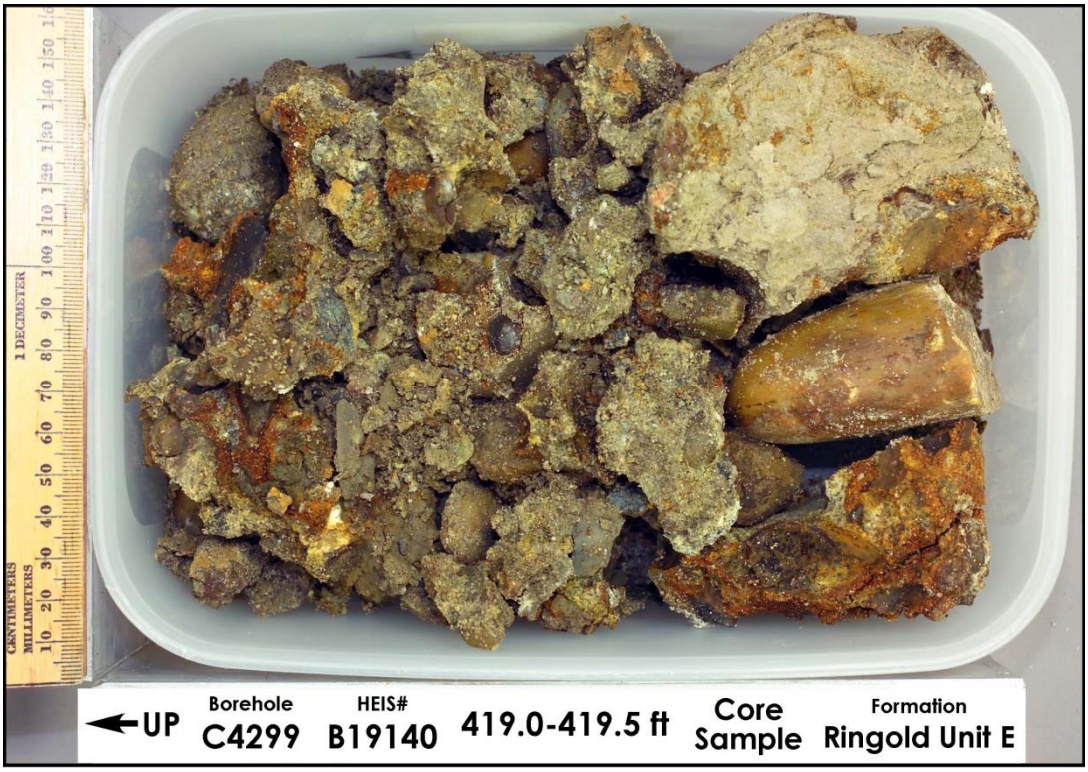

Figure C.3. Sediment in Core Liner B192140 from Borehole C4299. Core liner B192140 shows a significant amount of iron oxide coatings and cementing together of some of the grains. (Um et al., 2005)

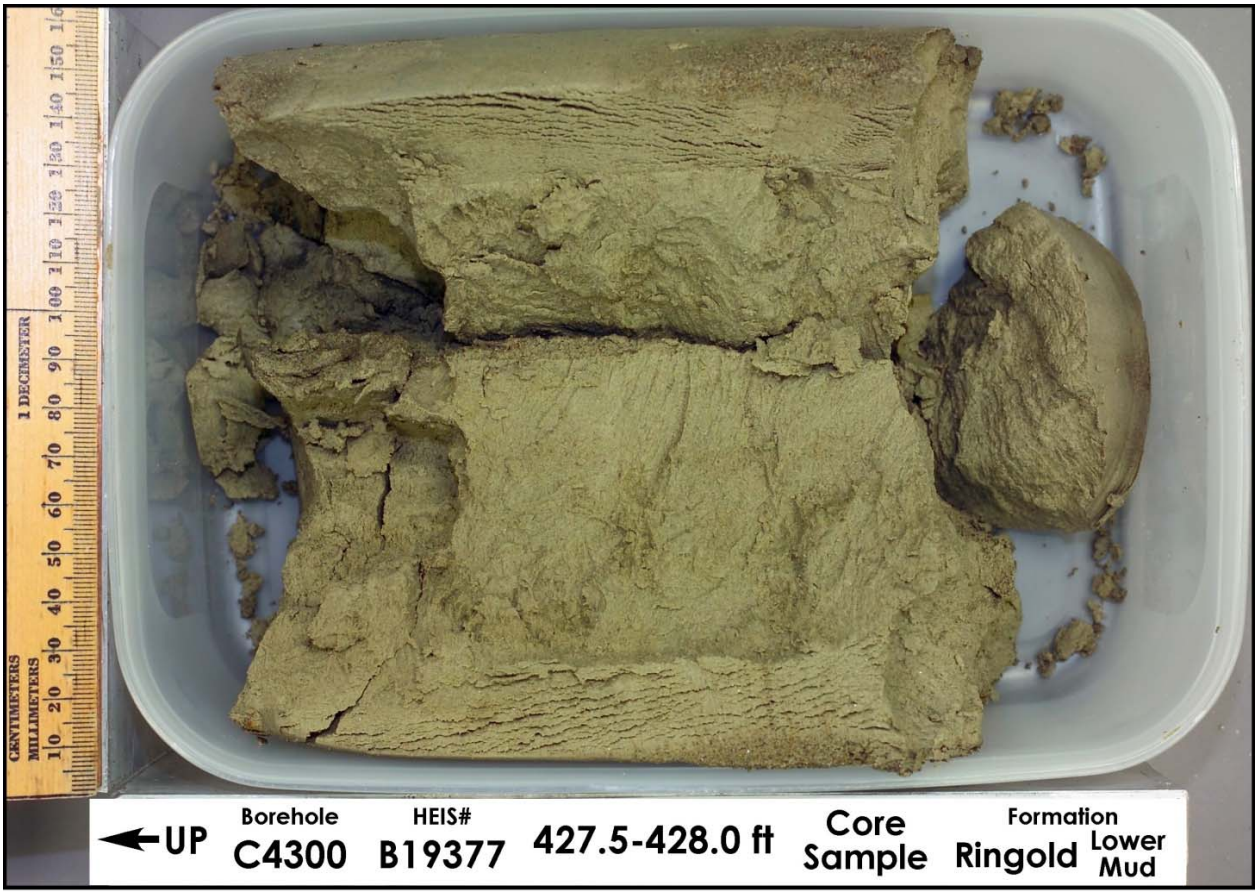

Figure C.4. Sediment in Core Liner B19377 from Borehole C4300 (Um et al., 2005)

The samples that were characterized were generated as follows (Table C.2):

Table C.2. Description of Intact Samples that were Characterized. Data are FIO. (Um et al., 2005)

Sediment Sample ID	Well	Formation	Sample Description
B192K1	C4298	Ringold Unit E	Bulk sample including gravel
B19136 and B19137	C4299	Ringold Unit E	Mixture of these two liners including gravel
B19136 and B19137	C4299	Ringold Unit E	Mixture of two samples without gravel
B19140	C4299	Ringold Unit E	Bulk sample including gravel
B19140	C4299	Ringold Unit E	Bulk sample without gravel
B19377	C4300	Ringold Lower Mud	Bulk sample. Because of mud formation there was no gravel in this liner.
NA	C4977	Ringold Unit E	Gravel (made up ~50 wt%) of bulk sediment was removed
NA	C4990	Ringold Lower Mud	Sandy silt from all 4 liners was composited.

C.1 Particle Size Data for Aquifer Sediments

Particle size distributions of the selected sediment samples described in Table C.2 are presented in Table C.3. Most of the samples are gravel and sand dominated sediments except B19377 and the four liners composited from C4990, which are Ringold Lower Mud. The other 200 West Area aquifer sediments are typical gravel- and sand-dominated Ringold Unit E formation, consistent with other geologic characterizations in the literature.

Table C.3. Summary of Particle Size Distributions for Bulk Samples as Determined by Dry Sieve/Hydrometer Method. Data are FIO. (Um et al., 2005)

Sediment Sample ID	Gravel (%)	Sand (%)	Silt (%)	Clay (%)
B192K1 (bulk)	25.9	68.5	4.90	0.60
B19136 and B19137(bulk)	42.0	52.2	4.34	1.46
B19140 (bulk)	55.0	26.7	13.2	5.10
B19377 (bulk)	0.0	20.8	69.3	9.83
C4977 (bulk)	50	22.8	25.3	2.0
C4990 composite (bulk)	0	9.1	74.6	16.4

C.2 Carbon Content of Aquifer Sediments

The total carbon and inorganic carbon content of the sediments described in Table C.1 are listed in Table C.4. The total and inorganic carbon content of the aquifer sediments are low.

Table C.4. Total Carbon, Inorganic Carbon and Organic Content (as wt%) of Sediments. Data are FIO. (Um et al., 2005)

Borehole	HEIS #	Total Carbon	Inorganic Carbon	Inorganic Carbon As $CaCO_3$	Organic Carbon
C4298	B192K1	0.026	0.001	0.010	0.027
C4298	B192K2	0.049	0.000	0.000	0.049
C4298	B192K3	0.017	0.000	0.000	0.017
C4298	B192K4	0.025	0.000	0.000	0.025
C4299	**B19136**	0.026	0.000	0.000	0.026
C4299	**B19137**	0.239	0.223	1.860	0.016
C4299	B19138	0.015	0.000	0.000	0.015
C4299	B19139	0.021	0.000	0.000	0.021
C4299	**B19140**	0.039	0.000	0.000	0.039
C4300	B19373	0.019	0.000	0.000	0.019
C4300	B19374	0.033	0.003	0.026	0.030
C4300	B19375	0.056	0.009	0.071	0.048
C4300	**B19377**	0.015	0.000	0.000	0.018
C4977	**NA**	0.19	0.00	0.00	0.19
C4990 composite	**NA**	0.09	0.02	0.17	0.07

The sample IDs labeled in bold were intact cores. The others contained slough.

C.3 Specific Surface Area of Aquifer Sediments

The specific surface area for different size fractions for four aquifer sediments are shown in the top portion of Table C.5. The specific surface area of the <2 mm fraction of the C4977 (Ringold Unit E gravel) and each of the four 6-in.-long liners from core C4990 (Ringold Lower Mud unit) are shown in the lower portion of Table C.5. Highest surface area was found in the Ringold Lower Mud samples from C4299 and C4990 boreholes, which are dominated by silt and clay-sized particles. Relatively high specific surface area was also found in the sand-sized fraction of B19140 sediments relative to the other samples (B192K1, B19136 and B19137, and B19377). This was attributed to a presence of the Fe oxide coatings around the surfaces of sand-size particles. These coatings are considered to be vesicular or porous, thus leading to high surface area. The highest specific surface area found in sample B19140 correlated well with the relatively high adsorption distribution coefficient (K_d) values found for this sediment compared with other samples (see Um et al. 2005).

Table C.5. Specific Surface Area for Aquifer Sediments from 200 West. Data are FIO. (Um et al., 2005)

Sample ID		Size Fraction	(m^2/g)
B192K1 (C4298)		<2 mm	1.94
B192K1 (C4298)		(0.125 < Size < 0.5 mm)	1.27
B192K1 (C4298)		<0.5 mm	2.24
B19136 and B19137 composite (C4299)		<2 mm	3.33
B19136 and B19137 composite (C4299)		(0.125 < Size < 0.5 mm)	0.97
B19136 and B19137 composite (C4299)		<0.5 mm	4.12
B19140 (C4299)		<2 mm	23.4
B19140 (C4299)		(0.125 < Size < 0.5 mm)	13.2
B19140 (C4299)		<0.5 mm	23.3
B19377(C4300)		<2 mm	8.40
B19377(C4300)		(0.125 < Size < 0.5 mm)	2.40
B19377(C4300)		<0.5 mm	8.71
C4977		<2 mm	2.62
C4990	404.7–405.2 ft bgs	<2 mm	29.4
	405.2–405.7 ft bgs	<2 mm	25.9
	405.7–406.2 ft bgs	<2 mm	29.8
	406.2–406.7 ft bgs	<2 mm	25.9

C.4 Cation Exchange Capacity of Aquifer Sediments

The cation exchange capacity (CEC) results for aquifer sediment samples are shown in Table C.6. The highest CEC value was found for the B19140 sediment, consistent with previous specific surface area results. Clay minerals and hydrous iron oxides generally have a greater CEC than other minerals. The minor difference, as opposed to the anticipated large difference, between bulk (with gravel) and without gravel samples for the B19136 and B19137 mixed sample was attributed to the presence of silt and clay mineral coatings on the gravel surfaces. The relatively higher CEC in both B19377 and B19140 resulted from the higher percentage of silt- and clay-sized particles in both sediments (see Table C.3) and the high ferric oxide coating in the latter sediment. The clay minerals present in the clay-sized fraction (see mineralogy discussion below) include smectite, chlorite, and illite, which have high cation exchange capacities.

Table C.6. Cation Exchange Capacity of 200 West Area Aquifer Sediments. Data are FIO. (Um et al., 2005)

Samples	B192K1 (<2 mm)	B19136&B19137 (Bulk with gravel)	B19136&B19137 (<2 mm)	B19377 (Ringold Low mud)	B19140 (<2 mm)
CEC (meq/100g)	1.66±0.34	3.28±3.29	3.39±0.21	17.12±2.45	44.91±9.25

C.5 Elemental Composition of Aquifer Sediments

The elemental composition of the intact sediments was determined by fusion and inductively coupled plasma (ICP) analysis, and the results are shown in Table C.7 for major elements and Table C.8 for minor elements. The elemental composition was converted to percentage oxide forms. The iron present in the sediments was assumed to be all ferric oxide, although some reduced ferrous iron oxide may also be present. The bulk chemical composition showed that silica and alumina were the most dominant oxides. Minor amounts of iron oxide were also found. The highest iron oxides were present in samples B19140 (C4299) and C4990, consistent with previous noticeable iron oxides seen when these liners were opened (Figure C.4).

Table C.7. Major Element Oxides (wt%) of Sediment Samples Using Fusion/ICP-MS. Data are FIO. (Um et al., 2005)

Element	SiO_2	Al_2O_3	$Fe_2O_{3(T)}$	MnO	MgO	CaO	Na_2O	K_2O	TiO_2	P_2O_5	LOI	Total
B192K1 Bulk	68.2	12.33	5.43	0.104	2.54	4.72	3.17	1.46	0.726	0.13	1.12	99.94
B19136 and B19137 Bulk with gravel	77.36	9.72	4.26	0.086	0.89	1.87	2.07	1.76	0.471	0.08	1.17	99.73
B19136 and B19137 w/out Gravel (<2mm)	75.64	10.67	3.37	0.069	1	2.35	2.86	1.69	0.413	0.1	1.35	99.52
B19140 Bulk with gravel	64.47	12.54	7.93	0.131	1.73	2.51	2.13	1.5	0.775	0.1	5.56	99.37
B19140 Bulk w/out gravel (<2mm)	66.67	11.54	6.66	0.12	1.23	1.79	1.96	1.87	0.673	0.1	7.28	99.9
B19373 Bulk	71.69	10.48	5.19	0.075	1.23	3.31	2.34	1.29	0.969	0.31	2.85	99.73
B19377 Bulk	68.15	12.89	4.12	0.037	1.95	1.09	1.42	2.61	0.62	0.12	6.55	99.56
Element	SiO_2	Al_2O_3	$Fe_2O_{3(T)}$	MnO	MgO	CaO	Na_2O	K_2O	TiO_2	P_2O_5	Others	Normalized
C4977 <2 mm	55.4	12.9	6.6	0.1	2.4	13.8	5.2	3.2	0.0	0.1	0.3	100
C4990 <2 mm	54.9	14.3	14.8	0.1	2.5	4.3	3.3	5.1	0.0	0.1	0.3	100

LOI= loss on ignition

Others= SrO and BaO; no loss on ignition performed on C4977 or C4990 and total normalized to 100%

Table C.8. Trace Element (mg/kg) of Sediment Samples using Fusion/ICP-MS. Data are FIO. (Um et al., 2005)

Elements	B192K1 Bulk	B19136 and B19137 with gravel	B19136 and B19137 without gravel	B19140 Bulk with gravel	B19140 Bulk without gravel	B19373 Bulk	B19377 Bulk
Sc	15	8	7	13	11	14	10
Be	1	2	2	2	2	1	2
V	133	56	57	116	97	123	82
Cr	60	50	30	60	70	50	50
Co	10	6	5	11	14	10	9
Ni	30	30	<20	40	40	30	30
Cu	30	20	10	20	20	20	20
Zn	40	<30	<30	60	60	40	60
Ga	13	11	11	15	16	13	17
Ge	1.3	1.4	1.1	1.2	1.3	1.1	1.4
As	<5	<5	<5	8	9	<5	<5
Rb	39	54	49	59	71	32	95
Sr	380	286	359	292	256	317	184
Y	19.5	21.5	18.3	24.3	26.7	24.5	29.3
Zr	124	176	165	157	171	128	289
Nb	7	12.9	10.5	9.8	11.6	7.7	17.3
Mo	<2	<2	<2	<2	<2	<2	<2
Ag	1.5	1	1	0.7	0.8	0.7	1
In	0.1	0.1	0.1	0.1	0.1	0.1	0.1

Elements	B192K1 Bulk	B19136 and B19137 with gravel	B19136 and B19137 without gravel	B19140 Bulk with gravel	B19140 Bulk without gravel	B19373 Bulk	B19377 Bulk
Sn	1	1	<1	1	2	1	2
Sb	0.7	0.4	0.3	0.4	0.6	0.4	0.5
Cs	1	1.4	1.2	3.5	3.7	0.9	4.5
Ba	642	609	650	638	684	543	621
La	16.2	28.3	21.9	20.8	26.4	21.1	44.8
Ce	32.8	55.8	43.8	44.5	67.4	40.5	90.7
Pr	3.89	6.04	4.85	5.19	6.55	4.85	10.2
Nd	14.9	21	17.4	19.3	24	18.7	36.7
Sm	3.18	3.66	3.16	3.96	4.76	3.88	6.95
Eu	0.932	0.883	0.813	1.05	1.08	1.16	1.44
Gd	3.43	3.61	3.16	4.17	4.79	4.1	6.56
Tb	0.57	0.58	0.5	0.7	0.78	0.68	0.95
Dy	3.23	3.36	2.84	4.06	4.34	3.86	5.14
Ho	0.65	0.7	0.59	0.85	0.87	0.78	0.98
Er	2.04	2.27	1.85	2.66	2.82	2.4	2.97
Tm	0.308	0.356	0.283	0.411	0.42	0.356	0.443
Yb	1.96	2.3	1.79	2.65	2.64	2.23	2.73
Lu	0.282	0.336	0.269	0.392	0.38	0.32	0.398
Hf	3.2	4.5	4.4	3.9	4.6	3.3	7.6
Ta	0.52	1.09	0.8	0.71	0.85	0.53	1.29
W	0.6	1.3	0.8	1	1	0.5	3.8
Tl	0.23	0.27	0.25	0.39	0.55	0.18	0.57
Pb	7	11	8	11	16	9	18
Bi	0.2	0.2	0.2	0.3	0.4	0.2	0.7
Th	4.38	8.02	7.28	6.34	8.14	4.71	13.7
U	1.07	1.64	1.5	1.87	1.93	1.47	2.96

C.6 Mineralogy of Aquifer Sediments

The aquifer sediment samples collected from boreholes in the 200 West Area were characterized by X-ray diffraction (XRD) to determine their mineralogy. XRD patterns representing the bulk, sand-, silt- and clay-sized fractions were characterized. Samples collected from borehole C4299 at depths of 271.5-272.0 ft bgs and 308.5 to 309.5 ft bgs were combined and treated as one sample. The XRD results taken from the bulk sediments indicated each interval was mineralogically similar. A typical example of an XRD tracing of the bulk sample collected in borehole C4299 (419.0-419.5 ft bgs) is provided in Figure C.5 along with the mineral powder diffraction files (PDF™) for comparison. The sample was dominated by quartz and feldspar, with minor amounts of hornblende and clays (smectite, chlorite, and mica). The feldspar was a combination of several different plagioclase and potassium feldspars; therefore, an exact match was not possible. Subtle differences were observed in the bulk patterns with the broad clay reflection at 5.9 °2θ, which is a combination of smectite and chlorite clays.

Examination of the silt- and sand-sized fractions from each sediment indicated a dominance of quartz and feldspar along with lesser amounts of hornblende (Figure C.6). As expected, the clay minerals smectite and chlorite were noticeably reduced or absent in the sand fraction. Micas were present in the sand fraction as biotite and muscovite flakes. In the silt fraction, one noticeable difference was observed with the mixed sample C4299 (B19136 and B19137). The clay mineral reflections in this mixed sample at lower angles (<10°2θ) were significantly more intense, indicating the sample had higher clay mineral content in the silt fraction compared to the silt fractions of the other samples. With the exception of intensity differences, the clay mineral assemblages from each aquifer sediment were the same.

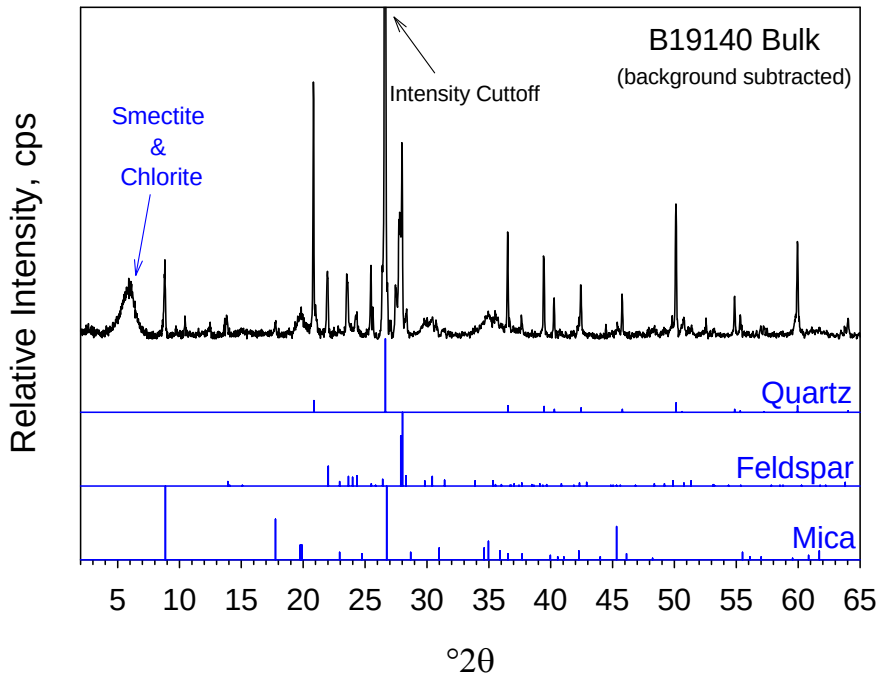

Figure C.5. XRD Tracing of B19140 Bulk Sample Collected from Borehole C4299. Data are FIO. (Um et al., 2005)

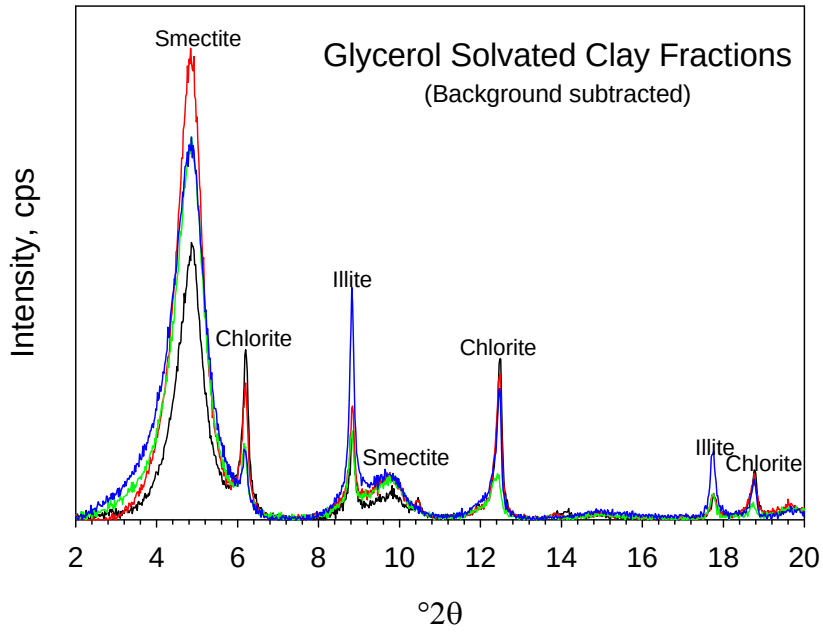

Figure C.6. XRD Tracings of Mg+2 Saturated, Glycerol Solvated Clay Fractions from Boreholes C4298 (B192K1) (black), C4299 (B19136&B19137) (red), C4299 (B19140) (green), and C4300 (B19377) (blue). Data are FIO. (Um et al., 2005)

Illite produced reflections at 8.8 and 17.7°2θ, which were easily distinguished from chlorite reflections at 6.15, 12.4, and 18.7°2θ. Figure C.6 shows that smectite, chlorite, and illite dominate the clay fractions. Minor amounts of non-clay minerals (quartz, feldspar) were also detected. No crystalline Fe2+ or Fe3+ compounds were identified in the XRD tracings of the clay fractions.

The XRD patterns and identified minerals for sample C4977 are given in Figure C.7 and Figure C.8. The sample was dominated by quartz, feldspar (orthoclase), and plagioclase (albite), with minor amounts of hornblende, mica (muscovite), and clays (montmorillonite). The XRD pattern at low angle (<30 in 2-theta) showed more distinctive peaks for clays (Figure C.8). The XRD patterns for composite sample C4990 showed similarities to that of sample C4977, except that orthoclase is dominant in sample C4990. However, based on the similar XRD patterns, all the aquifer sediment samples are considered to have similar mineralogical composition.

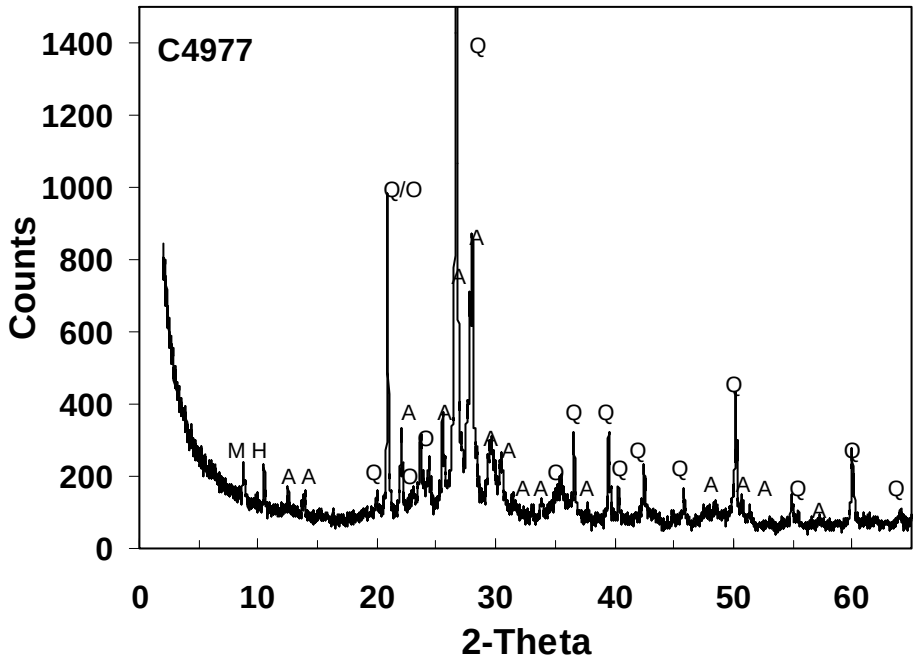

Figure C.7. X-Ray Diffraction Pattern of Borehole C4977 Sample and Identified Minerals. M = muscovite; H = hornblende; A = albite; Q = quartz; O = orthoclase. Data are FIO. (Um et al., 2005)

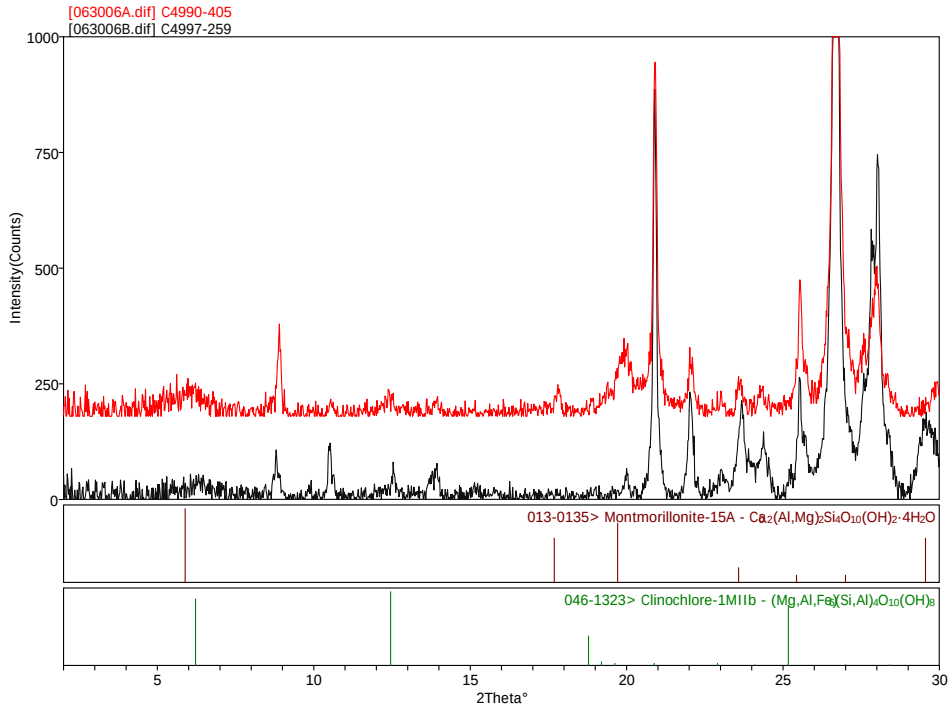

Figure C.8. X-Ray Diffraction Patterns of Montmorillonite and Clinochlore from Boreholes C4977 and C4990 in Low Angle. Data are FIO. (Um et al., 2005)

C.7 Characterization of Fe Oxide/Clay Coatings on Aquifer Sediments

Although ferric iron-rich coatings were found on the gravel surfaces of sediment in core B19140, the bulk XRD pattern of scrapings of the fine-grained and orange-colored material did not show any distinguishable crystalline iron oxides peaks such as hematite or goethite. Thus, the mass of crystalline iron oxides in the sediment is likely less than 5 wt%, or alternatively, the crystals are very small and not amenable to bulk XRD because small crystals lead to more diffuse and overlapping peaks in the XRD spectra. We thus resorted to more sophisticated micro analyses of the Fe oxide/clay coatings. The surface morphology, obtained from Field-Emission Scanning Electron Microscopy (FESEM), showed angular, platy shapes indicating crystalline minerals were present (Figure C.9). EDS also showed Si, Al, K, Mn, and Fe in the scrapings. These elements suggest the presence of both aluminosilicate clays and iron oxides in the coatings. Based on Figure C.9 findings, the needle-shaped crystals found attached to platy-shaped clay minerals are believed to be goethite.

The transmission electron microscopy (TEM) images yielded weak electron diffraction patterns, which are presented in Figure C.10. The TEM image of the same Fe oxide/clay coatings showed a needle-like structure, which is typical for goethite. Selected area electron diffraction indicates that this needle-like structure is indeed crystalline. However, due to the very limited orientation, identification of the phase based on one diffraction pattern is not possible. Based on previous bulk XRD analysis, smectite was one of the dominant clay minerals found in the Fe oxide/clay coatings. A weak electron diffraction pattern also suggested a small amount of goethite mixed with clay minerals.

The needle-shaped particle in the left image is tentatively identified as goethite. The right image, an electron diffraction image of the needle particle, indicates several crystalline materials are present. Amorphous materials would not yield the distinct “dots” and would look like an opaque cloud.

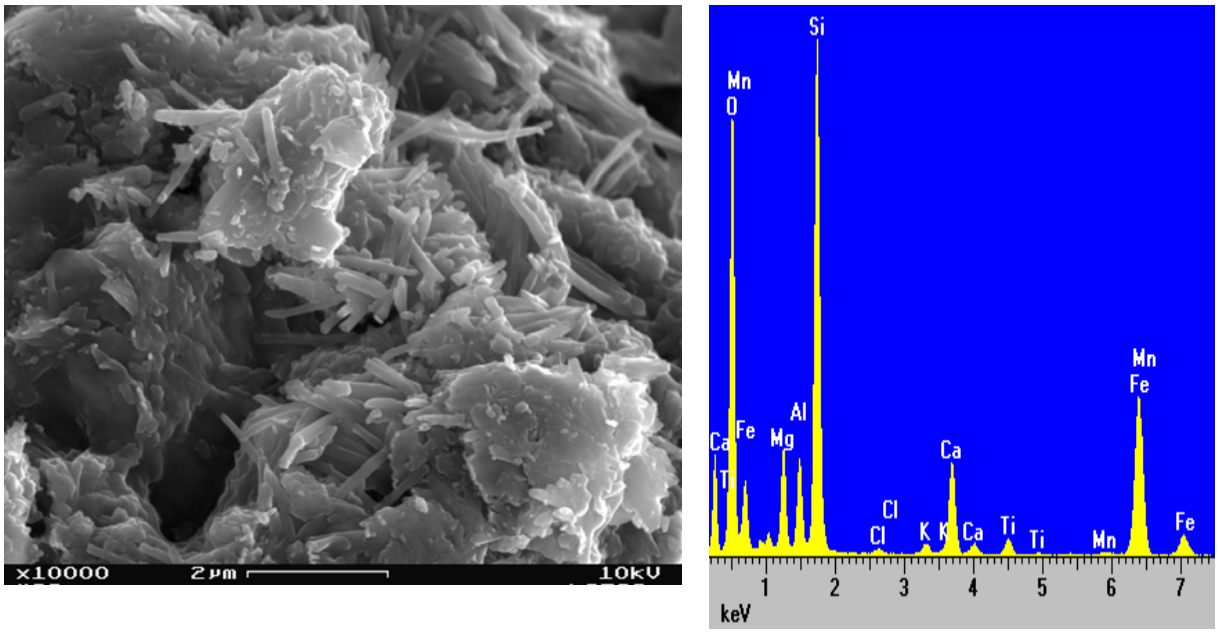

Figure C.9. FESEM Images with EDS of Fe Oxide/Clay Coatings Found in B19140 (C4299). Data are FIO. (Um et al., 2005)

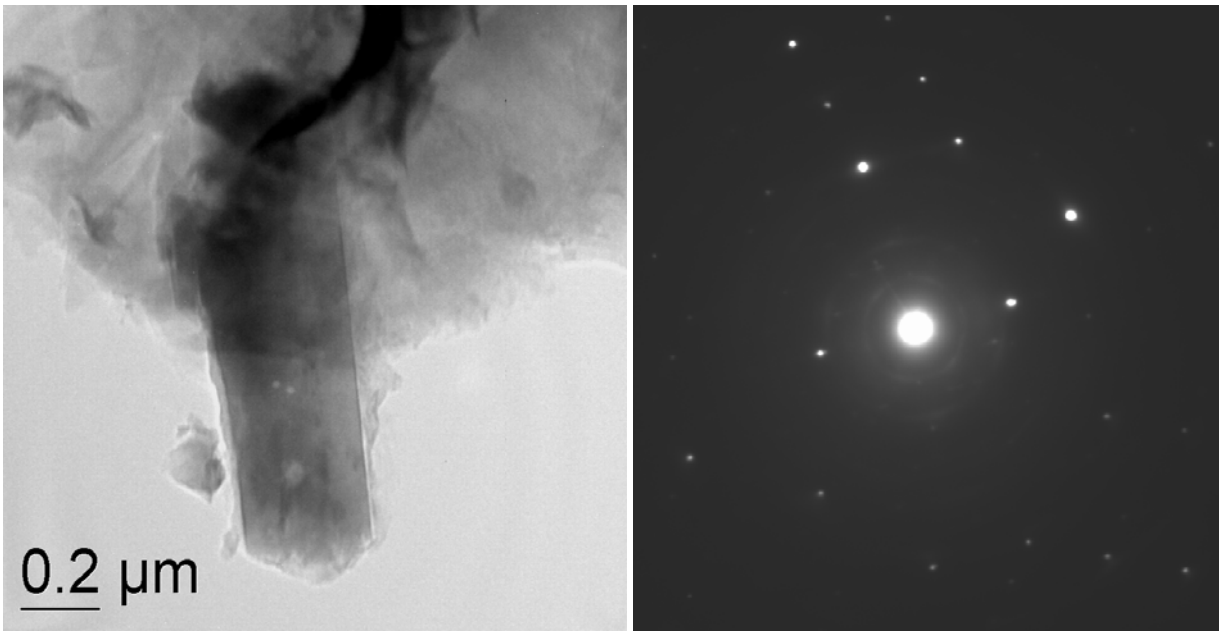

Figure C.10. TEM Image and Electron Diffraction Pattern of Fe Oxide/Clay Coatings from B19140. Data are FIO. (Um et al., 2005)

C.8 Fe and Mn Oxide Extraction of Aquifer Sediments

The extractable iron concentrations for 200-UP-1 and 200-ZP-1 aquifer sediments using three different methods are shown in Table C.9. The hydroxylamine hydrochloride (HH) and ammonium oxalate (Tamm's reagent) methods were used to quantify the amount of amorphous iron oxide (generally dominated by ferrihydrite) in the sediments. Tamm's method results showed significantly higher amorphous iron extractions than the HH method. One explanation for the different results is that the HH method chosen uses low concentrations (0.1 M hydroxylamine hydrochloride in 0.01M nitric acid) rather than 0.25 M hydroxylamine hydrochloride in 0.25 M hydrochloric acid used by Chao and Zhou (1983). If the extracted iron quantities from Tamm's method are assumed to represent all the amorphous and poorly crystalline iron oxide, which is dominated by ferrihydrite, in the sediment, the first three samples in Table C.9, (B192K1, B19136 and B19137 with gravel, and B19136 and B19137 without gravel), show that most of the iron oxides were present as amorphous iron oxides (ferrihydrite), especially in B192K1. Because Method 3 (dithionite-citrate-bicarbonate, DCB) quantified the total free iron-oxide content in the sediment, approximately 46% to 95% of the total extractable iron oxides in these 200-UP-1 sediments appears to be poorly crystallized iron oxide (ferrihydrite), as revealed by Method 2 (Tamm's reagent).

Table C.9. Results of Fe Extraction of 200-UP-1 Sediments Using Three Different Methods. Data are FIO. (Um et al., 2005)

Samples	Fe (μmoles/g of sediment)		
	Method 1 (HH)	Method 2 (Tamm's)	Method 3 (DCB)
B192K1 (C4298) Bulk with gravel	3.79±0.59	48.13±12.24	50.78±1.08
B19136 and B19137 (C4299) Bulk with gravel	1.71±0.39	21.03±7.45	38.35±5.85
B19136 and B19137 (C4299) without gravel (<2mm)	1.88±0.30	21.82±3.91	47.49±2.89
B19140 (C4299) without gravel (<2 mm)	3.27±0.38	16.37±0.62	111.21±2.60
B19377 (C4300) Ringold lower mud	1.38±0.35	4.74±0.11	37.41±0.33

Although the B192K1 sample was identified as slough material in the previous core description (see Table C.1), the B192K1 sample showed relatively higher amounts of amorphous iron oxide (95% of the total extractable iron oxides) compared with other samples from 200-UP-1. This high amorphous iron oxide content might result from newly precipitated amorphous iron oxide after oxidation of any fresh ferrous iron, released from broken gravel (generally basalt fragments containing ferrous iron) or from metal particles scraped off equipment during vigorous hard-tool drilling activities. Even though measurable soluble ferrous iron was not found in extracted pore water from this core, using the ferrozine method, significantly higher K_d values were found (see Um et al. 2005) for B192K1 sediments, especially for anions, Tc-99, and Cr(VI), which are usually considered to be non-reactive in most natural Hanford sediment conditions (Kaplan et al. 1996).

This hypothesis that new precipitates of ferrihydrite formed in the sediments because of hard drilling is also suggested by examining two other samples (B19136 and B19137 with gravel, and B19136 and B19137 without gravel). These samples also showed that ferrihydrite was 46% to 55% of the extractable total iron oxides (Table C.9), even though the absolute concentration of ferrihydrite is less than half the value found in the B192K1 slough material. Measurable ferrous iron concentrations were found in these two extracted pore water samples: 19 and 594 μg/L of Fe(II) in B19136 and B19137 pore water, respectively. Because the amount of ferrihydrite present was not different between samples (B19136 and B19137) with and without gravel, new precipitates of ferrihydrite might be present on all of the sediment particles as surface coatings or as mixtures with clay-sized particles that cling equally to all the bulk sediment. If the iron oxides were present as discrete particles, they would be expected to be small and not concentrated in the sample that had gravel removed. However, on a weight basis the amounts of extractable amorphous iron oxides (ferrihydrite) were the same with or without gravel removed (B19136 and B19137).

In addition, the first two samples in Table C.9, (B192K1, B19136 and B19137) were collected at relatively shallow depths (280-310 ft) compared to the bottom two samples, B19140 and B19377, collected at 420 and 428 ft, respectively. The top two samples collected at shallow depth had approximately 26% to 42% gravel in the bulk sample (Table C.3), which could be broken up by hard tool drilling activities thus releasing ferrous iron into their pore waters. Although sample B19140 also contained 55% gravel, it showed only 15% of the total extractable iron oxide was dissolved in the Tamm's reagent, which typically indicates the poorly crystalline ferrihydrite content. Most of the iron oxides in B19140 (85% of the total extractable iron oxide) was dissolved in the DCB step, indicating the presence of more crystalline ferric oxides such as goethite or hematite. This finding suggests that the iron oxide minerals in B19140 were originally developed a long time ago after exposure to a near-surface weathering environment. After long periods of aging, the amorphous iron oxides in sediment B19140

likely transformed into more crystalline iron oxides. High concentrations of extractable iron in sediment B19140, using DCB method, was consistent with previous characterization results, which showed many red-orange colored iron oxides in the sediment (Figure C.3). The presence of goethite in the B19140 sample was also identified by microscopic characterization of Fe oxide/clay coatings on gravel in B19140 (Figure C.9 and Figure C.10). Because no gravel was present in the B19377 sample (Ringold Lower Mud unit), and ferrihydrite was found to be only about 13% of the total extractable iron oxides in this sediment, most of the iron oxides in this sediment sample also exists as either goethite or hematite present as coatings or clay-sized particles.

The extractable aluminum (Al), silicon (Si), and manganese (Mn) was also measured, and the findings are reported in Table C.10. The highest extractable Al concentration was found via Method 2 (Tamm's) in all the sediments, suggesting ferrihydrite precipitates in association with Al-bearing minerals such as feldspar and clays. However, the highest Si concentration extracted was found via Method 3 (DCB), indicating that most of the aged iron oxides, such as goethite and hematite, were likely present with clays as coatings on the quartz surfaces of the natural Ringold Formation sediments. Because higher amounts of extractable Si was found via Method 3 (DCB) than Method 2 (Tamm's) for both B19140 and B19377 sediments, most of the iron oxides found in B19140 and B19377 were assumed to be goethite and goethite coatings on quartz or gravel surfaces that co-dissolved in the DCB step. Bulk XRD analyses did not identify any crystalline iron oxides because the absolute mass of iron oxides is small, and it is also difficult to find distinct XRD patterns for very small-sized particles such as coatings. The scanning electron microscopy and TEM characterization for clay-sized particles and coatings scraped off of sediment B19140 does show evidence of the presence of crystalline iron oxides.

Table C.10. Extracted Iron, Aluminum, Silicon, and Manganese in 200-UP-1 Sediments. Data are FIO. (Um et al., 2005)

		Samples				
Elements	Methods	B192K1 Bulk with Gravel	B19136 and B19137 Bulk with Gravel	B19136 and B19137 Bulk w/o Gravel	B19140 Bulk w/o Gravel	B19377 (C4300) Ringold Lower Mud
Fe (μmoles/g)	Method 1	3.79±0.59	1.71±0.39	1.88±0.30	3.27±0.38	1.38±0.35
	Method 2	**48.13**±12.24	21.03±7.45	21.82±3.91	16.37±0.62	4.74±0.11
	Method 3	**50.78**±1.08	38.35±5.85	47.49±2.89	**111.21**±2.60	37.41±0.33
Al (μmoles/g)	Method 1	2.40±0.43	2.26±0.44	2.36±0.37	4.70±0.45	4.48±0.79
	Method 2	4.18±0.30	4.63±1.05	4.88±0.57	**16.30**±0.17	**10.74**±0.26
	Method 3	2.28±0.20	2.30±0.25	2.51±0.07	8.45±0.21	6.26±0.12
Si (μmoles/g)	Method 1	1.59±0.34	1.33±0.19	1.40±0.21	5.17±0.43	3.11±0.42
	Method 2	5.33±0.45	3.55±0.89	3.45±0.60	7.98±0.42	3.53±0.32
	Method 3	7.52±0.52	8.73±1.09	9.66±0.15	**22.02**±0.31	**22.97**±0.74
Mn (μmoles/g)	Method 1	1.09±0.06	0.97±0.11	1.00±0.06	**11.78**±0.89	0.86±0.12
	Method 2	1.24±0.15	1.04±0.25	1.01±0.06	**12.72**±0.73	0.88±0.03
	Method 3	1.51±0.06	1.22±0.14	1.30±0.06	**11.68**±0.69	0.83±0.05

Bold values represent samples with high extractable quantities compared to the other sediments.

High concentrations of Mn were extracted in sediment B19140 via all three methods, suggesting Mn oxide coatings are also present in this sample and they were associated with Fe oxides. However, because all three chemical extractants dissolved similar amounts of Mn in each of the 200-UP-1 sediments, the

Mn oxides are likely highly amorphous and not associated with any specific type of iron oxide (either ferrihydrite or goethite/hematite).

Similar hydrous oxide extractions were performed on aquifer sediments from two 200-W ZP-1 operable unit boreholes (C4977 and C4990) using the DCB and Tamm's reagent methods and the results are shown in Table C.11 and Table C.12. Both Tamm's and the DCB methods yielded higher iron contents in sample C4977 compared to that for the composite sample C4990. Significantly higher iron content was found in the DCB extract from sample C4997 than resulted from the Tamm's extract. Because the DCB extraction method is selective for crystalline iron oxides and the Tamm's extraction method is selective for amorphous iron oxides, most of the iron oxides (74%) present in sample C4977 are considered to be more crystalline iron oxides such as hematite or goethite. However, sample C4990 showed that about 70% of iron oxide present in DCB extractant is from amorphous iron oxide (ferrihydrite). These iron oxide content differences between samples C4997 and C4990 may have originated from different weathering environments or history in the two different wells. Interestingly the Tamm's extraction removed more manganese from these two sediments than the more aggressive DCB extraction.

Table C.11. Results of Selective Iron and Manganese Extraction Using Two Different Methods. Data are FIO. (Um et al., 2005)

	Fe (μmol/g of sediment)	
Sample ID	DCB Method[(a)]	Tamm's Method
C4977	26.49 ± 0.13	18.52 ± 1.45
C4990 composite	149.28 ± 8.32	38.30 ± 1.15
	Mn (μmol/g of sediment)	
Sample ID	DCB Method[(a)]	Tamm's Method
C4977	1.13± 0.04	2.40± 0.11
C4990 composite	0.68±0.02	1.52±0.03

(a) DCB method indicates citrate-bicarbonate-dithionite extraction.

Table C.12. % of Total Fe and Mn that is Extractable by the Two Treatments. Data are FIO. (Um et al., 2005)

	Fe (%) Extractable	
Sample ID	DCB Method	Tamm's Method
C4977	3.20%	2.24%
C4990 composite	8.05%	2.07%
	Mn (%) Extractable	
Sample ID	DCB Method[(a)]	Tamm's Method
C4977	8.02%	17.03%
C4990 composite	4.82%	10.78%

C.9 References

Chao TT and L Zhou. 1983. "Extraction Techniques for Selective Dissolution of Amorphous Iron Oxides from Soils and Sediments." *Soil Sci. Soc. Am. J.* 47: 225-232.

Kaplan DI, RJ Serne, AT Owen, JA Conca, TW Wietsma, and TL Gervais. 1996. *Radionuclide Adsorption Distribution Coefficients Measured in Hanford Sediments for the Low Level Waste*

Performance Assessment Project. PNNL-11485, Pacific Northwest National Laboratory, Richland, Washington.

Um W and RJ Serne. 2006. *Characterization of 200-UP-1 and 200-ZP-1 operable unit aquifer sediments and batch adsorption distribution coefficients for contaminants of concern—Fiscal year 2006 Progress*. PNNL-16102, Pacific Northwest National Laboratory, Richland, Washington.

Um W, RJ Serne, BN Bjornstad, HT Schaef, CF Brown, VL LeGore, KN Geiszler, SR Baum, MM Valenta, IV Kutnyakov, TS Vickerman, and MJ Lindberg. 2005. *Characterization of UP-1 Aquifer Sediments and Results of Sorption-Desorption Tests Using Spiked Uncontaminated Groundwater*. PNNL-15502, Pacific Northwest National Laboratory, Richland, Washington.

Um W, RJ Serne, GV Last, RE Clayton, and ET Glossbrenner. 2009. "The effect of gravel size fraction on the distribution coefficients of selected radionuclides." *Journal of Contaminant Hydrology* 107(1-2):82-90.

Pacific Northwest National Laboratory

902 Battelle Boulevard
P.O. Box 999
Richland, WA 99354
1-888-375-PNNL (7665)

www.pnnl.gov